DISTRIBUTIONS AND BEHAVIOR OF SOME RADIONUCLIDES IN THE ENVIRONMENT

MASAMI FUKUI

DISTRIBUTIONS AND BEHAVIOR OF SOME RADIONUCLIDES IN THE ENVIRONMENT

MASAMI FUKUI

CONTENTS

Chapter 1
INTRODUCTION

The tasks of environmental assessment are closely interrelated with the general problem of ecology, agrochemistry, radiobiology, etc. because the migration of toxic substances occurs via air, soil and water. The many processes by which pollutants reach the living spaces from source terms are the major concern of this research. These processes are complex and highly variable in the environment. However, to estimate the human toxicological impacts, it is essential to increase our understanding of distributions and variations of harmful substances. With regards to radioactive contamination, concerns over the exposure by radiation have been increasing, not only of the nuclear energy industry but also of the natural environment.

Distributions and variations of radon-222 in the subsurface environment will be firstly dealt with in chapter 2, because radon and its daughter products are the major sources of radiation exposure in the natural environment. Radon is also used as a geochemical tool for subsurface investigations because it is basically an inert gas and has a relatively short half-life (3.82 days). Radon is supplied continuously as a decay product of radium-226 (a half-life of 1600 y) widely distributed in solid matrix in subsurface environment. Once formed in the Earth's crust, it diffuses into soil air/groundwater and then into the atmosphere. These processes in different phases are examined in chapter 2 using data in field investigations of the distributions and variations of radon concentration both in groundwater and soil air.

Radionuclides have usually been released under a controlled situation in nuclear facilities, and since the concentration of radionuclides is monitored the duration of release is known. However, the release of radionuclides may also occur in an uncontrolled situation such as during an incident and/or an accident. Chapter 3 addresses an incidental release of heavy water

containing tritiated water spilled from a tank. The tritiated water vapor was used as a tracer for a better understanding of dynamics of vapor in a containment building air, as well as a tracer of groundwater in subsurface. Effort was focused not only on describing the distributions of concentrations of tritiated water vapor in air through monitoring after an incident, but also on developing mathematical models to quantify the amount transferred into environmental compartments, thus enabling estimation of the exposure dose to man. Investigations on the behavior of HTO in an indoor environment, as dealt with in this chapter, would provide information for the radiation protection under a severe accident.

Toxic effects of contaminants can generally be minimized only when their behavior in the environment is understood, and the likely future impacts can be predicted. However, a basic tenet, especially for radiation protection, is to maintain exposures as low as reasonably achievable, taking economic and social considerations into account (ALARA concept). Application of this Japan has resulted in developing the techniques to reduce the routine release of radioactivity into the environment, which makes it difficult to detect radioactivities in the biosphere, except at specific locations surrounding the discharge points. For this reason, the use of models is helpful to forecast the contaminant spread in the environment. Chapter 4 addresses the fate of some radionuclides, which have been released routinely as low-level liquid wastes from nuclear power installations into coastal areas. Model parameters needed for the assessment, such as the association of radionuclides with both suspended particulate matters and coastal sediments, were obtained in the in vitro experiments. The procedures as shown in this chapter may be applicable to the forthcoming assessment for the environmental pollution of many non-radioactive substances whose chemical behavior is similar to specific nuclides.

Figure 1-1 summarizes the essential components of an evaluation of the likely effcts of radionuclides in the environment, including subjects mentioned above in relation to the overall assessment scheme.

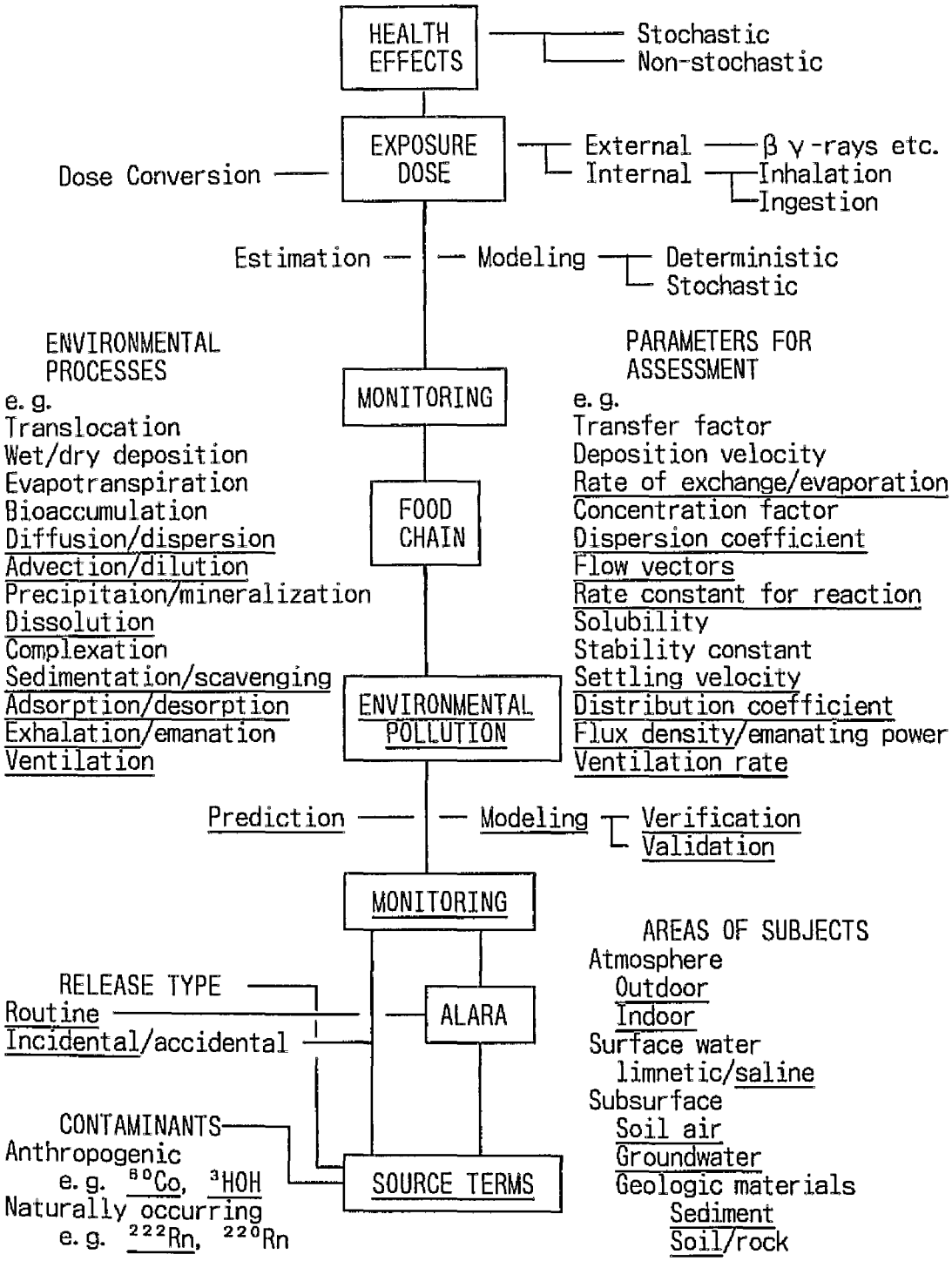

Fig. 1-1 Major steps in evaluating the effects of radionuclides in the environment and other factors needed for the assessment. The underlined topics were addressed in this project.

Chapter 2
RADON-222 UNDERGROUND

2. 1 INTRODUCTION

It is well known that radium-226 in the U-series is widely distributed in almost all soils, and that the daughter nuclide, radon (the term "radon" refers to ^{222}Rn unless otherwise specified), migrates from the geologic materials into both the saturated and unsaturated underground, and then discharges into the atmosphere. The measurement of radon has been performed from many standpoints, for instance, the mining industry (IAEA 1976; Goldsmith et al. 1980; NUREG 1980; NUREG 1989; IAEA 1991), geophysics and hydrology (Tarnner 1964; Kimura et al. 1975; Hess et al. 1979; Graves 1987), earthquake prediction (Bichard et al. 1976; Noguchi et al. 1977; King 1978; Nishimura 1979; Ikeda et al. 1981), and the health physics field (Hems 1966; Pohl-Ruling 1976; Sasser et al. 1978; Kataoka et al. 1979; Kiefer et al. 1980). However, the dynamics of radon is not well known due to the interference with meteorological effects. Several studies have reported on the effects of meteorological variables on the concentration of radon in soil gas (Hatsuda 1953; Okabe 1956; Biessell et al. 1973; Clements et al. 1974; Mochizuki et al. 1980; Schery et al. 1984; Wilkening 1990) but few reports have been made for shallow groundwater. Among the various atmospheric fluctuations which might alter the near surface radon concentration in the ground, only the effect of atmospheric pressure change may be reproducible (Kraner et al. 1964; Schery et al. 1984). In all the research fields mentioned above, it has been important to know the distribution of radon concentration in underground in greater detail. Continuous monitoring of radon concentration in soil gas and groundwater, however, has not been sufficient to prove meteorologic effects, including the groundwater level, especially near the surface in natural soil where radon content has not been elevated by U ore and/or mill tailings.

2. 2 VERTICAL DISTRIBUTIONS OF RADON IN UNCONFINED GROUNDWATER

2.2.1 Objective and Scope

Few general studies have reported on the anomalies of radon concentration in groundwater which may influence the dynamics of radon in the vadose zone near the interface between the water table and the soil air. In humid areas with a high groundwater table, such as Japan, the decrease in concentration of radon below the water table is probable.

In this study, the spatial and vertical distributions of radon concentration in unconfined groundwater were surveyed, and the change of the concentration in groundwater relative to pumping was investigated. The results are considered to be valuable in obtaining sampling condition of groundwater, which represents a normal concentration in contact with the Earth's crust. Knowledge of the level of radon concentration in water is also important to assess the internal exposure dose on public individuals caused by both ingestion of water and inhalation of radon after degassing.

2.2.2 Surveyed Area and Sampling Locations

The study was carried out at the site of the Research Reactor Institue, Kyoto University (KUR-RI), which is located on the Plio-Pleistocene Osaka Group (Fig. 2-1). The Group forms a hilly landscape on the basement rock of the Ryoke Granite (Paleozoic-Mesozoic) and is composed of many strata of fine sand and clay with a few meters depth for each (Itihara et al. 1975). The total depth of the Group is of about 200 m at the KUR site. The geology and stratification of the Osaka Group was surveyed by means of borings at ten locations, 30 m apart for each, in the KUR-RI site (Fukui and Katsurayama 1976b).

Figure 2-2 shows the ten locations of boreholes designated No. 1-10 from which groundwater samples were collected for

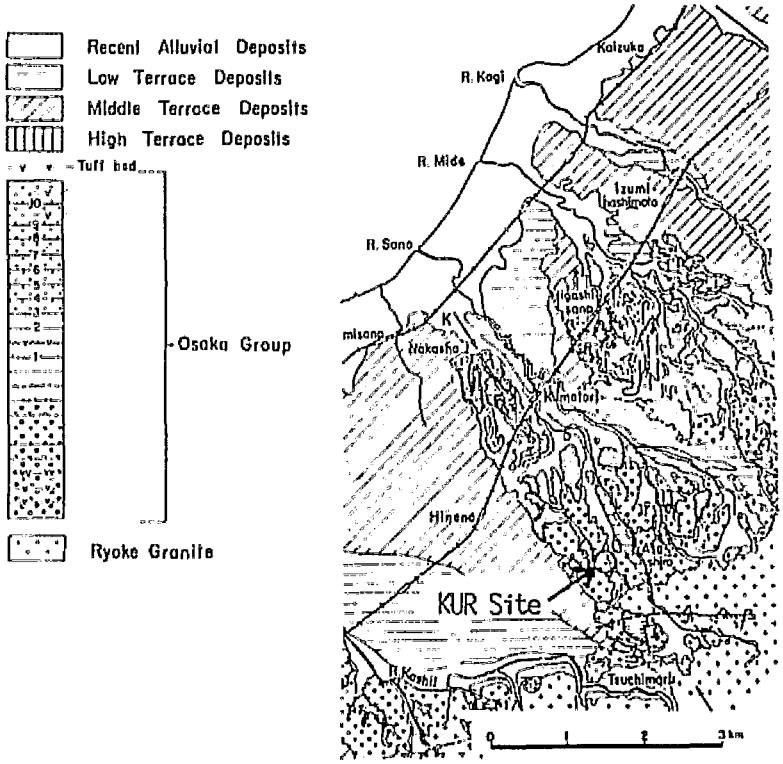

Fig. 2-1 Geological map of Sennan area (Icihara et al. 1975) and location of the KUR site.

investigation of the extent of, and variations in radon concentrations in near surface waters during a 6-month period. The locations where deep groundwater (100-200 m) was sampled were given to the north side of this figure as No. D-1 and No. D-2. In 1976 fourteen boreholes designated A-N, were also excavated near the borehole, No. 7, as shown in Fig. 2-2 to examine the groundwater flow. As this area is located in lower elevation, the groundwater levels appeared ordinarily within 2 m below ground surface and the changes of level in the boreholes were enhanced by infiltrating water due to precipitation when compared to those of boreholes set in the hill side.

The boreholes were completed with a PVC casing of 20-30 m length for No. 1-10 and 5 m length for No. A-N, wrapped with polyester filter. The diameter of casing was 10 cm for the longer

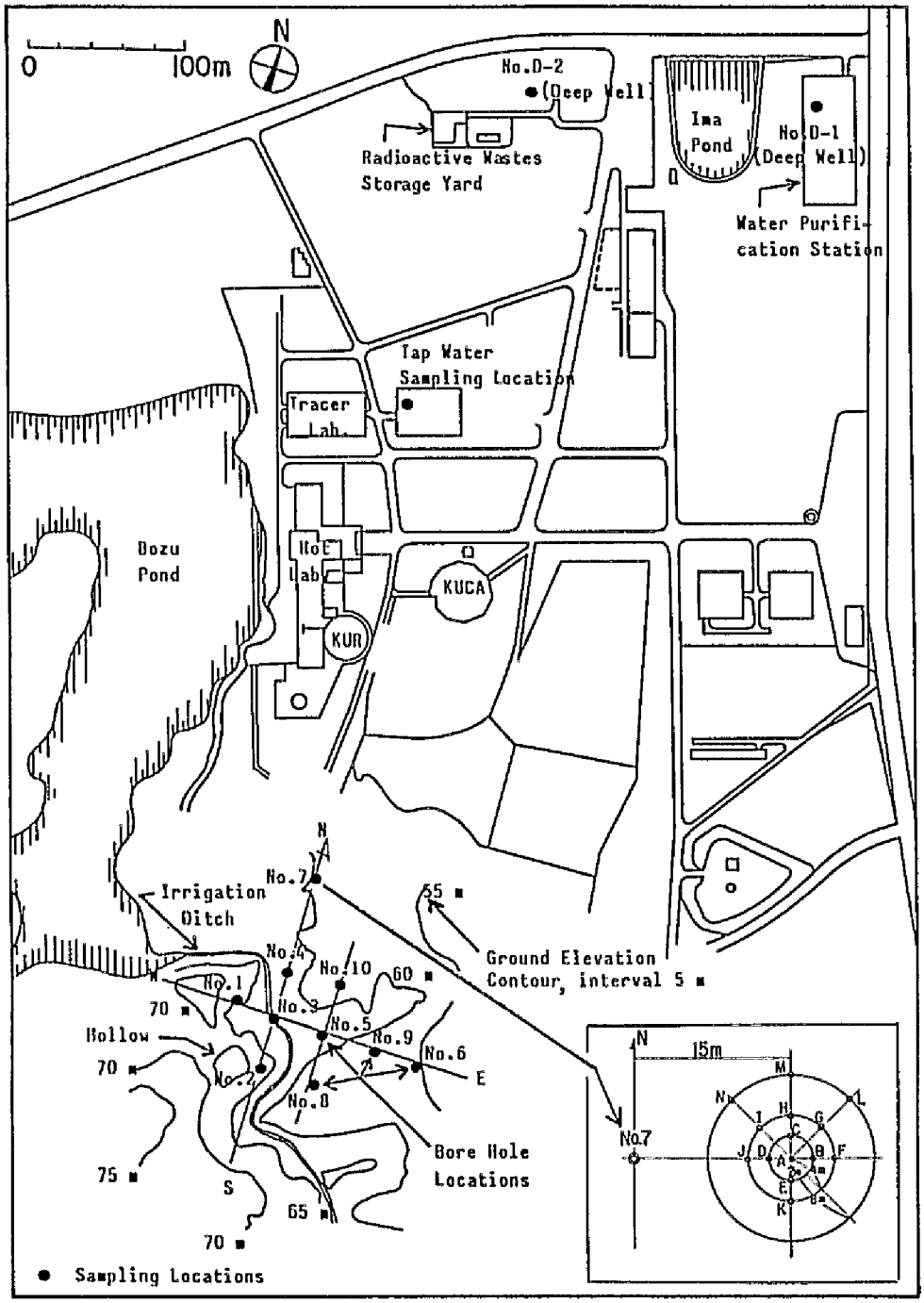

Fig. 2-2 Map and locations of sampled boreholes.

and 7.5 cm for the shorter (but 10 cm diameter in wells, A and N), screened with an annulus area of about 11% to the surface area of pipes below 50 cm from the top of the PVC casing.

2.2.3 Sampling Method and Measurement Procedure

The fact that radon is an inert gas, requires a special procedure for sampling and transferring of radon into the counting vial. An acrylic lucid column (50 mm I.D. and 700 mm in length) was used for collecting the shallow groundwater samples for No.1-10 boreholes from ca. 1 m below the water table, which is within 10 m depth. The sampled water was trasferred into a 1-L polyethylene bottle with overflow, which was then sealed so that the contained water did not come in contact with air. The sample was then allowed to settle in the laboratory for ca. 2 days, which promoted the precipitation of suspended particles, and allowed greater separation between the water and the toluene in the extraction procedure. Radon is highly soluble in toluene, a solvent generally used in liquid scintillation counting. In this study, radon concentrations were measured using the toluene extraction-liquid scintillation counting technique (Noguchi 1964) with minor modifications. One liter of sampled water, treated carefully as described above, is siphoned out of the polyetylene bottle at a constant flow rate less than 1 L min^{-1} into a flask loaded previously with 30 or 40 mL of toluene to prevent the loss of radon from water into the air. Then, the samples were shaken vigorously for ca. 3 min and allowed to settle for ca. 20 min until the mixtures separated so that the toluene, enriched in radon, could be collected into a glass vial for counting. Samples of lower turbidity, such as deep groundwater and tap water were introduced directly into a flask without the precipitation procedure, and then were treated in same way as the other samples. Because the solubility of radon in toluene is ca. 45 times higher than in water at 20 ℃, radon in water is easily extracted into the toluene. In the method described above, the radon concentration

in water, is estimated using the following equation (Wakita et al. 1976):

$$C = (V_a/D_t V_w + V_t/V_w + D_w/D_t)C_t \quad (2\text{-}1)$$

where

V_a, V_t, V_w : volumes (L) of air, toluene and groundwater, respectively, in the flask, and

D_t, D_w : distribution coefficients of radon in air to toluene and water, respectively.

The concentrations of radioactivity in the counting vial (C_t) is:

$$C_t = n \times \exp(\lambda t)/(11.1 \times V_{vt}) \quad (2\text{-}2)$$

where

V_{vt} : volume (L) of toluene in the counting vial,

n : integral counting rate (cpm) obtained by zero extraction at different bias settings,

λ : decay constant (7.56×10^{-3} h^{-1}) of radon, and

t : time elapsed from the sampling of water to the counting.

Because it takes ca. 3 h to establish secular equilibrium between radon and its short-lived progeny, the samples were counted for 50 min, at least 5 h after the extraction procedure. The lower limit of detection at the 95% confidence level by this method was 0.15 Bq L^{-1} in terms of the concentration in water. The scintillation fluid was composed of 4 g of PPO and 0.1 g of POPOP in a 1-L toluene solution.

A water pump was used to collect groundwater samples for boreholes, No.A-N, where electricity is available. This procedure is able to prevent loss of radon from water to air. Figure 2-3 shows the set-up for sampling the shallow groundwater, where a 1-L of flask was connected on the inlet side of the pump to prevent access of air into the sample. A glass-wool filter is set on the inlet side of this flask to provide for good separation between toluene and groundwater by eliminating the suspended solids from the water, which can cause foaming of the toluene phase, especially in summer, probably due to the increase of soluble organic matters in infiltrating water.

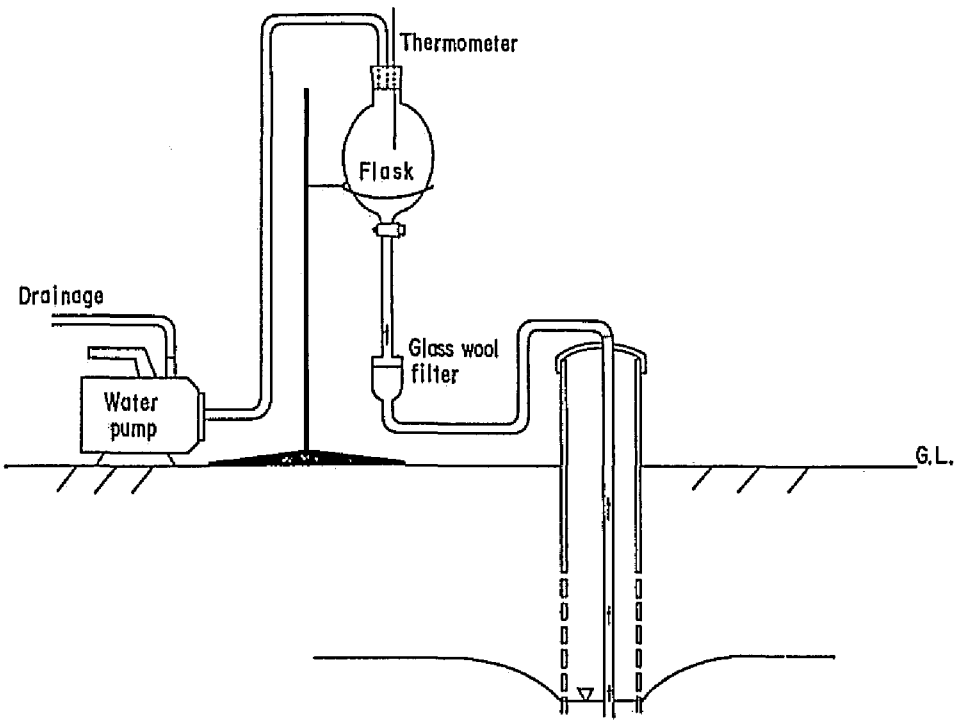

Fig. 2-3 Set-up for groundwater sampling.

The extraction procedure of radon from the groundwater sampled in the flask is as follows:

(1) measure the volume of the flask by the displacement method;

(2) hook-up pump, flask and filter to the hose connected to the PVC casing as shown in Fig. 2-3;

(3) pour a measured amount of toluene (40 mL) onto the water sampled in the flask in order to prevent loss of radon;

(4) after shaking, followed by settling the flask described above, transfer the toluene, enriched with radon, into a counting vial by forcing the water gently upward from the bottom of the flask without the use of a pipet. This procedure again serves to prevent loss of radon from toluene to air.

The weight of the toluene transferred into the vial was converted to volume by measuring the specific weight of the toluene. Subsequent procedures for measuring the radon concentration are as described above.

2.2.4 Results and Discussion

2.2.4.1 Preliminary investigation for radon measurement

(1) Hook-up of the flask to the pump.

The radon concentrations of the groundwater pumped were measured to investigate the effect of inhalation of air from the pump. Water samples were collected in three flasks which were hooked-up in a series on both inlet and outlet sides of the pump. The average concentration of those on the outlet side showed only 55% as much radon as those on the inlet side, when the hose was loosely connected to the pump. For this reason the flasks for the sample collection were hooked-up to the inlet side of the pump.

(2) Method of transferring toluene enriched with radon in the flask to the counting vial.

It was found that the use of a pipet to transfer the toluene resulted in decreasing the radon concentration in the toluene scintillator transferred to the vial. Therefore, the toluene was gently transferred to the vial by hydraulic pressure without the use of a pipet.

(3) Identification of the radionuclide trapped in the toluene.

The measurement of the same sample repeatedly over a period of several weeks indicated that the radionuclide has a half-life of about 3.8 days, which is the same as that of radon-222.

(4) Effect of the volumetric ratio of the three phases on the process of extraction.

Radon concentrations were measured with the varying volumes of toluene (20, 30, 40 and 50 mL) and water (500, 750 and 1000 mL). As shown in Table 2-1, the difference of concentration was found to be small, that is, the relative concentrations obtained are almost unity for these volume combinations.

Table 2-1 Relative concentrations of radon-222 in water volume sampled and toluene volume.

Volume of water (mL)	Volume of toluene (mL)	Relative concentration
1000	50	1.03
1000	40	1.00
1000	30	0.92
1000	20	1.00
750	40	1.02
500	40	1.06

2.2.4.2 Previous studies on radon concentrations in groundwaters in boreholes

In order to obtain the knowledge about the mixing of groundwater with surface water, groundwater samples in boreholes, No. 1-7, were analysed for radon content about once a week for a 6-month period starting October 1976. Figure 2-4 shows cross-sections of the shallow zone; the average annual groundwater level is shown in each borehole. As shown by the cross-sections, permeable layers are intercalated with impermeable layers, and all of these stratigraphic units dip NNW. The dashed lines at the boreholes (Nos. 2, 6 and 7) mean that they were fitted with PVC casing which is screened below the depth of 5 m, whereas in the other boreholes (solid lines), plain PVC casing extends only 5 m from ground level. Therefore, the water samples ordinarily were collected from just below the water table adjacent to a sandy layer (O_{s1} or O_{s2}).

Figure 2-5 shows rainfall intensity and elevation of groundwater for a year, which encompassed the period of radon measurements. The ground surface elevation of the seven boreholes is denoted at the left side of the figure.

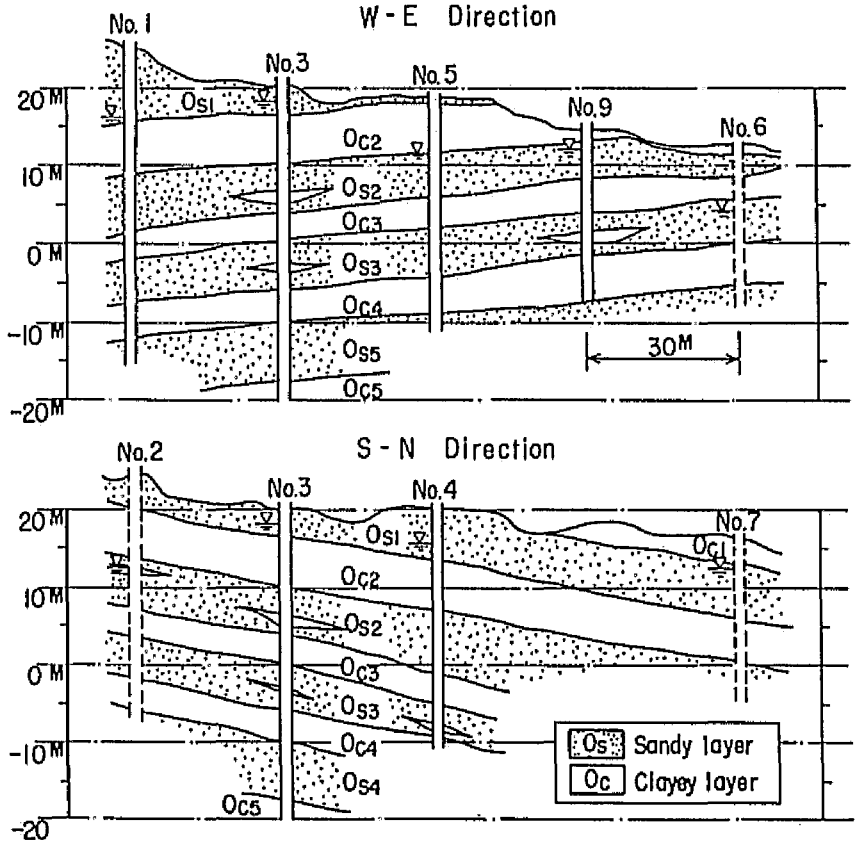

Fig. 2-4 Geological cross-sections of the area surveyed and normal levels of groundwater in boreholes.

Relative ground surface elevations were measured from an arbitrary datum 20 m below the No. 3 borehole elevation. As is shown by Fig. 2-5, the annual variation of groundwater levels was ca. 0.5-3.5 m except for the No. 2 borehole. Figure 2-5 shows that the water level in borehole, No. 2, rises abruptly after a precipitation event. This is because large amounts of rain water flow into a hollow ca. 1000 m^2 in size located near this borehole. Consequently, the water level in the No. 2 borehole rises for ca. 10 m $week^{-1}$ in response to more than 50 mm d^{-1} of precipitation. The generally high level of the groundwater table in the No. 3 borehole may be influenced by recharge from a nearby irrigation ditch (Fukui and Katsurayama 1983a).

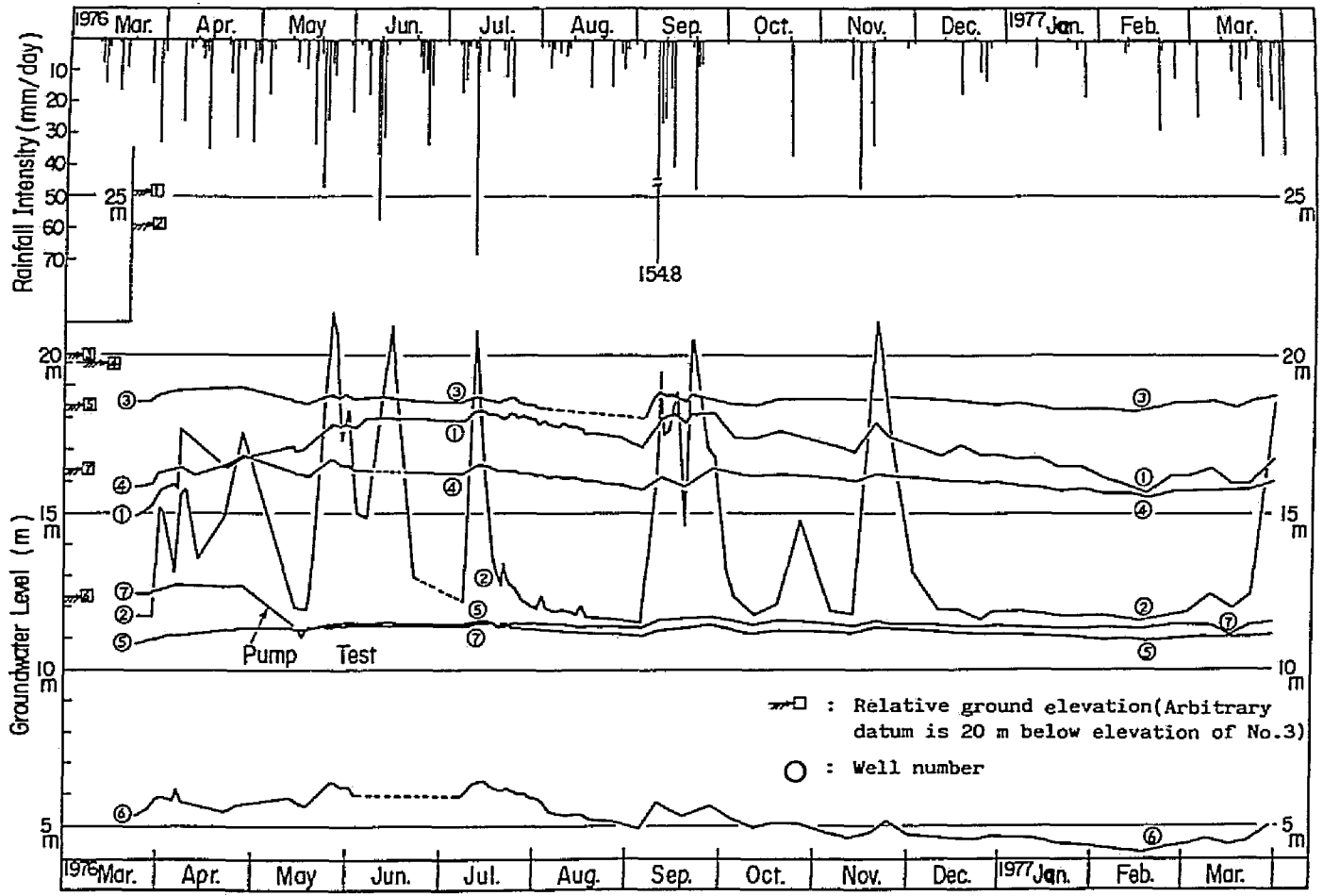

Fig. 2-5 Annual trends of groundwater levels in seven boreholes, and rainfall intensity.

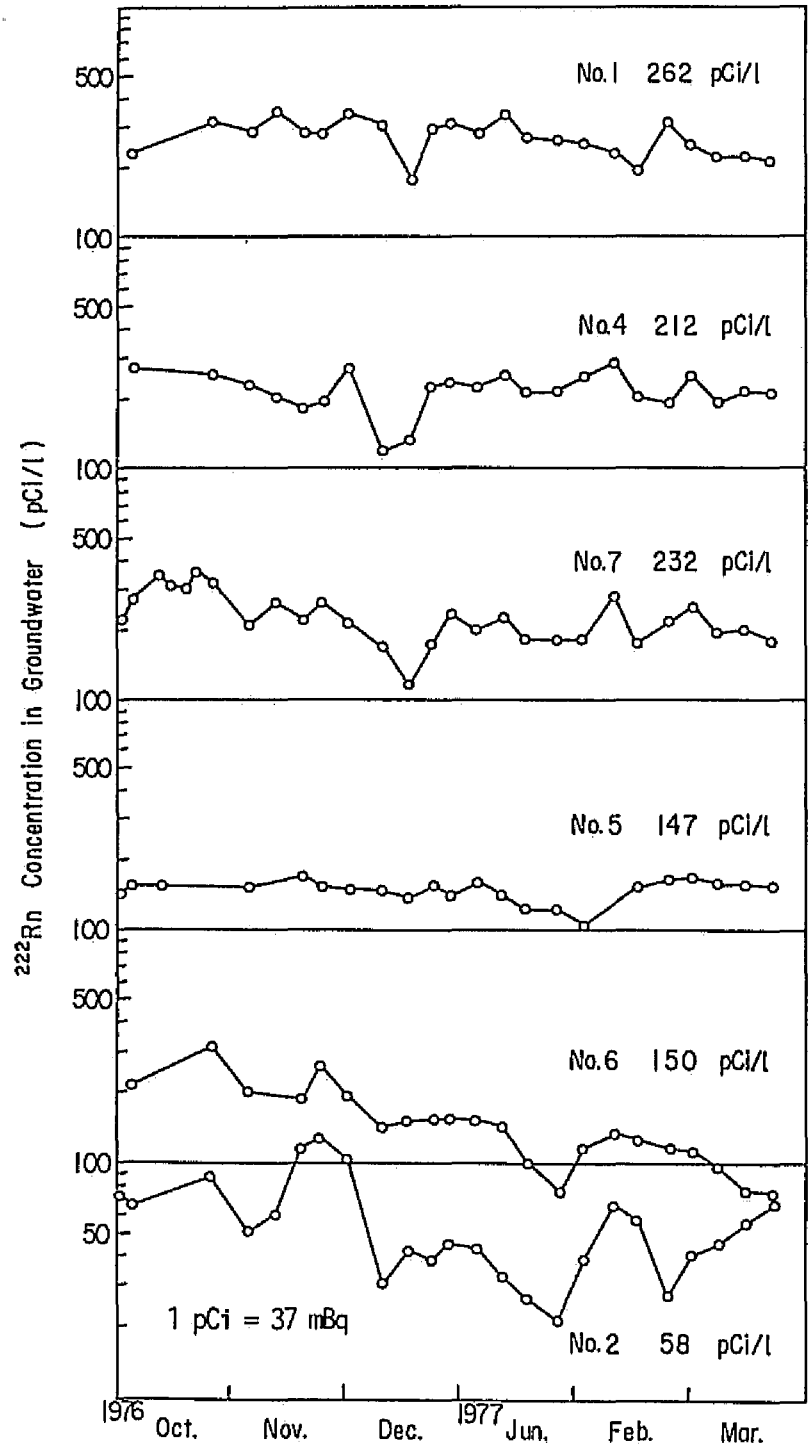

Fig. 2-6 Radon concentrations in groundwater in six boreholes for a 6-mo period. Data from No. 3 was not available due to the closure of the borehole.

Figure 2-6 shows the radon concentrations in water collected from six boreholes (Nos. 1, 2, 4-7), measured about once a week for 6 months. The variation of radon content is minimal in the No. 5 borehole, whereas it was notable in the No. 2 borehole. This fact and the water levels shown in Fig. 2-4 indicate that the impermeable layer (O_{c2}) above the sandy layer (O_{s2}) provides a more stable condition for groundwater flow near the No. 5 borehole than at the No. 2 borehole. That is, the lower concentration and the large scatter of radon content in water from the No. 2 borehole result from the effect of dilution by precipitation. However, the variations do not correspond exactly to the precipitation history, because of displacement of soil water by precipitation, and/or of the disequilibrium effect between radon and radium.

Table 2-2 Radon concentrations (Bq L^{-1}) in groundwater within ca. 10 m depth.

Sampling locations (Borehole No.) Levels of water table (m), stratum			Concentrations in 1977 March 9	March 16	March 23
No. 1	7 - 8	O_{s1}	8.0	7.9	7.5
No. 2	3 -12	O_{s2}*1	1.7	2.1	2.6
No. 3	1 - 2	O_{s1}*2	1.4	1.7	3.1
No. 4	3 - 4	O_{s1}	6.9	7.8	7.7
No. 5	7 - 8	O_{s2}	5.9	5.9	5.8
No. 6	5 - 7	O_{s3}	3.6	2.9	2.9
No. 7	4 - 5	O_{s1}	7.2	7.4	6.6
No. 8	~ 3	O_{s2}	5.0	4.7	5.7
No. 9	~ 3	O_{s2}	3.6	3.9	3.9
No. 10	~ 3	O_{s2}	3.7	6.0	5.3

*1 : Decreased by mixing with infiltrating water

*2 : Decreased by mixing with irrigation water and by escape of radon.

The lower levels of radon concentration in water in the No.3 borehole (Table 2-2), where the water table is within 2 m of the ground surface, indicates that the emanation effect and/or the steady mixing with the infiltrating water from the irrigation ditch, has a direct effect on the measurement. Below a borehole depth of 4-5 m, however, the radon content of groundwater seems to be less affected by these variables. As a whole, radon concentrations in water collected for boreholes, Nos. 1, 4 and 7, were higher than those in Nos. 2, 5 and 6 over the 6-month period. The groundwater in ten boreholes (Nos. 1-10) have been classified by the degree of the radon concentration, which corresponds to the geoliogic formation. As shown in Table 2-2, the radon concentrations analysed during March 1977 were 6.6 - 8.0 Bq L^{-1} in wells, No. 1, 4 and 7, in which the water table ordinarily was in the upper sandy layer, O_{s1}. The concentrations for wells, No. 5, 8 - 10, in which the water table was in the lower sandy layer, O_{s2}, were 3.6 - 6.0 Bq L^{-1}. These relationships suggest that the radon content in groundwaters below 4 - 5 m may depend mainly on the presence of strata which contain sources of ^{226}Ra rather than meteorological parameters.

Tap water at the KUR-RI site is supplied by a water purification station, where groundwater is pumped from depths greater than 100 m through two wells, Nos. D-1 and D-2, ca. 200 m apart from each other (Fig. 2-2). Samples of water from these wells were taken from branch pipe faucets installed as near as possible to the wells. Six samples for measurement of radon content were taken from the No. D-1 well during a 5-h period after a few hours of pumping on 9 December 1980. The average value was 13.6 Bq L^{-1} with a standard deviation of 0.31 Bq L^{-1}. Almost the same value (13.3 $\pm$0.36 Bq L^{-1}) was obtained for four samples taken on the next day. For No. D-2 well the results of measurement showed similar data, though they show more scattered values (13.3 $\pm$2.1 Bq L^{-1} for 9 samples taken on 15 December 1980 and 14.4 $\pm$1.1 Bq L^{-1} for 10 samples on 17 December 1980, respectively) when compared with those values for No. D-1 well. Thus, these values of radon content in water from the deep wells

are about twice as great as the average radon content of the shallow groundwater sampled from ca. 1 m below the water table at depths greater than at least 4 - 5 m.

The radon content in laboratory tap water samples supplied from the deep wells showed lower values, on the order of 1/7 to 1/5 of comparative values for samples from the previously discussed deep wells. This relationship is due primarily to the loss of radon during water purification such as percolation, and to decay during storage and/or distribution. Thus, the estimation of the depletion of radon content in the supplied tap-water may serve to evaluate the residence time of water in the plumbing systems.

2.2.4.3 Spatial distribution

After completion of boreholes, No. A-N, at the sites indicated in Fig. 2-2, the groundwater flow was investigated by both aquifer-testing and a tracer test. The results showed that the velocity of groundwater was about 0.5 m d^{-1}, which corresponds to the dip of strata in this site rather than to the slope of ground surface. The fluctuations of groundwater levels were also investigated, where measurements were made almost every week for eight months. In this investigation it was found that the groundwater levels followed by precipitation show the same extent of variation in all the boreholes. The flow direction of groundwater demonstrated by the tracer test was coincided with that expected by the decline of the hydraulic head of groundwater.

Radon concentrations were measured three times during January 1980 at eleven boreholes (see Table 2-3) under the same condition of pumping about 2 L of groundwater from each of the boreholes prior to sampling. The water levels in these boreholes were usually within 1 - 2 m below the ground surface. The variations of concentration were found to be significant among these boreholes in this limited area of less than 200 m^2. These concentration anomalies may or may not be due to the groundwater flow, though the variation of groundwater levels shows the same pattern after the precipitation events.

Local geologic differences and/or the small differences in the amount of groundwater pumped may affect the radon concentrations. Wells A, C, D, G and H, which are close to each other, were observed to have higher concentrations of radon more than 9.3 Bq L^{-1}, when compared with the other boreholes. Futher investigation is needed to obtain information about both the extent of concentration changes of radon and vertical distribution in the shallow groundwater in greater detail, which will be described in the following sections.

Table 2-3 Spatial distribution of radon-222 concentration in unconfined groundwater.

Borehole	8 Jan.	23 Jan.	31 Jan.	Ave.
A	8.1	10.2	10.0	9.4
C	10.9	9.6	10.6	10.4
D	9.8	11.7	11.1	10.9
E	6.3	6.3	7.0	6.5
F	7.4	6.1	8.5	7.3
G	7.8	9.3	9.4	8.8
H	9.6	9.3	9.1	9.3
I	6.9	8.3	6.5	7.6
J	8.0	7.8	7.0	7.6
M	6.9	9.1	6.5	7.5
N	6.9	6.9	6.1	6.6

(Unit in Bq L^{-1})

2.2.4.4 Vertical distribution

It has been supposed that the radon concentration in groundwater decreases near the water table due to diffusion of the gas from groundwater to unsaturated zone if the groundwater level is close to a ground surface, although the radon gas is supplied continuously from the soil particles. Accordingly the vertical distribution of radon concentration was investigated to test this assumption both in summer and in winter. For the water sampling, special precautions

were taken to avoid mixing of the stagnant water in the borehole. Figure 2-7(a) shows the results measured at well N in summer, which reveals the clear tendency of increase in radon concentrations with the depth of groundwater, and also suggests the radioactive decay of radon in the well casing, as all the concentrations of 26 August, for example, decrease with declining water level compared with those of 12 August. Radon concentration at the deepest position in summer was as much as three to five times that of near the water table, whereas it was only twice as high in winter as shown in Fig. 2-7(b). This difference is not surprising because in winter, the groundwater in the casing mixes more due to density differences than in summer when the groundwater stagnates owing to the stability of vertical density distribution. This tendency of inverse stability is verified by the temperature distribution as shown in Figs. 2-7(a) and (b).

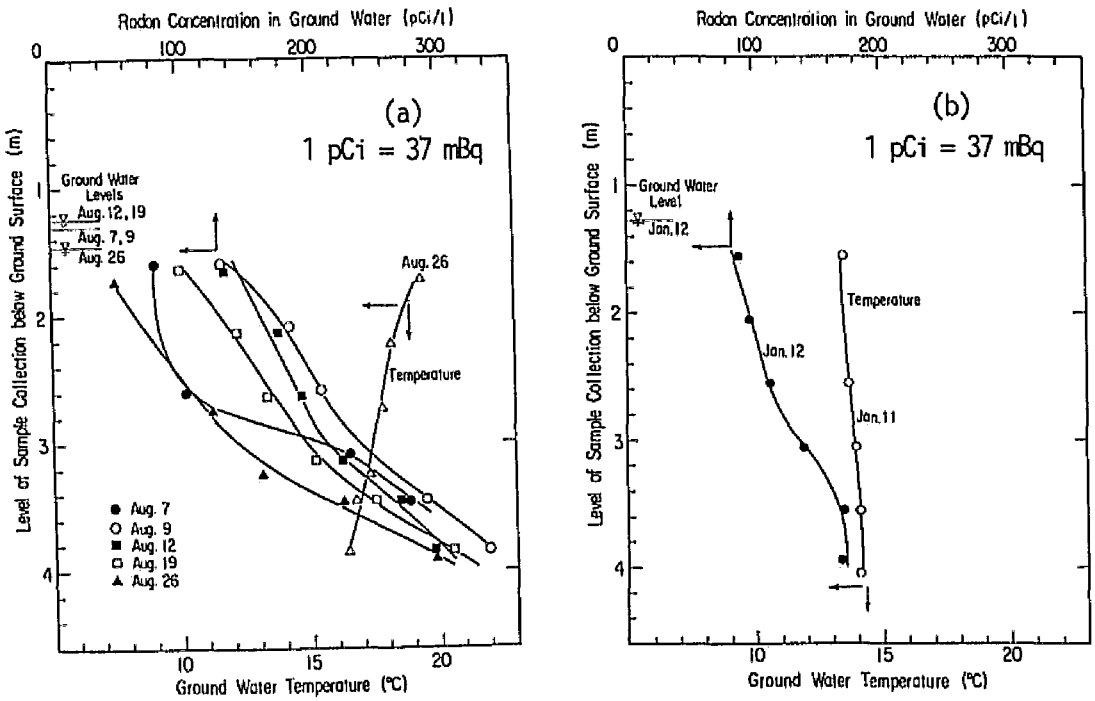

Fig. 2-7 Vertical distributions of radon concentration and groundwater temperature both in summer (a) and winter (b).

2.2.4.5 Effect of the extracted groundwater volume on radon concentration

In Figs. 2-8～2-10 the changes of radon concentration in groundwater, and the fall of groundwater level at well N and adjacent wells M and I, are shown in relation with the cumulative water volume extracted from the depths of 2, 3 and 4 m below the ground surface, respectively. The extraction of groundwater was continued for several days in December 1980 with a pumping rate of 0.2-0.8 L min^{-1}. These figures show the intensive increase of the radon concentration along S-shaped curves, and that the increase of the rate is most intensive between 10 and 100 L. Considering the water volume to be 7.8 L per 1 m of 10 cm diameter casing, the difference in sampling depth may influence the slope of the curves: as the sampling depth increases, the slope becomes gentler. This suggests that the attenuation of radon in the groundwater is due to exposure to air and/or radioactive decay in the borehole. Indeed, after pumping about 1 m^3 at all three depths, the concentrations all reach a maximum value of ca. 15 Bq L^{-1}, which coincides with that measured for deep groundwater pumped from 100 to 200 m depth in

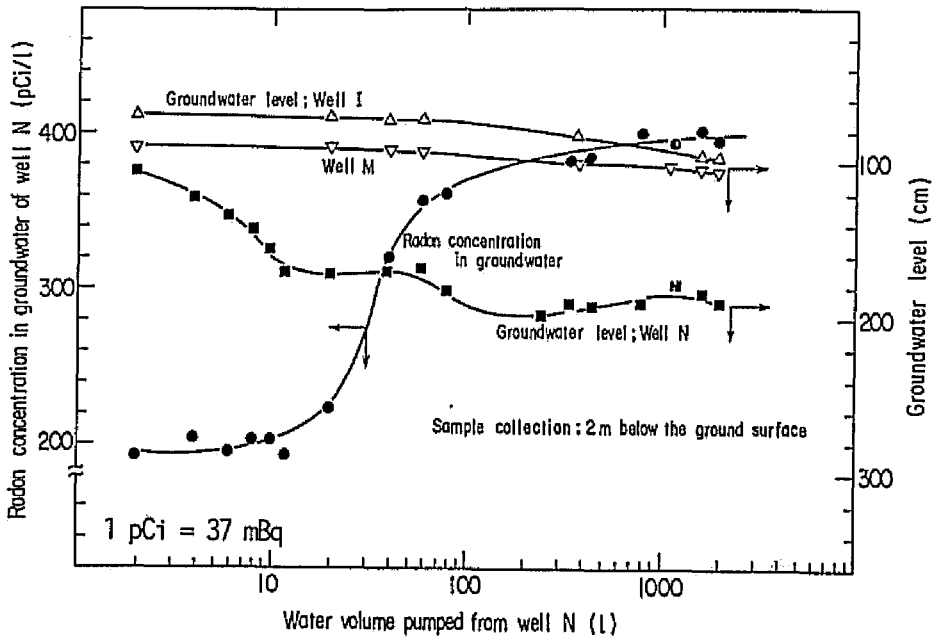

Fig. 2-8 Variation of radon concentration with pumping well N, from 2 m below the initial water table, 5-11 December 1980.

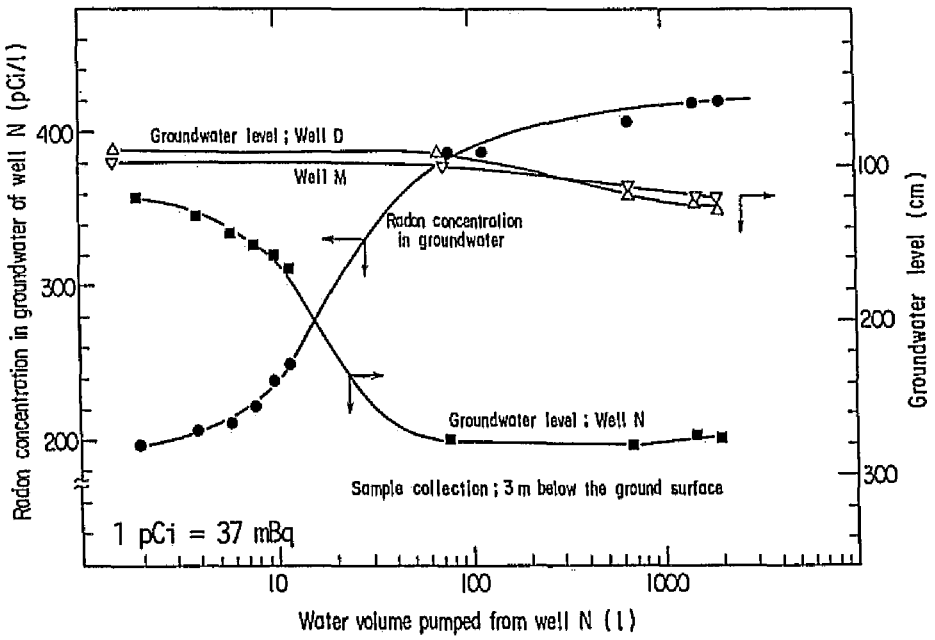

Fig. 2-9 Variation of radon concentration with pumping well N, from 3 m below the initial water table, 14-17 December 1980.

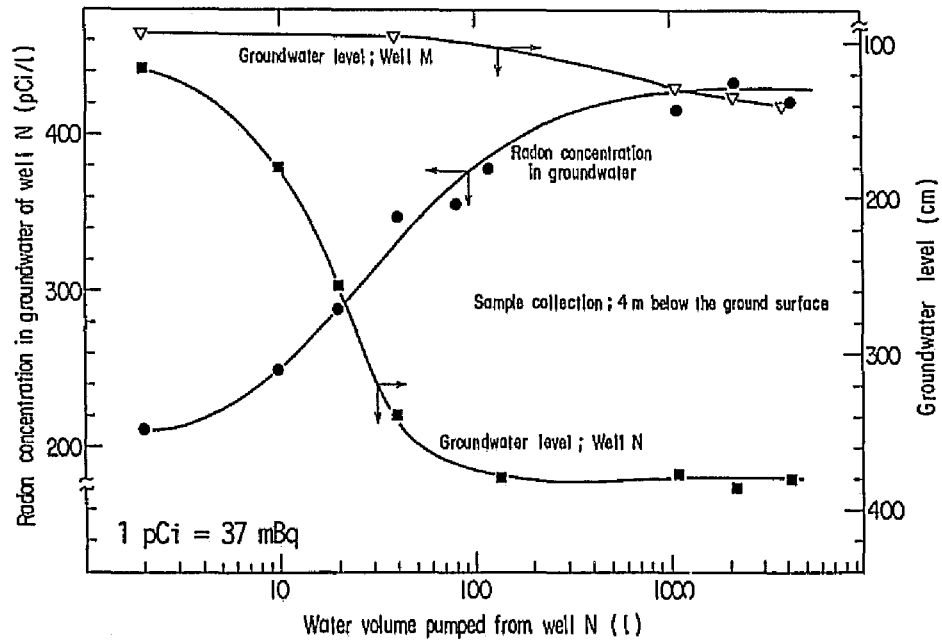

Fig. 2-10 Variation of radon concentration with pumping well N, from 4 m below the initial water table, 20-24 December 1980.

the same geologic sequence at the northeast side of KUR-RI (Fukui and Katsurayama 1983a). This indicates that to obtain samples for radon analysis representative of the unconfined groundwater, a water volume of more than 1 m^3 should be withdrawn before sampling. This volume may be different depending on the size of casing used and the type of screen.

2.2.5 Conclusions

The distribution and changes of radon concentration in unconfined groundwater were investigated, after preliminary investigation of concentration changes.

The findings in this section are as follows

(1) Spatial distribution of radon concentrations in groundwater, in the limited area of less than 200 m^2, showed rather large variation, ranging from about 6.3 to 11.1 Bq L^{-1}. This may be from differences in geology, as the boreholes which show the higher concentration of 9.3-11.1 Bq L^{-1}, are close to each other, and/or from small differences in volume of groundwater withdrawn during sampling.

(2) The radon concentration of groundwater shows a distinct increase with depth in groundwater, which is more apparent in summer when the water stagnates in wells' casings due to temperature and density stability, whereas cooler air temperatures in winter cause instability and mixing.

(3) The extraction of groundwater leads to approximately a two-fold increase of radon concentration compared with the initial value in the borehole. The rate of increase is steepest in the range of 10 - 100 L water extracted.

(4) A steady state concentration, ca. 15 Bq L^{-1}, is reached after the extraction of about 1 m^3 of water, which is comparable to the radon concentration measured in deep groundwater nearby, pumped from 100 to 200 m depth. Thus, it is necessary to pump more than 1 m^3 to obtain a representative concentration of a steady state in unconfined shallow groundwater depending on the local geology.

2. 3 VARIATIONS OF RADON CONCENTRATION IN UNCONFINED GROUNDWATER

2.3.1 Objective and Scope

An earlier investigation (Fukui 1985a) revealed that radon concentration of unconfined groundwater in cased boreholes varies due to radioisotopic decay and exhalation, and that more than 1 m^3 of groundwater should be drawn from a well so as to obtain representative radon concentration of water. Excessive withdrawal of groundwater, however, would mask the change of the radon concentration caused by precipitation. In this study, a method for continuous monitoring of radon in unconfined shallow groundwater is described which allows examination of the concentration change by meteorologic effects. This gives not only the boundary concentration for radon dynamics in the vadose zone, but also a better understanding of soil-water/groundwater hydrology. This method developed for radon would be adaptable for monitoring the ^{226}Ra in groundwater, which may migrate from mill tailings and/or from disposal sites for nuclear wastes.

2.3.2 Tracer Test for Groundwater

As the area of investigation is located on a lowland, the levels of groundwater in wells, A-N are usually within 2 m of land surface. The fine sandy stratum near the ground surface slopes to the NNW about seven degrees. The difference in groundwater level between wells, K and M 12 m apart (Fig. 2-2), has been observed as about 1.2 m. After boring, the groundwater in these wells was allowed to stabilize for about six months before field investigations. Prior to the survey of radon concentration in groundwater, a tracer test in a fine-sandy aquifer was carried out for obtaining knowledge of the groundwater hydrology, where the Br^- ion was selected as a tracer in the chemical form of $CaBr_2$ (1.8×10^{-2} mol L^{-1} as $CaBr_2$). The ion has a high sensitivity using

a neutron activation analysis. Moreover, it is supposed to behave in similar manner as the I^- ion which has been used as a tracer of groundwater because of the low affinity with soil, as it belongs to the halide group. The volume of the solution injected into a borehole was restricted as little as possible, so as not to disturb the natural groundwater flow. Aliquot of water sampled was dryed and irradiated for 10 min to measure the concentration quantitatively using the pneumatic tube equipment installed at the Research Reactor (KUR). The evolutions of Br^- concentration at well A, and observation well C, 2 m apart were obtained in terms of C_A/C_0 and C_C/C_0, where C_0 is the initial concentration at well A. The decrease of concentration at well A, was extensive during the first day of experiment, whereas the relative concentration (C_A/C_0) remained at about 10^{-2} for the successive 20 days, although the concentration, C_A/C_0 at injection well A, was usually higher than that (C_C/C_0) at the observation well C. This fact and the tailing out of tracer at well A, suggests minimal exchange of groundwater with aquifer, which would cause radioisotopic decay of radon in the casing, although Kimura et al. (1969) observed in laboratory experiments, that the water in a casing was exchanged smoothly with a sandy aquifer, provided that the ratio of annulus area is greater than 10% of the surface area of the casing. At observation well C, the threshold concentration of the Br^- ion was detected after about 1.5 days following injection and the peak concentration was observed in about 7 days. Supposing that the velocity of groundwater is represented depending on the transit time to the point of inflection in the tracer evolution curve, velocity was evaluated at about 0.5 m d^{-1}. The laboratory test using the soil sample at well B, gave a hydraulic conductivity of about 2.6×10^{-3} cm s^{-1}, and the velocity of interstitial water was estimated at about 0.6 m d^{-1}, which corresponds almost exactly to that obtained by the tracer test. Considering that the peak concentration of tracer injected into a well A, as a pulse, does not move easily to the downstream, i.e., less exchange of water volume in a casing, it is neccessary to

withdraw part of the water in the casing continuously. This results in being able to monitor the radon concentration without isotopic decay in unconfined groundwater corresponding to the history of precipitation and hence the mixing with infiltrating water. The following arguments are focused on testing the feasibility of monitoring radon concentration in groundwater continuously by measuring the radon gas being exhaled from the water.

2.3.3 Continuous Monitoring of Radon Concentration in Groundwater

2.3.3.1 Preliminary investigation of radon concentration in groundwater

Measurement of the radon concentration was performed daily at well M, from 14 September to 20 November 1980 to investigate daily changes due to precipitation and changes in groundwater level. As withdrawing more than 1 m^3 will mask the meteorological effect on the radon concentration, only a minimum volume of groundwater, 300 mL which is necessary for sample collection was pumped prior to each sampling at a standard depth of 30 cm below the water table. As clearly shown in Fig. 2-11, radon concentration decreased on 9 October and 3 November owing to the dilution effect of heavy rainfall with groundwater level rises greater than about 50 cm, whereas the radon content increased on 21 September and 30 October following light rainfall. The phenomenon of increase in radon concentration may be less reasonable than that of decrease following rainfall, because the radon concentration in rain water is generally two orders in magnitude lower than that in groundwater. It is inferred that the groundwater with radon concentration lowered due to radioactive decay and/or the exhalation in the casing, partially exchanges with fresh groundwater enriched with radon being directly in contact with soil. Thus, the radon concentration increased, when the groundwater level rose less than about 50 cm following light rainfall. In this area, the change of groundwater level is commonly greater than can be accounted for by local precipitation, because the area is lowland

and collects runoff water. After a decrease in concentration level caused by the dilution effect of heavy rainfall, the radon content seems to return to its former level gradually as shown in Fig. 2-11 (9-15 October). However, the relation between radon concentrations in groundwater in a borehole and the dilution effect by infiltrating water had not been clearly shown by the intermittent measuring method for the groundwater. Continuous observation of radon in unconfined groundwater will give more detailed information about the effect of meteorological parameters on the concentration.

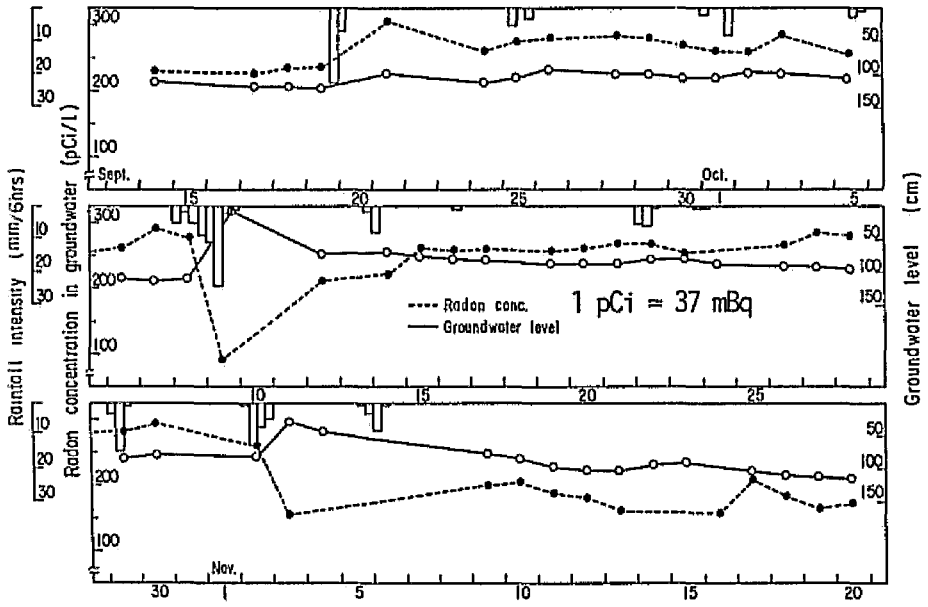

Fig. 2-11 Daily change of radon concentration in shallow groundwater at well M, 15 September-20 November 1980.

2.3.3.2 Set-up for continuous monitoring

A ZnS(Ag) scintillation counter was used as an instrument for the continuous measurement of radon gas, exhaled from confined groundwater for earthquake predictions (Noguchi and Wakita 1977), and an ionization chamber with vibrating-reed electrometer was used for the monitoring of radon gas in a vadose zone for the same purpose (Nishimura 1979).

As indicated in a previous section, excessive withdrawal of unconfined groundwater close to a ground surface masks the change of radon concentration in a casing caused by meteorologic effects such as precipitation, although it gives a representative concentration of radon associated with soil. Thus, it is necessary to monitor the actual concentration in unconfined groundwater with depressed radon gas by sampling groundwater continuously near the water table. For this purpose, a spray nozzle as shown in Fig. 2-12, was installed in the PVC casing of well H. Groundwater was pumped and sprayed to force the exhalation of radon gas for the monitoring. Part of the water pumped was discharged initially, and later was injected into well J or F (see Fig. 2-2), to maintain the natural level of groundwater. In this investigation, an ionization chamber of effective volume (1.5 L), was used for the measurement, after ascertaining that the radioactive gas exhaled from the sprayed water was radon-222, by determining the half-life of the gas suctioned in the chamber. The groundwater-level recorder was installed in well B, about 3 m apart from the precipitation gauge.

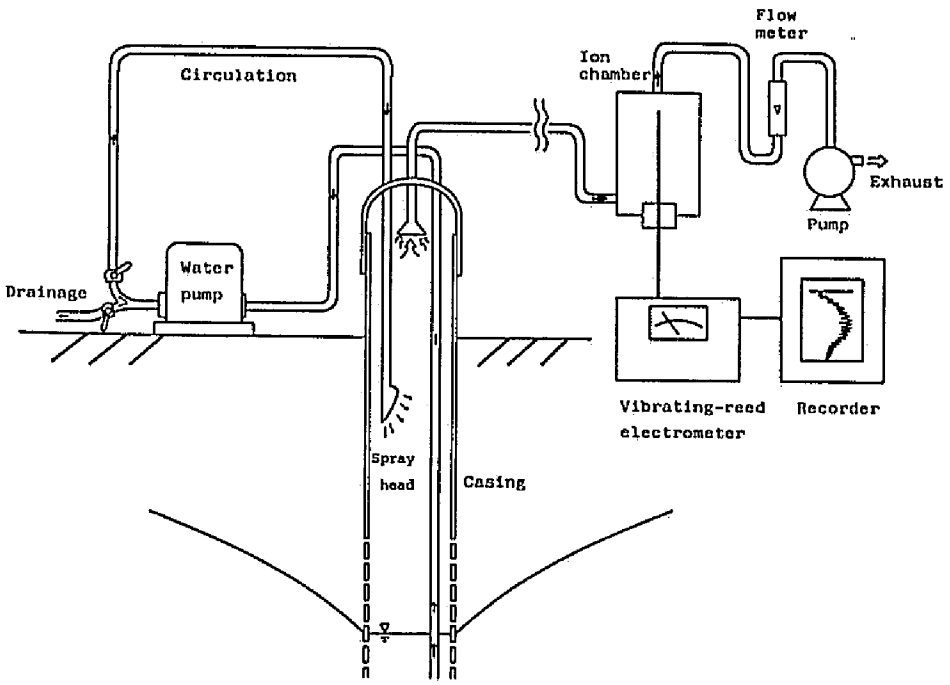

Fig. 2-12 Instruments for measurement of radon and continuous monitoring system.

2.3.4 Results and Discussion

The concentrations observed using the ionization chamber were low when all the water pumped was circulated (2.3 L min^{-1}) in the borehole to maintain the natural groundwater level, and was sprayed in the same casing, so that little fresh groundwater in contact with soil flowed into the casing. Figure 2-13 shows the response of radon concentration in the casing for different groundwater volumes extracted, up to 40 L from the circulation system at well H, where the flow rate of gas into the chamber was set at about 100 mL min^{-1}. Curves, C and D, in this figure show that the pumping rate does not affect the peak concentration if the total volume of groundwater extracted remains the same, although the peak is reached sooner at higher pumping rates. The peak concentrations, however, increase with increase of the water volume extracted. This suggests that for monitoring, it is necessary to pump and discharge continuously a certain quantity of unconfined groundwater so as to attain a concentration equilibrium not affected by fluctuaion of water level.

The transit time of air from well H, to the ionization chamber was measured to examine the concentration response between them. In this investigations, out of 2.3 L min^{-1} pumped, 1.0 L min^{-1} of groundwater was circulated and sprayed, thus about 1.3 L min^{-1} of water was drained from the faucet at well H, and discharged into well J, to maintain the natural groundwater level. Figure 2-14 shows the concentration responses of radon gas exhaled from the water sprayed in the casing at several air-flow rates into the 1.5 L chamber. This figure indicates that it takes more than 5 h to detect the change of the concentration in air corresponding to that of unconfined groundwater, if the flow rate of gas into the chamber is less 50 mL min^{-1}. The flow rate of about 100 mL min^{-1} seems to be adequate for monitoring, as it takes about 3 h to establish secular equilibrium between Rn-222 and its short-lived progenies.

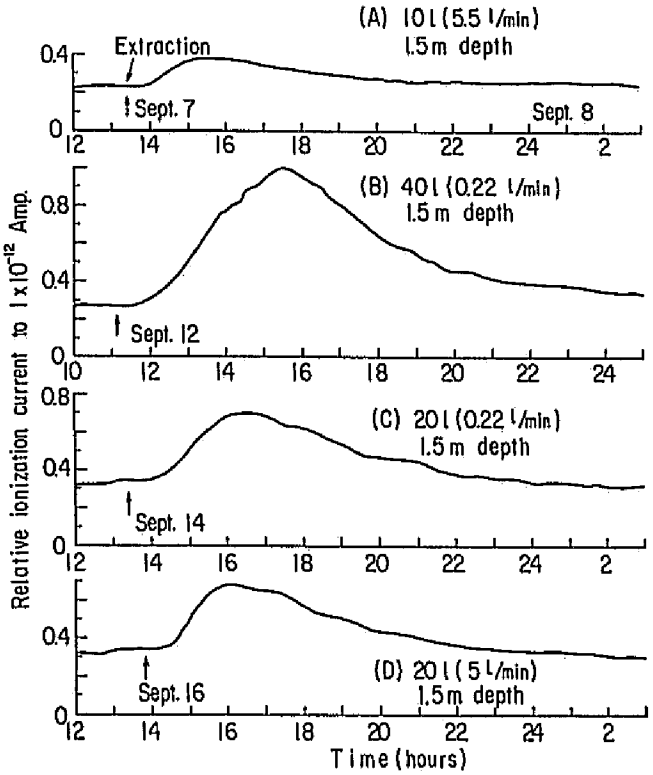

Fig. 2-13 Responses of radon concentration exhaled from groundwater under different conditions of the extracted water volume and the flow rate.

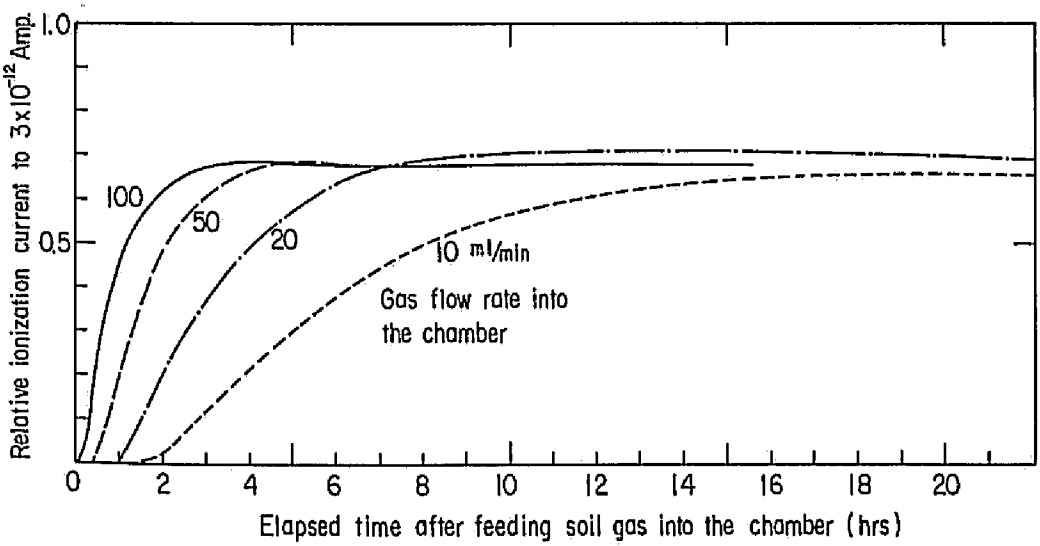

Fig. 2-14 Breakthrough curves of radon gas inhaled into ionization chamber from borehole casing H.

For higher flow rates of exhaled gas (more than 100 mL min^{-1}) the concentration shows a slight tendency of decrease due to the exhaust from the casing via the ionization chamber. Hence, circulation system of the exhaust air into the same casing is recommended for the continuous monitoring.

Prior to monitoring, the relation between the concentration of radon gas and the volume of groundwater sprayed in the casing should be analysed to examine the error caused by the change of flow rate of groundwater being circulated. In Fig. 2-15, the concentration of gas based on ionization current is shown both for slow rates of drained and sprayed (circulated) systems, with the concentrations in groundwater circulated. The corresponding concentrations of radon in water in the borehole were simultaneously measured by the toluene extraction-liquid scintillation method mentioned previously.

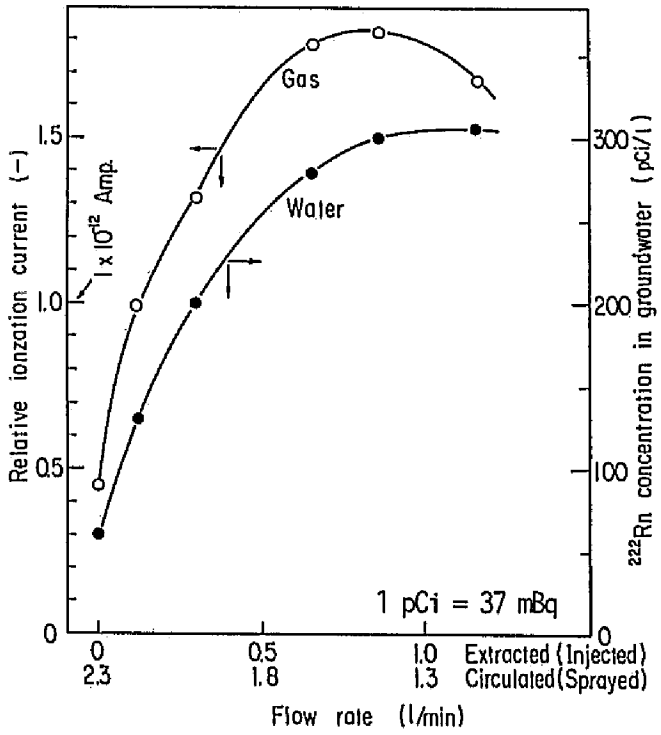

Fig. 2-15 Change of radon concentrations depending water discharge rates in air inhaled and in groundwater as measured by liquid scintillation method.

It was found that the concentrations in exhaled gas in the casing increase with increase of discharge rate of groundwater up to about 0.7 L min^{-1} due to the inflow of fresh groundwater into well H. Above this discharge rate, the flow rate of groundwater circulated and sprayed from the nozzle drops. This resulted in reducing the quantity of exhaled radon gas and decreasing the radon concentration in air in the casing, despite actual increase in concentration in the circulated water, as confirmed by the liquid-scintillation method. Thus, the monitoring system described above can be useful for discharge rates less than about 0.7 L min^{-1}, where the concentration of radon gas corresponds to that of ground water, provided that the flow rates of pumping, circulation, and discharge are kept constant.

Radon concentrations in air in well H, monitored continuously by this method, are shown in Fig. 2-16, together with records of precipitation and the groundwater level. For the phenomena of precipitation, the tendency toward reduced radon concentration due to the dilution effect of groundwater by infiltrating water is well monitored and corresponds to rise of the groundwater levels. On 1 and 5 October 1981, the radon concentration did not change with the light rainfall, because the groundwater levels were at summer low levels and most of the infiltration was retained in the soil in the aerated zone. For the light rainfall shown on 21 and 23 June, the concentrations returned to their initial levels quickly, whereas, for the heavy rainfall, as on 5 July, the decreased concentration continued for a few days and seems to have returned to the former level within a week. In October, the radon concentration was higher compared with that monitored in June and July when the groundwater levels were close to the ground surface. Considering that the radon concentration in groundwater typically is greater as the water level declines (Fukui 1985a), this result indicates that the monitoring method developed here is highly effective for measuring the radon concentration in unconfined groundwater.

As shown in Fig. 2-17, the concentrations in radon exhaled from the groundwater well coincide with those in the grounwater itself.

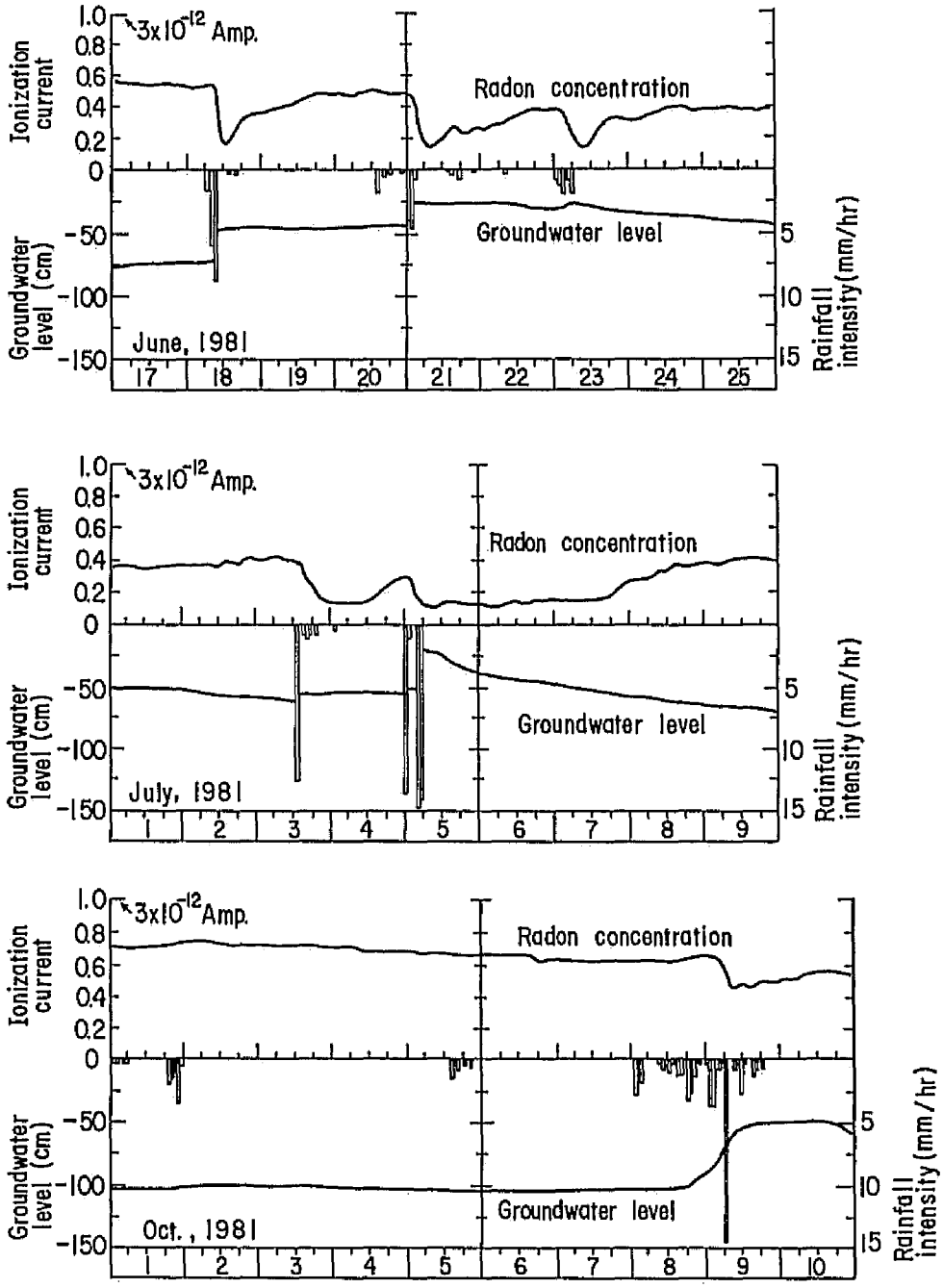

Fig. 2-16 Radon concentrations monitored continuously during June, July, and October 1981.

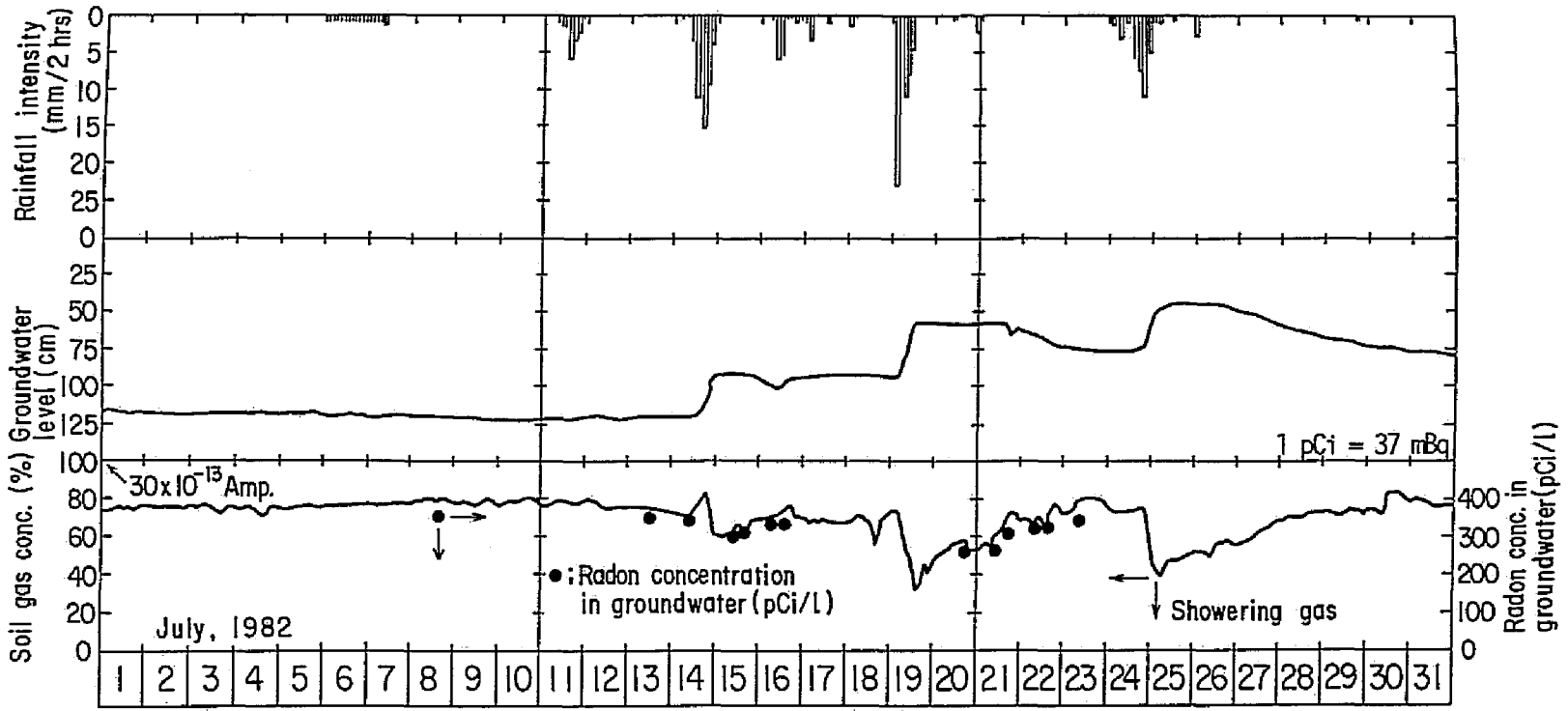

Fig. 2-17 Daily change of radon concentration in groundwater measured by ionization chamber and liquid scintillation counter at well N, July 1982.

2.3.5 Conclusions

The feasibility of continuously monitoring radon concentration in unconfined groundwater was investigated by measuring the radon gas exhaled from sprayed groundwater in a well casing. Using the tracer (Br^-), for which concentrations were measured by the activation analysis, it was found that part of the unconfined groundwater in well casings stagnates, although the tracer front moved at a velocity of about 50 cm d^{-1}. A monitoring system of radon concentration in groundwater was designed involving pumping shallow groundwater, in which part of the water pumped was recirculated in the same borehole by spraying, and the other part was drained, followed by injection into another borehole to attain the concentration equilibrium in the semi-closed subsurface hydrosystem. This led to maintain the natural level of the unconfined groundwater in the borehole. In this system, the radon concentration in unconfined groundwater is well monitored by measuring the radon gas exhaled from the sprayed water. The effects on gas concentration were investigated for the following factors:

(1) water volume pumped and drained under the fully circulating system;

(2) the transit time of radioactive gas from the borehole to the ionization chamber;

(3) the ratio of discharge to that recirculated under the partially discharging system, and so on. The radon gas concentration in unconfined groundwater was followed closely by monitoring the radioactive gas exhaled in the casing, provided that the water flow rates such as amounts pumped, circulated and discharged are kept constant and the circulation rate of groundwater in the same casing is greater than about two-thirds of that pumped (2.3 L min^{-1}).

(4) the radon concentration in unconfined groundwater diluted by infiltrating water from precipitation recovers to its former level within ca. 1 wk depending on the rainfall intensity, the duration, the amount of precipitation and the groundwater level.

2. 4 DISTRIBUTIONS AND VARIATIONS OF RADON IN SOIL GAS

2.4.1 Objective and Scope

There has been increased concern about exposures associated with the natural radiation environment, especially from radon and its short-lived progeny (UNSCEAR 1982) which are major radiation sources in soil gas. Continuous monitoring of radon has been undertaken in many research fields as mentioned in section 2.1. It has been important to recognize the vertical motion of radon in the ground not only as the main source of radiation exposure, but also in the assessment of subterranean waste disposal in which flow could be critical.

In humid areas with a high groundwater table, an effect of precipitation on the radon concentration in soil gas is probable. In previous sections, vertical profiles and variations of radon content in unconfined groundwater were measured, and the depression of radon content near the water table and a dilution effect in groundwater due to infiltrating water following precipitation were observed.

The concentration profiles of radon in a vadose zone near the surface above the water table are measured in the field by using the toluene trap-liquid scintillation counting technique, bubbling soil gas, developed in this study. The rate of exhalation of radon gas from the earth into atmosphere could be evaluated by this vertical profiles.

The concentrations of radon in soil gas below the ground surface are also monitored continuously using an ionization chamber to have a better understanding about the vertical motion of radon. These results will be used to estimate the radon exhalation which would be affected by meteorological parameters.

2.4.2 Experiments

2.4.2.1 Site

The location of the radon surveys in soil gas is the same area as that of the groundwater in the KUR site. This area was chosen as being rather uniform stratigraphically within the strata of a few meters depth, which dip by ca. 7 degree to the north/northwest. The surface slopes downward from both the west and southeast to the immediate survey area, then the low drainage line runs to the northeast from the southwest edge of a 5-m escarpment. As the area of investigation is located on lowland, the levels of ground-water are usually within 2 m of the land surface and the slope of the water table was about one-tenth to the north. The radon concentrations in groundwater, which were lessened by the infiltrating water, recover to the level within 1 wk. The arrangement of experimental devices is indicated in Fig. 2-18.

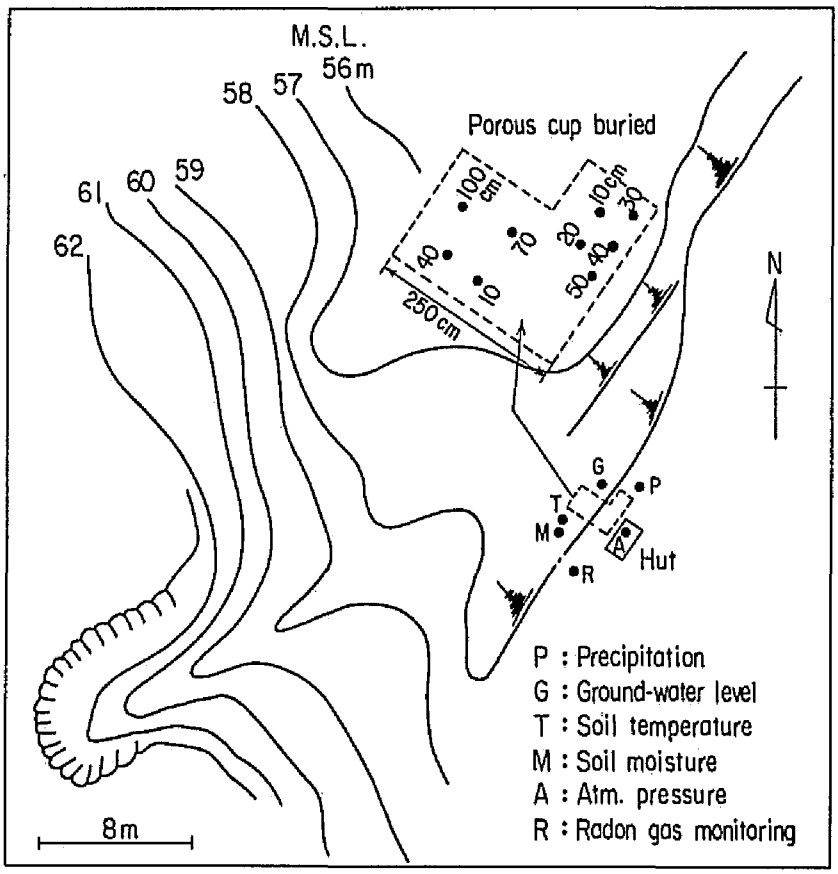

Fig. 2-18 Topographical map of investigation area and arrangement of experimental devices.

2.4.2.2 Sampling method

Sampling of soil gas in a vadose zone has been performed using perforated stainless steel cups (10 cm in length and 10 cm in diameter; Fig. 2-19(a)) buried in auger holes to examine the vertical profiles, and from a PVC rectangular box (50x50 cm^2 and 33 cm in height; Fig. 2-19(b)) with many holes drilled in the walls to investigate the change of radon concentration with time in soil gas. All cups were a minimum of 10 cm deep, the deepest being 100 cm. Double annulus pipes were connected to the top of each sampling cup as shown in Fig. 2-19(a). The inner one, for exhaust, is inserted into the center of the cup, and it projects about 10 cm above the ground and branches off. The soil gas in the buried vessels (both the cup and box) and a tray (Fig. 2-19(d)) was circulated by a pump through a flow meter so as to sample the ambient air at a specific depth in the ground, which was referred to elsewhere (Blue et al. 1989). Especially in a buried cup, this circulation system for measuring the radon concentrations with a small flow rate such as 100 mL min^{-1} has less disturbance of the radon profile due to a small change of suction pressure, since soil gas is not withdrawn.

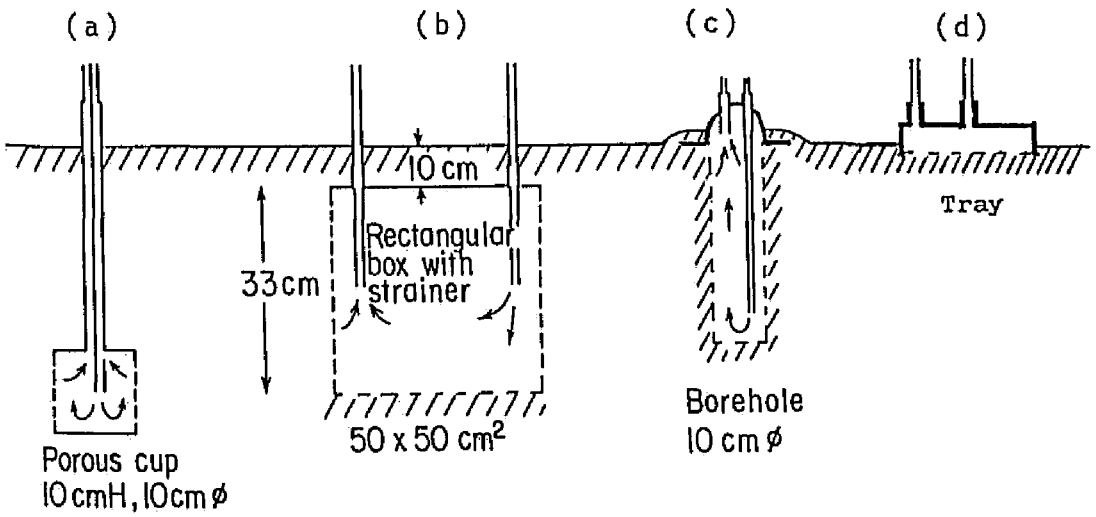

Fig. 2-19 Diagram of sampling vessels buried in ground, boreholes drilled and a tray for radon measurement.

2.4.2.3 Measurement of radon concentration

A toluene extraction-liquid scintillation method, which was developed for measurement of radon concentration in water was adapted to radon gas trapping and measurement (Fukui 1983b). As shown in Fig. 2-20, soil gas inhaled from buried sampling cups was introduced into a pyrostat where two or more vials are arranged in a series to trap radon gas at a constant temperature, usually 20 ℃. Fifteen milliliters of toluene in individual vials which contain a scintillator (liquid scintillation fluid, PPO and POPOP) was measured for 40 min, using a liquid scintillation counter, at least 5 h after the trap procedure. The background was always less than 45 counts min^{-1} and the lower limit of detection, at a 95% confidence level via this method, was about 0.04 Bq L^{-1} in air. The trap conditions required to attain equilibrium concentration of radon between toluene and soil gas will be described in a later section.

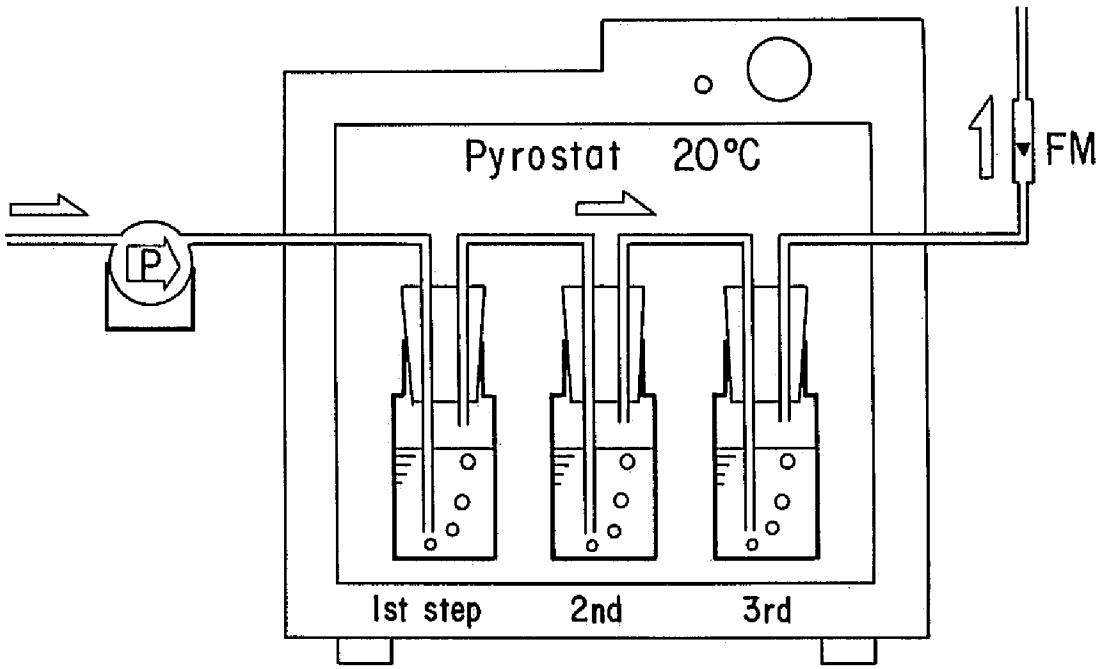

Fig. 2-20 Set-up for trapping radon gas in 15 mL of toluene. FM : Flow meter

An ionization chamber with an effective volume of 1.5 L was also used to measure the radon gas continuously in the ground. The details of this instrument were described previously. Both repeated countings of the scintillation vials, which contain radon trapped by toluene, and readings by the ionization chamber, where the soil gas inhaled was allowed to decay in the closed circuit of the chamber, indicated that the decay curves coincide with that of radon-222. The radon concentration in the soil gas trapped in toluene was evaluated by using the following equation.

$$C_{air} = C_t/D_t \qquad (2\text{-}3)$$

where

C_{air} and C_t : radon concentration in soil air and in toluene, and

D_t : distribution coefficient of radon in air to toluene which is expressed by the following empirical formula (Wakita et al. 1976).

$$D_t = 18.2\exp(-T/46.5) \qquad (2\text{-}4)$$

where

T : ambient temperature (℃).

The concentration of radioactivity in the counting vial (C_t) is expressed in eqn (2-2).

2.4.2.4 Measurement of meteorological parameters

At the investigation area, the following parameters were observed simultaneously with radon concentration.

(1) Precipitation.

Rain water was collected in a graduated cylinder (20 cm) and was recorded with every 0.5 mm of precipitation accumulated.

(2) Groundwater level.

A water table was recorded using a float in a casing (10 cm) fitted into an augered borehole B.

(3) Soil moisture and soil temperature.

These probes were buried at 10 cm below the ground surface.

(4) Atmospheric pressure.

This device was installed in the hut near the site where the ionization chamber and the instruments described above were

situated.

The arrangement of these instruments is shown in Fig. 2-18.

2.4.3 Results and Discussion

2.4.3.1 Trap condition for the attainment of radon equilibrium

To confirm the establishment of radon equilibrium between trapped soil gas and toluene, air, enhanced with radon released from the groundwater by spraying in a casing as described in previous section (2.3), was introduced into three vials as shown in Fig. 2-20. The gas flow-rate was set at 20 mL min^{-1} because for a flow rate greater than 50 mL min^{-1}, a part of the toluene was transferred into the downstream vials by bubbling air.

Figure 2-21 shows the radon concentrations in bubbling gas, which were converted from the concentrations trapped for 5, 10, 20, 30, 60 and 90 min in toluene, respectively. The figure also indicates that for more than 60 min, more than 1200 mL of air volume should be bubbled into the 15 mL of toluene to achieve

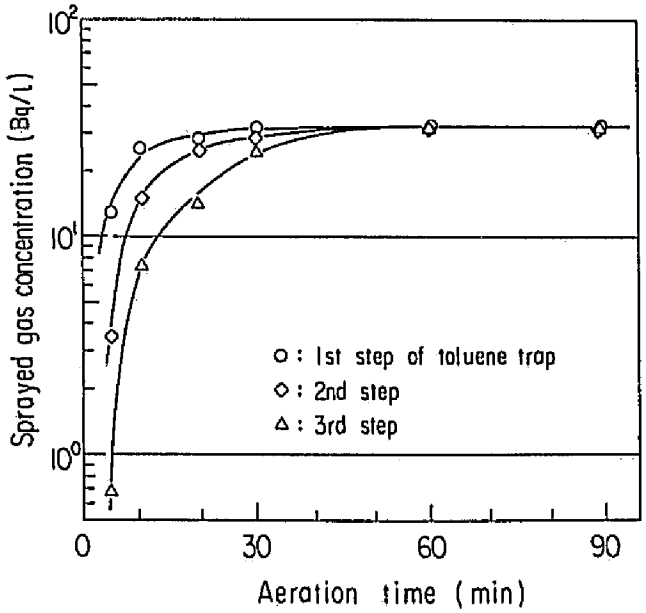

Fig. 2-21 Achieving radon equilibrium between toluene in three vials and bubbled gas, which was inhaled from the groundwater sprayed in casing in borehole.

equilibrium, where each concentration in the three vials arranged in a series shows the same value. Because this method for measuring radon in soil gas is convenient and economical, it might be adaptable even for spatial surveys of ground, such as in a mountainous terrain.

In Fig. 2-22, concentrations (Bq L^{-1}) measured by the toluene trap method described above, are compared with ionization current (ampere: A) measured by the ionization chamber, where soil gas from an augered borehole (Fig. 2-19(c)) was circulated through the chamber, and part of the gas was by-passed into the pyrostat with a certain flow rate. In this experiment, bubbling time was fixed at 60 min and the flow rate was controlled to be 10, 20, 30 and 40 mL min^{-1}, respectively. The calibrated value obtained by the ratio of these data measured by different methods was 1.6×10^{1} Bq L^{-1} pA^{-1} except for the flow rate of 10 mL min^{-1} for which equilibrium was not attained when less than 1200 mL of soil gas was bubbled into the 15 mL of toluene. These results indicate that the toluene trap method developed in this study may have broad and practical utility.

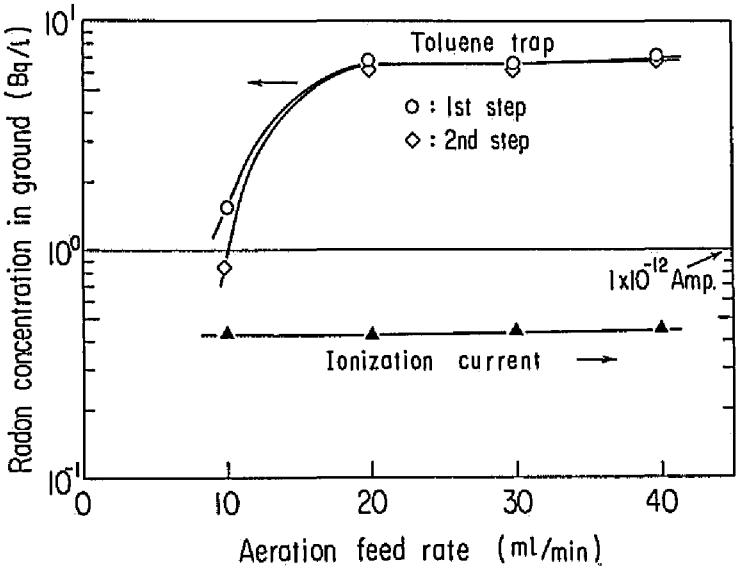

Fig. 2-22 Comparison of radon concentrations measured by the toluene trap method with those using ionization chamber. Air volume bubbled into a 15 mL-toluene: 1.2 L.

2.4.3.2 Vertical profiles of radon content in ground

Sampling cups (Fig. 2-19(a)) buried at depths of 10, 40, 70 and 100 cm in individual boreholes were allowed to settle for about 2 months to tighten the backfill.

Figure 2-23 shows the variations of radon concentrations as a function of time, where soil gas was inhaled continuously by an once-through system at depths of 10 and 40 cm, respectively, and bubbled in 15 mL of toluene for every 5 min with a flow rate of 20 mL min^{-1}. The breakthrough curve of radon at a 10-cm depth, which has a peak in the measured concentration, suggests the possibility of inhalation from air above the ground even for the small flow rate, though equilibrium was not attained in these samples due to the short time of aeration, 5 min. This also indicates that another technique for sampling of soil gas should be used instead of an once-through inhalation system. Then, a circulation system, in which exhaust from the vial was introduced into each buried sampling cup, was used to measure radon concentrations under a steady state condition in the following experiment.

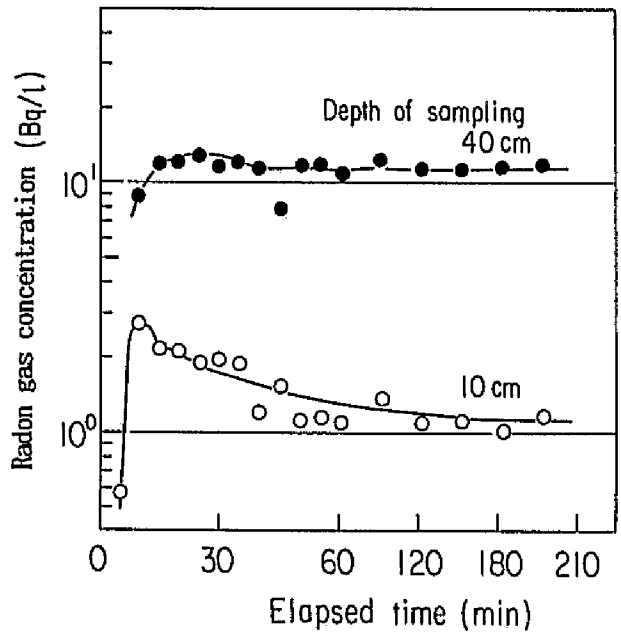

Fig. 2-23 Variations of radon concentration with time in soil gas. Aeration feed volume into toluene: 100 mL.

The changes of radon gas concentrations in the ground measured continuously using the ionization chamber in the circulation system, are shown in Fig. 2-24, where the initial effective volume of 1.5 L of air in the chamber was replaced with that above the ground except for the case of a 70-cm depth. For this case, a sampling hose connected to the mandrel of the cup buried at a 40-cm depth was changed to that of the 70-cm cup without ventilation. Figure 2-24 indicates that radon concentrations are at a steady state after about 15 h of gas circulation (40 cm), provided that the chamber was degassed previously. Whereas the reading approaches more quickly a different steady state within 5 h (70 cm) for a small buried cup, if the soil gas introduced into the chamber was not ventilated by fresh air.

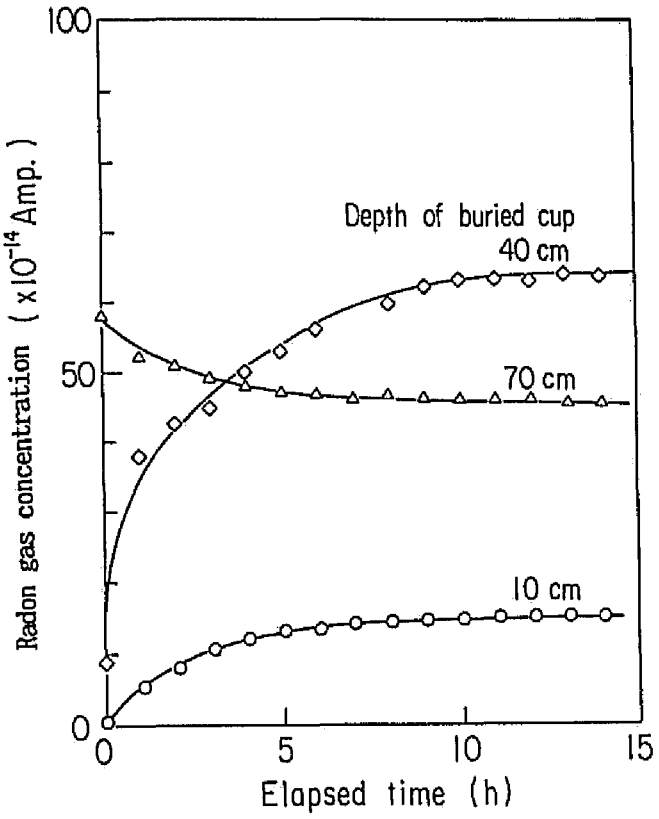

Fig. 2-24 Change of radon concentrations in ground measured at 10, 40 and 70 cm using an ionization chamber.

Figure 2-25 shows the radon concentration profiles in the ground measured by the toluene trap method according to the experimental conditions described previously, such as aeration period, gas feed rate and so on. All of these profiles show the maximum concentrations near a 40-cm depth, and this tendency for concentration decreases near the ground surface and the groundwater table could not be explained by the simple one-dimensional diffusion theory previously proposed (Fleischer et al. 1979). The groundwater level on 13 May was 105 cm, which is just below the sampling position of radon at a depth of 100 cm. On 2 and 10 December, it was about 125 cm. It is possible that the greater the soil-moisture content is, the less the radon content of the soil gas due to the decay process during diffusion in soil water region (Fleischer 1983). In addition, a decreased radon exhalation was shown for greater rainfall (Megumi 1973). The appearance of a peak in the concentration profiles may stem from both reductions near the surface caused by exhalation and from the decay process

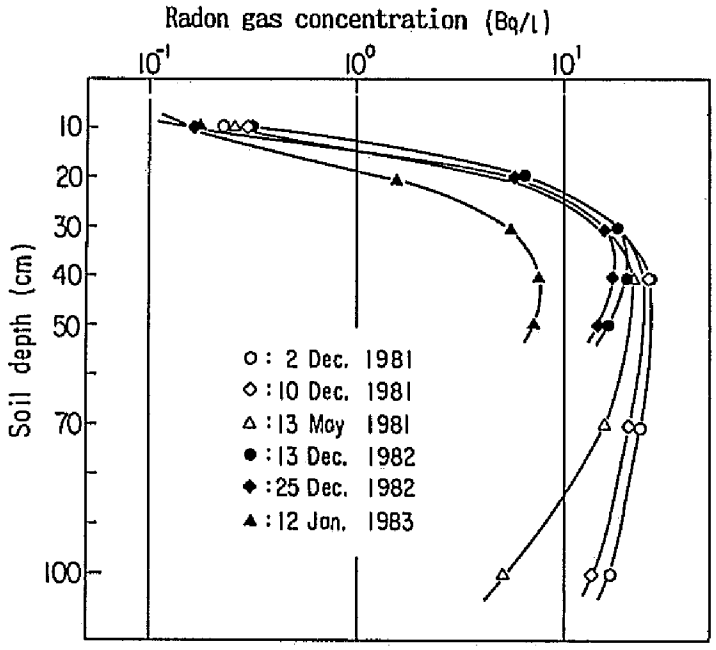

Fig. 2-25 Radon concentration profiles with depth measured using toluene trap method.

during the travel of radon from the soil particle surface. The diffusion layer of radon in pore water includes inter-granule layer. These resions usually absorb much water due to the capillary force near the groundwater table. On the other hand, the concentration peak was not observed when the soil gas was trapped from the augered borehole of various depths (10-100 cm) as shown in Fig. 2-19(c), and lower concentrations along soil depths were obtained in comparison with those measured for the buried cup. This is not suprising because the difference is clearly caused by mixing air through the hole, instead of using the cups buried in soil (Fig. 2-19(a)). These experimental results also indicated that the buried cup is preferable to monitor the radon concentration in soil gas at a specified depth. The concentration mixed in an augered borehole through 1 m was about 70% of that measured for a cup buried at 1 m.

Readings by ionization chamber of the radon content, which are higher at 40 cm than at 70 cm deep as shown in Fig. 2-24, may confirm this inverse relation. These findings may be predicted by the theoretical treatment that the radioactive decay effect becomes more significant above the groundwater table than in the region of less soil moisture, since it takes more traveling time for radon to diffuse toward lateral direction as indicated by the two site-model (Fukui 1976a, Neretnieks 1980). In the investigation area, five boreholes were drilled to examine the depth profiles in greater detail. Porous cups of equal size as shown in Fig. 2-19(a) were buried at a depth of every 10 cm, increasing in the individual boreholes from the surface to a 50-cm depth. As shown in Fig. 2-25 (closed circles), the maximum concentrations in these profiles also appeared near the 40-cm depth in spite of the fact that the concentration of profile recorded on 12 January was reduced due to precipitation and the groundwater level was only 95 cm. These profiles suggest considerable influence of groundwater level and soil moisture content, though there have been few reports on these meteorological parameters which may affect the fluctuation of radon content in soil gas.

Though it was found that the vertical profiles have a peak concentration due to the effect of soil moisture content, rough estimation for the surface flux density could be possible assuming semi-infinite and homogeneous soil with pure diffusion as follows (Schery et al. 1984) :

$$J_0 = C_m(\varepsilon \lambda D)^{1/2} \quad (2\text{-}5)$$

where

J_0 : surface flux density (unit m^{-2} s^{-1}),

C_m : concentration of ^{222}Rn in soil pore at the infinite depth and is equal to ϕ / λ (unit m^{-3}),

λ : radon decay constant (s^{-1}),

ϕ : source terms (unit m^{-3} s^{-1}),

ε : porosity (-), and

D : effective diffusion coefficient (m^2 s^{-1}).

Setting these constants 0.35 for ε, 2.1×10^{-6} s^{-1} for λ, 1.0×10^{-6} m^2 s^{-1} for D (Nielson et al. 1984; Rogers et al. 1991) and 8-30 kBq m^{-3} for C_m (see maximum concentration in Fig. 2-25), the flux density was estimated to be in the range of 6.9 to 2.6×10^1 mBq m^{-2} s^{-1}, which show good agreement with a figure of 1.7×10^1 mBq m^{-2} s^{-1} for continental soils given elsewhere (NCRP No. 97 1988).

2.4.3.3 Fluctuations of radon content in soil gas

The difficulty of continuous monitoring of radon concentration in the soil arises because of the withdrawal of the infiltrating water following precipitation into the ionization chamber. To avoid this trouble, soil gas was circulated for continuous monitoring. The feed rate of soil gas was set at 200 mL min^{-1}. This method moderates the possibility of withdrawing soil water into ionization chamber following precipitation, which may happen in an once-through inhalation system. Figure 2-26 shows the radon concentration in soil air near the ground and five meteorological parameters: precipitation, atmospheric pressure, and the soil temperature at a 10-cm depth during an one-month period. In Fig. 2-26 soil gas below ground surface ((a) and (c)) was taken from a buried box as shown in Fig. 2-19(b) and that close to the ground surface

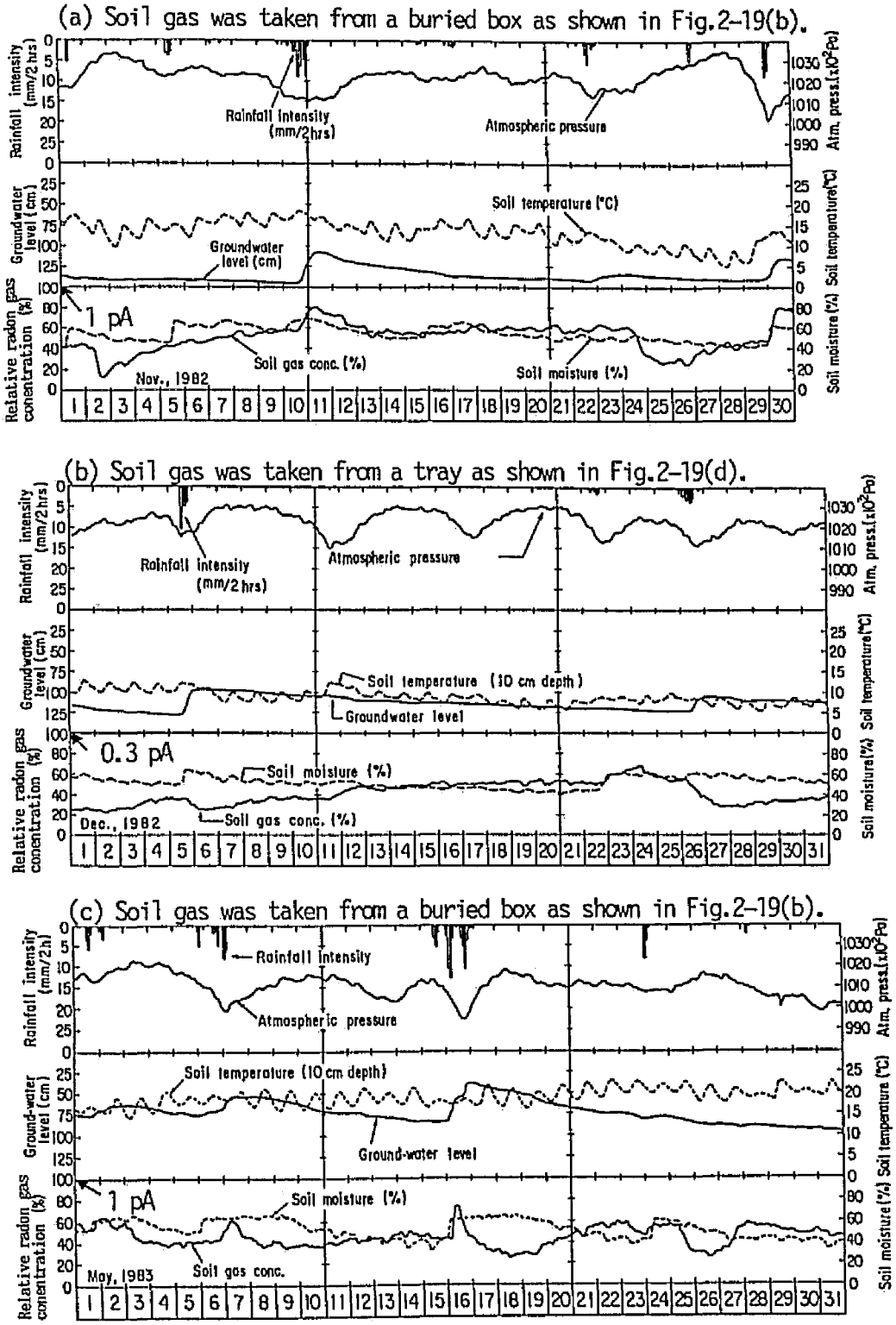

Fig. 2-26 Variation of radon concentration near surface of ground with five meteorological parameters.

was inhaled from a tray as shown in Fig. 2-19(d).
There is close correlation among these meteorological parameters, except for soil temperature, with either high or low radon readings. An explanation for the intermittent radon increase in soil gas in buried vessels would be the up flow of gas caused by raising the water table as indicated on 11 Nov., 30 Nov., 2 May, 7 May and 16 May.

On 2 Nov., 25-26 Nov., and 25-26 May, the radon concentration in soil gas in buried vessels was decreased by mixing with air from above-ground due to high atmospheric pressure. However, for other durations showing the decreases in radon concentration, the effect of atmospheric pressure (alternate intakes and emission of gas by the earth) is not so clear due to the variations superimposed by the change of water table and soil wetness. The change in concentrations is probably caused by the disequilibrium due to dilution by infiltrating water and by emanating power decreased due to covering the surface of soil particles with water. This effect of soil moisture is evident especially, on the surface soil where soil particles can easily absorb and evaporate water. Monitoring data of the gas in surface soil show that the cyclic changes of atmospheric pressure did not alter the radon concentration during no precipitation starting 10 to 20 Dec. whereas, the concentration was affected by the precipitation on 26-27 Dec. The same explanation applies for the week starting 5 Dec., though on a smaller scale. A reciprocal phenomenon is clearly shown during the period of 6-21 Dec., i.e., the radon concentration in soil gas increased as the level of groundwater table decreases during the period. This may be caused by increasing the emanating power of radon from soil particles due to decreasing content of soil moisture and/or by radon in pores equilibrating with soil water as demonstrated previously by continuous monitoring of the radon concentration in groundwater.

2.4.4 Conclusions

Vertical profiles of radon were investigated in a vadose zone where the groundwater table is close to surface and variations of radon in soil gas were monitored continuously for 1 mo. Before measuring the profiles, the measurement of radon by bubbling into toluene was examined. To establish equilibrium of concentraion for radon between in air and 15 mL of toluene, more than 1200 mL of gas was required to be bubbled through the toluene, when the feed rate of air was set at 20 mL min^{-1}. Circulating gas flow is preferable to bubbling gas into toluene and/or monitoring the concentration in soil continuously using an ionization chamber, since the ambient air could be inhaled at a specified depth without a change of suction pressure in soil gas. Also, there is less possibility of withdrawal of soil water into the ionization chamber, which may be accompanied by inhaling the soil gas from a sampling vessel in the ground.

Vertical profiles of radon concentration in soil gas, which were measured by the toluene trap-liquid scintillation method, showed a peak concentration at around a 40-cm depth in an area where the groundwater table is about 100 cm below the surface. So, it was proven that in an unsaturated zone, the radon concentration just above the water table decreases due to decay process during diffusion of radon in the soil moisture.

Based on a reasonable data set, the surface flux density was estimated to be in the range of 6.9 to 2.6×10^{1} mBq m^{-2} s^{-1}, at the site of interest.

The change of the radon concentration in the ground near the surface was interpreted as follows; the radon concentration in the ground near the surface increased for a while following precipitation, since the rising of the water table due to infiltrating water acted to pump the soil gas upward. The radon concentration in soil gas then decreased due to the coupled effects of dilution of soil water by infiltrating water, decrease of the emanating power due to increasing soil moisture, and by the intake of air through the soil which is caused by increasing barometric pressure after precipitation.

Chapter 3
TRITIUM BEHAVIOR IN A CONTAINMENT BUILDING

3. 1 INTRODUCTION

There is a continuing interest in the biological effects of tritium (^3H) and its behavior in the environment because of the potential for increased releases from proposed/planned fusion reactors in Japan (Okada 1988). Tritium is considered one of the least hazardous of the radionuclides because it is a weak beta emitter and has a relatively short biological half-life.

At present, atmospheric releases of tritium from nuclear facilities are not significant from the point of view of health hazard, and the tritium concentration in exhaust air is low and does not fluctuate so much during routine operation (Langhorst et al. 1981; Amano et al. 1988). However, an increase in tritium concentration can be expected resulting from unplanned releases (Kurzeja et al. 1988; Champ et al 1990).

In this chapter, we describe the monitoring efforts as well as the methods of recovery of tritiated water (HTO) released as a result of a leak within the containment building of the Kyoto University Reactor (KUR). The mechanisms responsible for HTO contamination of the containment building were examined and the monitoring data were used to validate the proposed mathematical models for describing the transfer of HTO vapor from air to water. Laboratory studies were conducted to provide estimates of the required model parameters and to verify the model.

There are a few experimental and model studies (Vaadia et al. 1963; Liss et al. 1974; Kline et al. 1974; Belot et al. 1979; Garland 1980; Murphy 1984) dealing with the exchange between HTO vapor in air and water/soil moisture/leaf tissue-water describing the transport mechanism that is relevant to the phenomenon discussed here.

3. 2 INCIDENTAL RELEASE OF TRITIUM AT KUR

3.2.1 Objective and Scope

In this section, the structure of the KUR facilitiy is outlined to understand the tritium behavior in the containment building. Monitoring efforts and survey as for the leak incident are also stated before and after closure to the tritium leak in connection with activities for the sealing and isolation of the sources.

3.2.2 Tritium Leak Incident

The Kyoto University Reactor near Osaka, Japan was initially operated at 1 MW_{th} (which hereafter denoted by MW) in 1964. Its power was raised to 5 MW in 1968. This reactor is usually operated for 70 - 80 hours per week with a ventilation system. The discharge rate of radioactivity from the KUR, operating at 5MW ranges from 0.2 - 0.3 GBq MWh^{-1} (Fukui et al. 1989a). The main radionuclide in the ventilation exhaust is ^{41}Ar (ca. 10^{-2} Bq cm^{-3}). The concentrations of other anthropogenic radionuclides are 10^{-6} Bq cm^{-3} of HTO, 10^{-8} Bq cm^{-3} of ^{133}I, and 10^{-9} Bq cm^{-3} of ^{131}I. Because of the low detection limits, as measured by a 22-L ionization chamber set for the exhaust streams, the presence of these radionuclides is usually masked by ^{41}Ar for minor releases during normal operation of the reactor; this is especially true for HTO. For this reason, monitoring of HTO vapor in the exhaust is carried out twice a year during the operation of the KUR using liquid scintillation counting of water samples collected by condensation from the air exhausted from the containment building.

During such a routine check in fall 1987, a member of the KUR Radiation Control Division noticed a relatively high concentration of HTO vapor in the exhaust. This result, however, was attributed to probable contamination of experimental devices. A water sample was not taken from the exhaust during the next monitoring period

(spring 1988) because the operation of the KUR had been suspended over a 3-mo period begining in April by the Science and Technology Agency (STA). The reason for this suspension was that work on the secondary coolant system of the KUR was required to repair a coolant leak in the pump. Although passing over data from the exhaust air monitoring, had delayed the confirmation of HTO leakage, there was another indicator of leakage. The monitoring data for waters obtained by the Research Reactor Division had showed that the HTO concentration in water pools in the containment building had increased gradually. This was especially the case in the sub-pool (ca. 1.0 $m^2 \times 1.7$ m deep) where the HTO concentration in the water had increased 20-fold during the period of 3 mo (May - July 1987) until this water was replaced in August 1987.

Investigations into the source of this increase in the HTO concentration in water were focused mainly on the presence of irradiated materials such as lithium and boron which could be a source of HTO production by a neutron activation process. Nobody except for the members of KUR safety committee, had been informed the increase in the HTO concentrations in pool waters until August 1988. A smear test revealed significant contamination on the front surface of a heavy water tank (see Fig. 3-1), and a high HTO concentration was detected in the atmosphere near the D_2O tank using a 1.5-L portable ionization chamber. However, this instrument could not detect the HTO concentrations in air a few meters apart from the D_2O tank due to the low detection limit and interferance by radon which emanates from the concrete walls. These findings led to the conclusion that HTO increases were the result of leakage of the heavy water. Nevertheless, the mechanisms by which HTO concentrations of both the sub-pool and the primary coolant water (about 30 m^3 and 9-m deep) had increased ca. 60-fold and 5-fold, respectively, during 1 year since May 1987, were unknown. Further investigations mandated by STA to locate the probable source of leak focused on pipes in pools that might be linked to the D_2O tank; however, no connections of pipes to the tank were found and the cause of the increases in HTO concentrations remained inderminate.

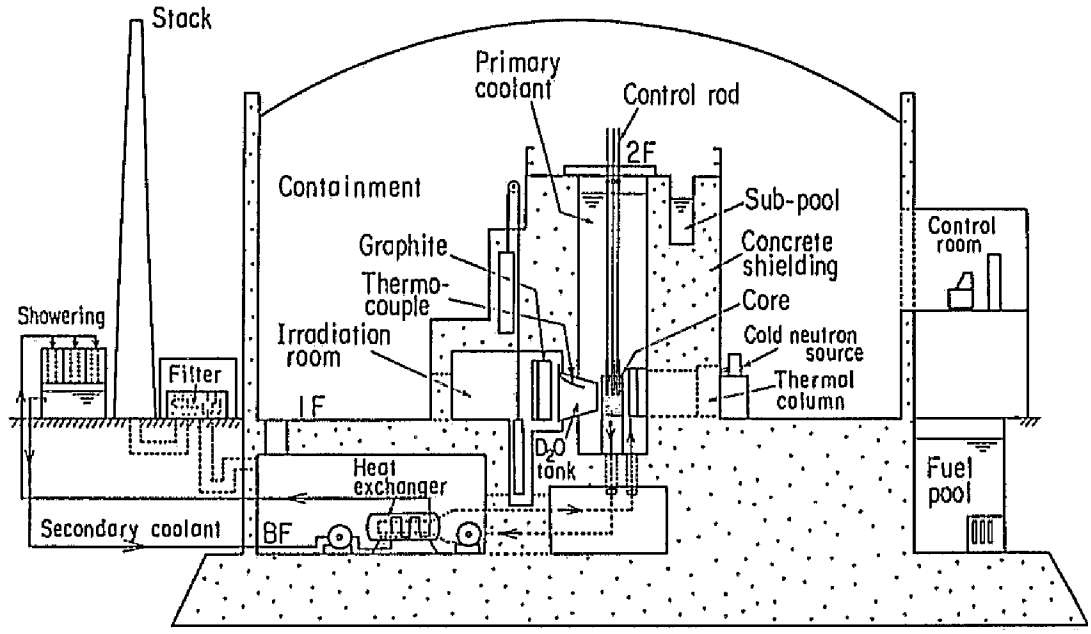

Fig. 3-1 Cross section of KUR containment building.

3.2.3 Isolation of the HTO Leak

Under normal conditions, the aluminium D_2O tank contains approximately 2.2 m^3 of heavy water with a purity of 99.7%. It is used to remove fast neutrons. As is shown in Fig. 3-1, one face of the D_2O tank, ca. 1.8 m in dia., is adjacent to a graphite block layer (ca. 1.5 m^3), 48 cm thick, with a bismuth plug. The space in front of this layer is used as an irradiation room with dimensions ca. 2.4 m × 2.4 m × 2.4 m. It is covered with high density concrete identical to the biological shielding of the reactor core. By 5 October 1988, the concentration of HTO in condensed water near the tank was found to be as much as 2.2 MBq cm^{-3}. Then, a 6-wk program was started by the staff of the Research Reactor Division to lower the moisture in the air in the irradiation room using an air conditioner and a water trap, through which

ambient air was bubbled. On 16-17 November, the heavy water in the D_2O tank was withdrawn into 200 L drums and replaced by light water to carry out a leak test. An estimated loss of 28.2 L of heavy water was made by comparing the weight of the water removed with that initially loaded into the D_2O tank. Inspection with a remote TV camera failed to locate the source of the leak in any of the suspected areas such as joints or flanges in the pipes. The high density concrete shield of the irradiation room was dismantled on 21 November 1988. The graphite layer adjacent to the D_2O tank was removed and stored in a container (2 m^2 ×2 m in height) on 19 January 1989. In early February, air, heated to 90 ℃ was circulated through this container over a 2-mo period to remove any HTO absorbed by the graphite blocks. On 25 January 1989, less than 100 mL of water was found in a guide tube in the D_2O tank used to hold a thermo-couple. The HTO concentration of this water was 7.9 MBq cm^{-3}, which was close to that of the stagnant heavy water (8.1 MBq cm^{-3}) in the dead space of the D_2O distribution system, and two thirds the concentration of the heavy water in the D_2O tank itself (1.2×10^{1} MBq cm^{-3}). Therefore, the source of the HTO leak was located somewhere in the guide tube. The guide tube was cut on the upper part of the tank where the tube had been inserted, and the resulting hole was welded shut. This resulted in the isolation and sealing of the main sources of HTO in the reactor containment building by early April 1989.

3. 3 DEVELOPEMENT, VERIFICATION AND VALIDATION OF A MODEL FOR HTO VAPOR TRANSFER FROM AIR TO WATER

3.3.1 Objective and Scope

This section deals with the development of a model to describe the transfer of HTO vapor between air and water. This model is used to explain the increase in the HTO concentration in the water pools. The objectives in this section are as follows:

(1) the verification of a transfer mechanism and development of a mathematical model for HTO exchange between air and water, based on laboratory experiments, and acquisition of parameters to assess the increases in the HTO concentration in water pools;
(2) the validation of the model by field observations of HTO concentrations in water; and
(3) the model development for the estimation of the mean HTO concentration in air to which the occupational workers may have been exposed during the leakage period, especially when no monitoring took place.

3.3.2 Modeling the HTO Vapor Dynamics between Water and Air

As illustrated in Fig. 3-2, the transport of HTO vapor to and from a water surface is mainly governed by the driving force based on the difference in the specific activity of tritium between water vapor in the turbulent air and the water in a pool (HTO exchange), by evaporation and by deposition.

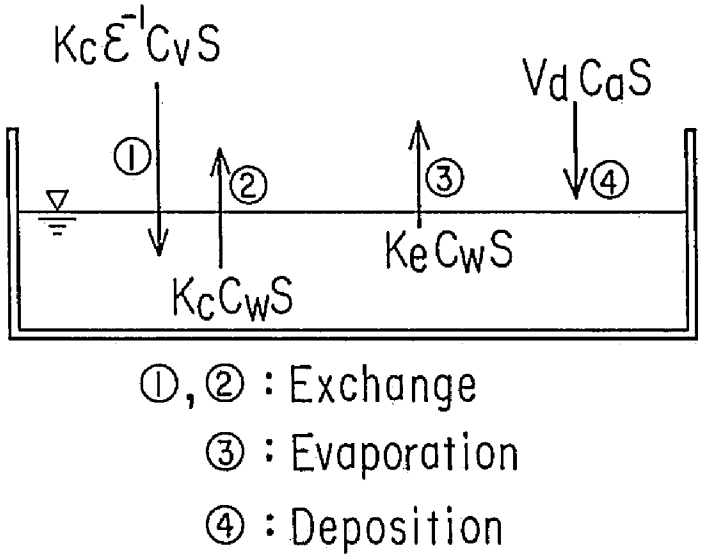

Fig. 3-2 Transfer mechanisms of HTO between water and vapor in air.

These processes can be represented mathematically by the following equation:

$$d(V_wC_w)/dt = -k_c(C_w - \varepsilon^{-1}C_v)S - Q_eC_w + V_dSC_a \quad (3\text{-}1)$$

where

V_w : volume of the water in the pool (cm^3),
C_w : concentration of HTO in the water in the pool (unit cm^{-3}),
C_v : concentration of HTO in the water vapor in air (unit cm^{-3}),
ε : isotopic ratio in HTO vapor and water (—),
C_a : concentration of HTO in the air (unit cm^{-3}),
S : surface area of the water/air interface (cm^2),
Q_e : rate of evaporation ($cm^3\ h^{-1}$),
V_d : deposition velocity ($cm\ h^{-1}$),
k_c : exchange rate constant ($cm\ h^{-1}$), and
t : elapsed time (h).

The evaporation rate, Q_e, is given as follows, assuming the humidity and temperature in the air is constant:

$$-dV_w/dt\ (=Q_e) = k_eS. \quad (3\text{-}2)$$

Equation (3-2) is rewritten as follows:

$$V_w = (H - k_et)S \quad (3\text{-}3)$$

where

k_e : apparent evaporation rate constant ($cm\ h^{-1}$), and
H : initial depth of water (cm).

The concentration, C_a, is related to C_v by the following equation:

$$C_a = KC_v \quad (3\text{-}4)$$

where

$$K = 2.9\times10^{-4}P_i^{-1}(273+T_i)^{-1}R/100 \quad (3\text{-}5)$$

and P_i : saturated vapor pressure (mm Hg) at the temperature T_i(℃) (Anazawa et al. 1972), and
R : relative humidity (%).

Equation (3-1) can be rewritten by substituting eqns (3-2) and (3-4), as follows:

$$d(V_wC_w)/dt = -k_c(C_w - \varepsilon^{-1}C_v)S - k_eSC_w + V_dSKC_v. \quad (3\text{-}6)$$

At equilibrium, i.e., $d(V_wC_w)/dt = 0$ in eqn (3-6), the HTO concentration in water, C_{we}, is given by:

$$C_{we} = C_v(k_c \varepsilon^{-1} + V_dK)/(k_c + k_e) \qquad (3\text{-}7)$$

The average rate constant, k_e, can be determined from eqn (3-2) by measuring the rate of evaporation of a volume of water over a given time period in the environment.

To determine the exchange rate constant, k_c in a laboratory, we considered the transport of tritium from water in a small dish to a large volume of ventilated air, as shown in Fig. 3-2, because this transport between water and air can be considered to be reversible. Under these conditions, the HTO concentration, C_v, in eqn (3-6) can be neglected. With this assumption, the following analytical solution can be obtained for the concentration, C_w, in water at time t, by substituting eqns (3-2) and (3-3) into eqn (3-6) and setting $C_v = 0$:

$$C_w/C_0 = (1 - k_e t/H)^{k_c/k_e} \qquad (3\text{-}8)$$

where

C_0 : initial concentration of HTO in water in a glass dish (unit cm^{-3}).

Rearrangement of eqn (3-8) gives the rate constant, k_c, as follows:

$$k_c = k_e \ln(C_w/C_0)/\ln(1 - k_e t/H). \qquad (3\text{-}9)$$

This model can be validated by comparing the dependency of the exchange rate constants obtained from eqn (3-9) for various concentrations with time and initial depths.

In addition to verifying the model as mentioned above, equation (3-6) can be used to estimate the increase of HTO in water pools via air as follows. In the reactor containment building, the primary coolant and the water in the sub-pool are usually circulated to remove heat from the core during reactor operation and to purify the water using ion exchange columns. The relatively high temperature (>30 °C) in these bodies of water leads to enhanced evaporation which is followed by the addition of a volume of HTO-free water to maintain the water levels. Consequently, the HTO concentrations in the water in these pools decrease intermittently,

and the volumes of the water, V_w, can be set constant in eqn (3-6) to satisfy this dilution condition mentioned above. Assuming a constant concentration, C_{vo}, in the air averaged over the period after the heavy water leak took place, the solution of eqn (3-6) is given by:

$$C_w/C_{vo} = r\{1-(1-r^{-1}C_iC_{vo}^{-1})\exp[-(k_c + k_e)H^{-1}t]\} \quad (3\text{-}10)$$

where

$$r = (k_c\,\varepsilon^{-1} + V_aK)/(k_c + k_e) \quad (3\text{-}11)$$

and C_i : initial concentration of HTO in the water (unit cm^{-3}), and

C_{vo} : average concentration of HTO vapor in air (unit cm^{-3}).

Equation (3-10) represents the HTO concentration in the water in the pool resulting from the transfer of tritium from air to water. At infinite time, the relative concentration in eqn (3-10) become equal to r. Thus, the HTO concentration in the water in the pools becomes r times that in the HTO vapor in the air at steady state condition. Note that the factor r includes coefficients for the effects of physical and isotopic dilution, and deposition.

3.3.3 Verification and Validation of HTO Exchange Model

3.3.3.1 Method for parameter acquisition to assess the HTO dynamics

Three procedures were used to obtain the key parameters, k_c and k_e, required to predict the HTO behavior between water and air. First, in September 1988, laboratory tests were carried out as follows. Ten to 40 mL of tracer solutions were placed in glass dishes (ca. 9 cm diameter) to measure both the changes in concentration of HTO and the amounts of water loss by evaporation over a 4-day period. Aliquots taken for radiometric assay were restricted to 0.1 mL at each sampling so as to minimize reduction in volume; the total volume of water sampled was adjusted to account for losses via evaporation. Temperatures during these experiments varied from 22 - 27 °C, and the relative humidity ranged from 53 - 59 %.

A second method was designed to represent the case of HTO vapor absorption from air in the containment building. As will be shown in a later section, air monitoring by measuring HTO activity in samples of condensate had indicated that a few days after turning off the ventilation in the containment building, the concentration of the HTO vapor had essentially reached a near-steady state. To compare the parameters, k_c and k_e, obtained in the laboratory with those near the heavy water facility, two glass dishes with 40 mL of HTO-free water were placed near the facility in containment for a period of 1 wk starting on 10 January, 1989 when the ventilation had been turned off for more than 2 wk. This experiment would demonstrate the transport of the HTO from air to water, in the opposite direction from the laboratory experiment. The temperature ranged from 12 - 15 °C and relative humidity was ca. 65% during this experiment. The procedure to estimate the parameters was the same as that described earlier.

In the third method, in situ k_e values for the sub-pool water were obtained by measuring water levels of the sub-pool over a period of 1 mo, starting on 8 May and again on 19 June, 1989. The in situ values are likely to be better suited for estimating the HTO concentration changes in water under conditions different from the laboratory experiments using small glass dishes. It is, however, difficult to obtain the in situ k_c values for the 1-mo period because of the small changes in HTO concentration in a pool water volume of ca. 1.7 m^3. Furthermore, large fluctuations in the HTO concentration in air resulting from the ventilation of the containment building make it difficult to estimate the average concentration, C_{v0}, in air, which is needed for assessing the increase in concentration of HTO in water (see eqn (3-10)). In the following argument, it will be described how to estimate the rate constants, k_e and k_c, not only for the procedure using small glass dishes containing HTO tracer solution in a laboratory but also in the in situ field in spite of the difficulty mentioned above.

3.3.3.2 Estimation of values of the parameters and verification of model

The laboratory experiments to obtain the rate constants for k_e and k_c were carried out as follows: the initial levels of the HTO-containing water samples in the four glass dishes were 0.242 (case ① in Fig.3-3), 0.387 (case ②), 0.553 (case ③) and 1.049 cm (case ④) for the 10, 20, 30 and 40 mL samples, respectively. Figure 3-3 shows the relative HTO concentrations (C/C_0) and the water levels as a function of time. It is apparent that the change in the relative HTO concentrations in the water is greater for lower initial water levels.

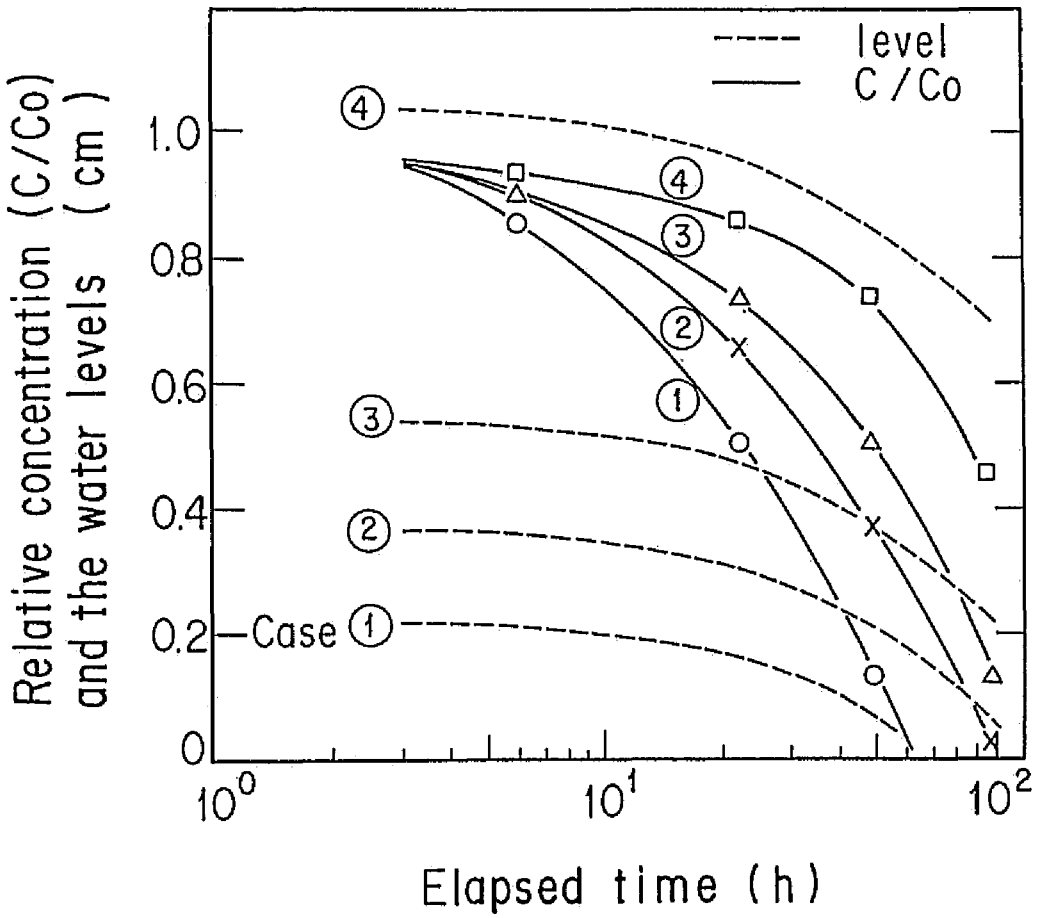

Fig.3-3 Relative HTO concentrations (C/C_0) in water and water levels in glass dishes with initial water levels for cases ①, ②, ③ and ④ respectively, as a function of time.

The evaporation rate in these dishes was almost constant with time and the average rate constant, k_e, in eqn (3-2) was readily calculated to be 3.3×10^{-3} cm h^{-1} using the weight loss per unit time and unit surface area. The exchange rate constant, k_c, as a function of elapsed time, was calculated from eqn (3-9). The k_c values are listed in Table 3-1, together with the changes of relative concentration of HTO in the water. The differences between the k_c values for various water levels are small, usually within a factor of two. The average value for this rate constant was found to be 6.8×10^{-3} cm h^{-1}, which is almost twice as high as the k_e value.

Table 3-1 Relative concentrations (C/C_0) for HTO in glass water dishes for four different water depths and exchange rate constants (K_c).

		Relative concentration C/C_0 (-)			
		Case ①	Case ②	Case ③	Case ④
Initial depth (cm)		0.242	0.387	0.553	1.049
Elapsed time (h)	6	0.855	0.912	0.907	0.936
	22	0.506	0.659	0.737	0.861
	48	0.124	0.367	0.508	0.743
	96	---	0.024	0.134	0.456
		Calculated k_e value ($\times10^{-3}$ cm h^{-1})			
		Case ①	Case ②	Case ③	Case ④
Elapsed time (h)	6	6.09	5.77	8.86	11.4
	22	6.32	6.64	7.15	6.89
	48	6.51	6.28	6.62	5.98
	96	---	7.20	7.79	7.19

This experiment was carried out during 1-5 September 1988.

The small variation in the experimental k_c values demonstrates the verification of this model on the HTO transfer mechanism. This is clearly shown from Fig. 3-4, where relative concentrations, C/C_o, obtained by experiments for the four initial water levels (case ① - ④), were plotted against the theoretical curve, calculated using average rate constant, k_e, and the ratio, k_c/k_e (=2), described above.

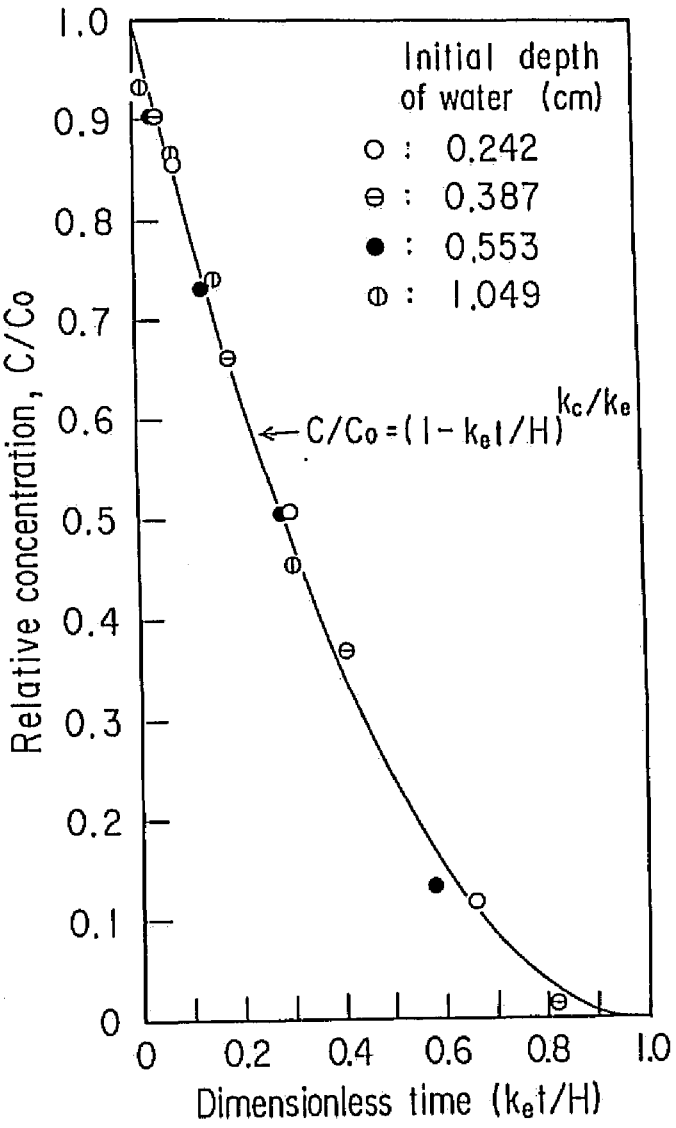

Fig. 3-4 Comparison of the change in relative concentrations observed in water with the calculated by the transfer model.

The rate constants for exchange and evaporation obtained from the glass dishes containing 40 mL of water which were placed in the reactor containment building for 1-wk period in a HTO vapor atmosphere were 4.3×10^{-3} and 2.4×10^{-3} cm h^{-1}, respectively with a ratio, k_c/k_e of 1.8. These values are rather close to those obtained in the laboratory in September, despite the difference in the direction of the HTO transfer. The in situ rate constants are recomended for use in a real case since the effect of temperature on the values of these parameters is small.

For 1-mo period with the ventilation operating continuously from Monday morning to Friday evening of every week, the in situ k_e values for the sub-pool water were found to be 1.81×10^{-2} and 1.94×10^{-2} cm h^{-1} (1.88×10^{-2} cm h^{-1} as an average) for May and June 1989. These values are larger by a factor of 5 than those obtained for glass dishes; this is attributed to a higher temperature in the sub-pool water near the reactor core compared to that in the atmosphere, which resulted in an increase in the rate of evaporation of water from the pool. In the following section the in situ exchange rate constant k_c value was adopted to be 3.7×10^{-2} cm h^{-1}, which was derived from the k_c/k_e ratio obtained by the laboratory tests.

3.3.3.3 Validation of transfer model

It should be noted that, in eqn (3-11), the conversion factor K value is usually on the order of 10^{-6}, and the value in V_d is on the order of 10^{-2} cm s^{-1} for elementary tritium (Förstel 1986). That is, the value for V_dK value is expected to be on the order of 10^{-4} cm h^{-1}, which is smaller than the observed rate constants k_e and k_c. In addition, the isotopic ratio, ε, is close to unity (0.90 to 0.92) at ambient temperatures in a natural environment (Sepall et al. 1960). The value for r therefore, becomes lower than unity, indicating that the r value is a reasonable factor for physical and isotopic dilution. It may be difficult to measure the deposition rate separately. However, it is not necessary to determine the value V_d because the evaporation rate of HTO

includes the deposition velocity as a net rate when the loss of water is determined by weighing. Given this, terms containing V_d can be neglected in all equations described above.

Figure 3-5 illustrates the increases of HTO concentration in the primary coolant water and in the water in the sub-pool together with predictions based on eqn (3-10), using the in situ rate constants and taking into consideration intrinsic water levels of pools. Two average concentrations of HTO vapor in air, 4×10^{2} and 6×10^{2} Bq cm^{-3} were selected for both reservoirs as boundary concentration because of the lack of data during the period before the leak had been detected.

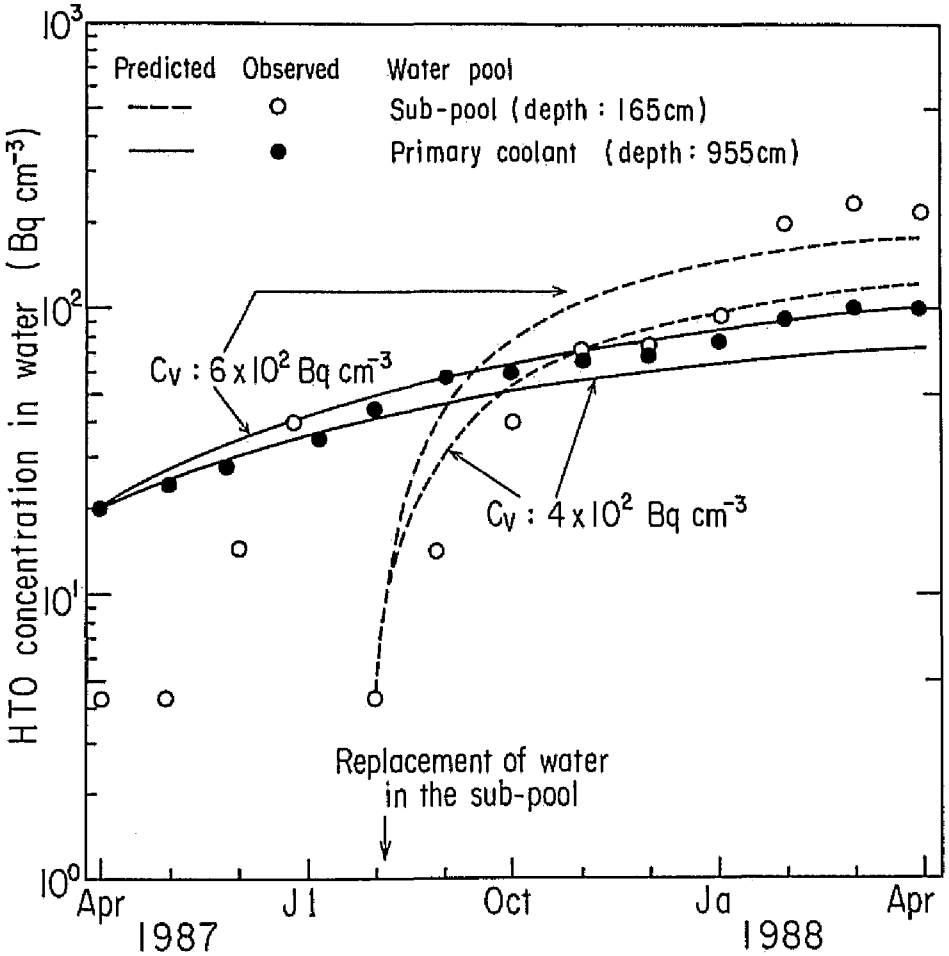

Fig. 3-5 Measured and calculated HTO concentrations in primary coolant and sub-pool waters as a function of time resulting from leakage of heavy water.

As is shown in this figure, the HTO concentrations in the water in the sub-pool decreased abruptly in August because all of the water was replaced at that time. For both reservoirs, the HTO concentrations measured after April 1987 show values lower than those calculated using a value of 4×10^{2} Bq cm^{-3} and higher values than those calculated using a value of 6×10^{2} Bq cm^{-3} after January 1988. This difference with time may be due to changes of leak scenario, i.e., our results suggest that the leak flux from HTO sources including the graphite layer may have increased with time. Nevertheless, the increases in concentrations in water are quite well reflected by this simple model.

Before removing the 2.2 m^{3} of heavy water into 200 L drums in mid November 1988, only a few samples were collected in the reactor containment building and the HTO concentration of the vapor in the atmosphere was determined. Two days after the ventilation had been turned off, the HTO concentration was 1.5×10^{3} Bq cm^{-3}. After the ventilation had been turned back on, this level had decreased to 1.7×10^{2} Bq cm^{-3} after 3 d. Thus, the values, $(4\text{-}6)\times10^{2}$ Bq cm^{-3} assumed for fitting the equation to the data in Fig. 3-5 are well within this range, and are quite reasonable. The HTO absorbed by the graphite block, 4.6×10^{1} GBq, was recovered from the isolation chamber in which it had been placed over a 2-mo period starting late January 1989. After isolating the graphite block in the containment building, the amount of HTO and the concentrations in the water in the sub-pool were monitored over a 1-y period. The results are shown in Fig. 3-6. A linear regression of the log-linear plots gave a half-life of approximately 15 wk after the removal of HTO. Assuming a HTO concentration in air of zero, an estimated half-life of the HTO concentration in the sub-pool water of 13 wk was obtained, using the transformation of eqn (3-10). The difference of half-lives is most likely caused by the contribution to the HTO concentration in air from the final source, i.e., HTO absorbed in the concrete in the containment building.

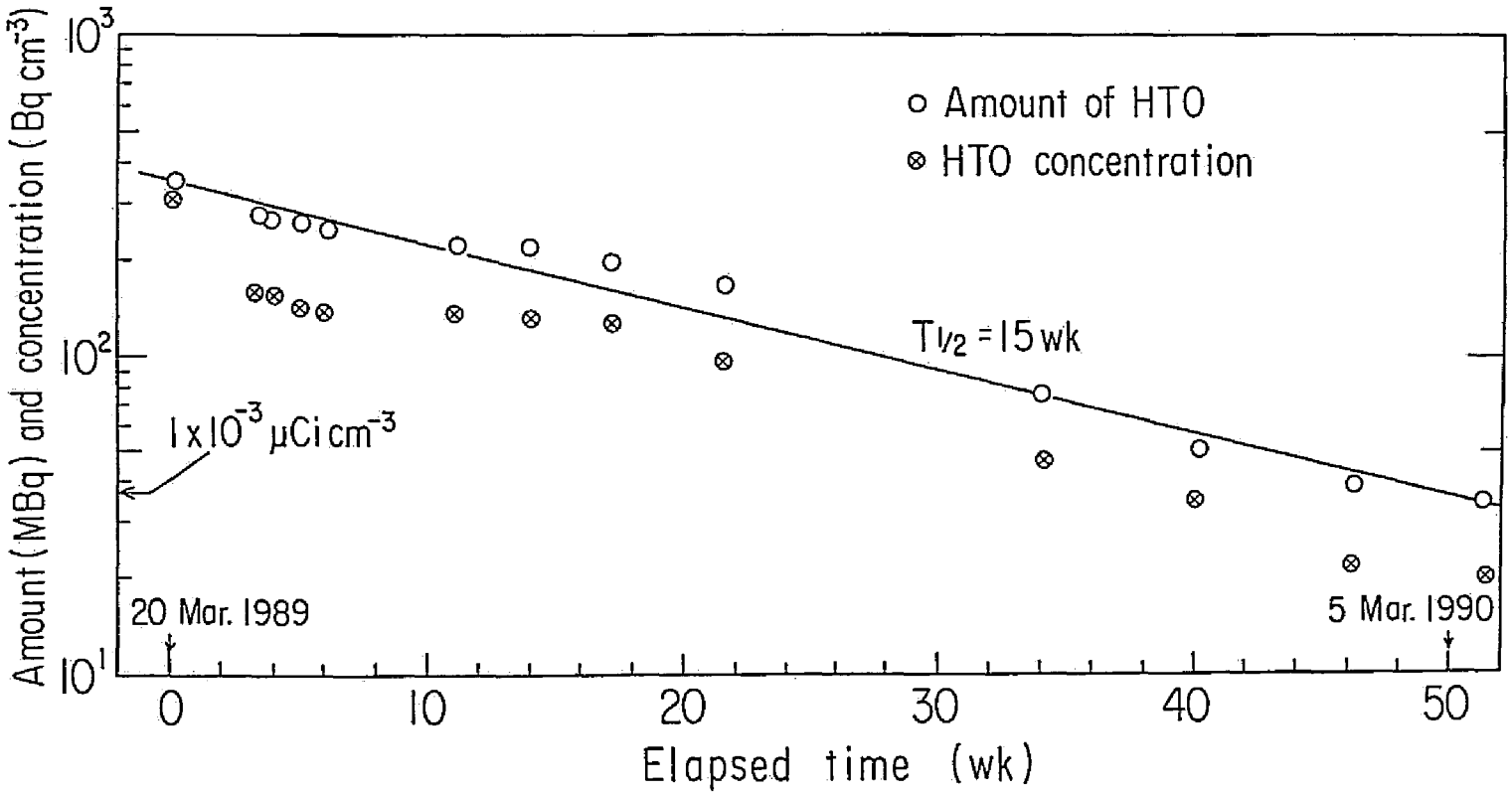

Fig. 3-6 Decrease in the amount and concentrations of HTO in the sub-pool water after removal of HTO sources in the containment building.

Solving eqn (3-6) by setting $C_w=C_{wo}$ at $t=0$ and neglecting V_dK as mentioned previously, the average concentration of HTO vapor, C_{vo}, for the duration of the HTO decrease from C_{wo} to C_w can be given by:

$$C_{vo}=aH\varepsilon k_c^{-1}(C_w-C_{wo}e^{-at})(1-e^{-at})^{-1} \qquad (3\text{-}12)$$

where

$$a=(k_c+k_e)H^{-1},$$

and C_w : HTO concentration in water at time t,

C_{wo} : HTO concentration in water at time 0, and

t : elapsed time after removing sources.

Using a value for ε of 0.92, the mean concentration, C_{vo}, in the air in the reactor containment building was calculated as 3.6×10^{1} Bq cm^{-3} after 50 wk when the amount of HTO in the sub-pool water had decreased by a factor of 10 as shown in Fig. 3-5. This indicates that the mean concentration, C_{vo}, was lowered by more than an order of magnitude after removing HTO sources in the containment building, when compared to the estimated concentrations before removing sources as is shown in Fig. 3-5.

At the end of the monitoring period in March 1990, the HTO vapor concentration in the air ranged from ca. 5×10^{1} Bq cm^{-3} to a few Bq cm^{-3}, depending on whether the ventilation system was operating. This again indicates that the estimated values of 3.6×10^{1} Bq cm^{-3} falls in the range monitored and that the model developed in this section is valid. Since eqn (3-12) provides reasonable estimates of time averaged concentration in air, given the change of relative HTO concentration in a pool of water in contact with the air, it may serve to estimate the long-term HTO exposure dose to occupational workers in the absence of air monitoring data.

The previous section addressed both the behavior of HTO vapor from air to water and its modeling based on the concept of the average concentration in air. In the following section the changes in concentration of HTO vapor in air will be described in more detail in relation to the ventilation histories and emission from the concrete material.

3. 4 CHANGES IN HTO VAPOR CONCENTRATIONS IN AIR AND THE ESTIMATION OF AMOUNT ABSORBED IN CONCRETE MATERIAL

3.4.1 Objective and Scope

In the previous sections the concept of average concentration of HTO in air has been described. The results show that the dynamics of HTO vapor between air and water can be modelled successfully. However, the HTO concentrations in air showed large fluctuations with ventiing over time by the process of the so-called soaking effect (Numata et al 1991), even after the HTO sources had been removed. Thus, it becomes important to better understand the change in concentration of HTO vapor in greater detail for short periods of less than 1 wk which cover one ventilation cycle, as well as for periods longer than 1 y to determine the amount of HTO remaining in the concrete walls of the KUR building. This section specifically deals with the following:

(1) the development and validation of a model for the dynamics of HTO concentrations in the atmosphere as a function of the venting in the containment building, and
(2) the estimation of the quantities of HTO remaining in the concrete walls after the removal of existing HTO sources in the containment building.

3.4.2 Modeling the Changes in HTO Concentration in Air after Removing the Main Sources

The monitoring data of the HTO vapor in the containment building showed that, even after removal and isolation of the main sources, the HTO concentration in air increased after the ventilation was shut down every Friday. This was followed by a decrease due to resumption of the ventilation on the following Monday. This behavior suggested the existence of a residual HTO source in construction materials such as concrete with a behavior similar to that of radon (Fukui et al. 1989a). In general, the HTO concentration

decreased drastically with an attenuation rate, Λ, just after resuming the ventilation, followed by a gradual decrease over a 1-wk period as shown in Fig. 3-7. The mass balance equation of HTO in air in the containment building with the emission of HTO from the concrete as the source is given by:

$$d(C_a V)/dt = P(t_i) - \Lambda C_a V \qquad (3\text{-}13)$$

where

$P(t_i)$: HTO production rate at time t_i (unit d^{-1}),
t_i : elapsed time after resumption of the ventilation (d),
Λ : total attenuation rate ($= \nu + \mu + \lambda$) in the HTO concentration (d^{-1}),
ν : ventilation rate (d^{-1}),
μ : leak rate in the containment building (d^{-1}),
λ : radioactive decay constant (d^{-1}),
C_a : HTO vapor concentration in air in the containment building (unit m^{-3}), and
V : volume of the containment building (m^3).

As shown in Fig. 3-7, the production rate $P(t_i)$ in eqn (3-13) cannot be considered a constant even within 1 wk.

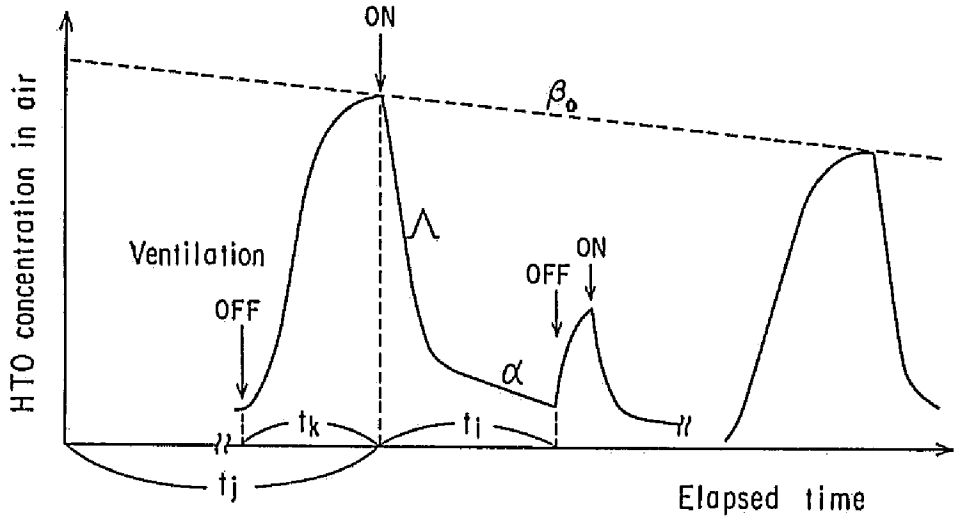

Fig. 3-7 Typical change in concentration of HTO in containment building air showing the effect of ventilation.

Based on the monitoring data, the production rate can be expressed by:

$$P(t_i) = P_{io} \exp(-\alpha t_i) \qquad (3\text{-}14)$$

where

P_{io} : initial value of the HTO production rate at $t_i = 0$ within one cycle of ventilation, and

α : the attenuation rate constant of the production rate within one cycle of ventilation.

Setting $C_a = C_{ao}$ at $t_i = 0$ and substituting eqn (3-14) into eqn (3-13), the HTO concentration at time t_i is given by:

$$C_a / C_{ao} = (1-K_p)\exp(-\Lambda t_i) + K_p \exp(-\alpha t_i) \qquad (3\text{-}15)$$

where

$$K_p = P_{io} C_{ao}^{-1} V^{-1} (\Lambda - \alpha)^{-1}. \qquad (3\text{-}16)$$

Then, the amount of HTO discharged during t_i (usually < 1 wk) is :

$$E_i = \int C_a Q dt$$
$$= (1-K_p) C_{ao} Q \Lambda^{-1} \{ 1 - \exp(-\Lambda t_i)\} + K_p C_{ao} Q \alpha^{-1} \{ 1 - \exp(-\alpha t_i)\} \qquad (3\text{-}17)$$

where

Q : the rate of air flow ($m^3\ d^{-1}$) from the containment building.

If the period without ventilation is short, the steady state condition of the HTO concentration is not attained between the air and the concrete. In this case the concentration C_{ao}, in eqns (3-15) and (3-16) at the short times of t_k after the shut down of the ventilation should be replaced by the value of eqn (3-18) which is easily obtained from eqn (3-13) with minor transformations assuming $C_{ao} = 0$, $v = 0$ and $\lambda = 0$ (i.e. $\Lambda = \mu$) at $t_k = 0$, and $P(t_i) = P_{io}$ (i.e. $\alpha = 0$) for small t_i in stead of eqn (3-14):

$$C_{ao} = P_{io} \mu^{-1} V^{-1} \{ 1 - \exp(-\mu t_k)\} \qquad (3\text{-}18)$$

where

t_k : elapsed time after ventilation shut down (usually <3d).

Over longer time periods(t_j), the saturated concentrations, C_{ao}, in the air under the quasi-equilibrium conditions at the shut down of ventilation decreased exponentially with a half-life, β_o, as a

result of the attenuation of the HTO content in the concrete as shown in Fig. 3-7. This suggests that the production rate, P_{io}, in eqns (3-16) and (3-18) is not constant but can be expressed as follows :

$$P_{io} = P_o \exp(-\beta_o t_j) \quad (3\text{-}19)$$

where

P_o : initial production rate just after removal of the main sources of HTO,

β_o: attenuation rate constant of the HTO content in the concrete, and

t_j : elapsed time after removal of the sources of HTO.

Substituting eqns (3-18) and (3-19) into eqn (3-17), the quantity of HTO released from the containment building within 1 wk at t_j is given by:

$$E_i = (A+B)\, P_o Q V^{-1} \exp(-\beta_o t_j) \quad (3\text{-}20)$$

where

$$A = [\{1-\exp(-\mu t_k)\} - \mu(\Lambda-\alpha)^{-1}] \times \{1-\exp(-\Lambda t_i)\}(\mu\Lambda)^{-1}, \text{ and}$$

$$B = \{1-\exp(-\alpha t_i)\}\alpha^{-1}(\Lambda-\alpha)^{-1}.$$

In eqn (3-20), the first term indicates the amount of HTO vapor initially present in the air during the period when the ventilation was shut down, and which was subsequently discharged during the resumption of the ventilation. The second term represents the amount of HTO emitted from the concrete during the period t_i.

3.4.3 Air Monitoring and Estimation of the Amount Absorbed in Concrete Material

3.4.3.1 Changes in HTO concentrations in air

Figure 3-8 shows the HTO vapor concentrations in the KUR containment building over a 15-mo period following November 1988 when ca. 2.2 m^3 of heavy water was transferred and isolated into the 200 L drums. Circles with cross mark (⊗) indicate HTO concentrations monitored during the shut down of the ventilation, while the open circles represent concentrations during operation

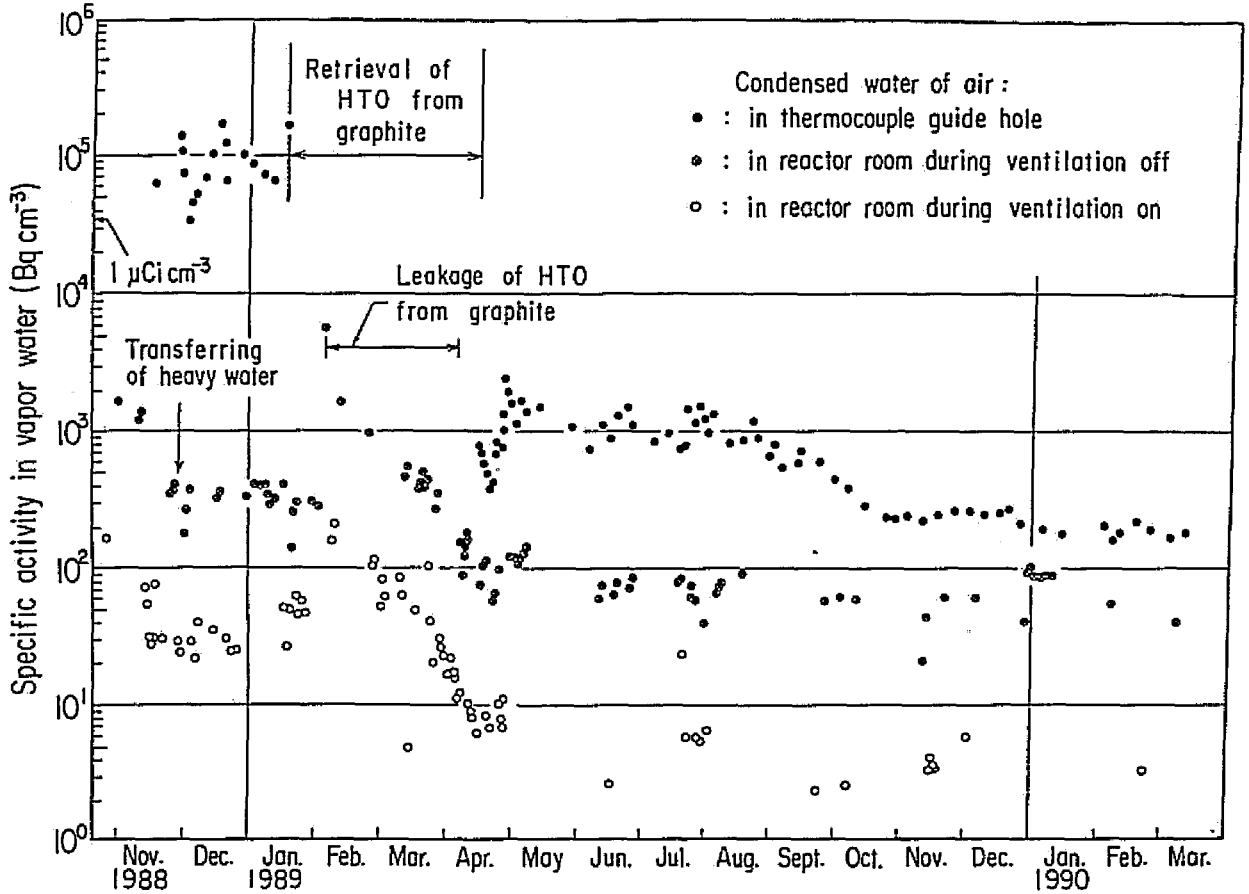

Fig. 3-8 Monitoring data of HTO concentrations in air over a period of 15 months. Closed circles are concentrations in condensate in thermo-couple guide hole. Open circles and marks (⊗) are those in containment building air during ventilation resumption and shut down, respectively.

of the ventilation. On the whole, the former concentrations are roughly one order of magnitude greater than the latter; however, as expected, the extent depends on the ventilation history. In this figure, there are two abrupt changes in HTO concentration during the monitoring period. The changes in late November 1988 coincide with the transferring of the heavy water from the tank into the drums which resulted in decreased concentrations of HTO in air due to the reduction of the leak rate through the thermo-couple. The abrupt increase in early February 1989 was caused by the leakage of HTO vapor from the graphite block in the isolation chamber during the process of dehumidifying by heating at ca. 90℃ (see the changes in HTO concentrations for a 1-wk period as shown on the right hand side of Fig. 3-9). As discussedin previous sections, the validation of the HTO vapor transfer model between air and water in the pools is demonstrated by air monitoring data. Closed circles indicate HTO concentrations in condensate of air taken from the guide hole of the thermo-couple, which is a main root for tritium leakage from the heavy water tank into the containment building air. A two-orders decrease in the HTO concentration for the period of a few months in early 1989 indicates that the process of dehumidifing from the graphite block is quite effective in reducing the emission of HTO. Setting back the graphite block and the heavy density concrete of irradiation room in front of the D_2O tank increased the concentration by about one order in April 1989. However, this process did not influence the HTO concentration in the containment building air during the period of both ventilation shut down and resumption due to the limited volume of air around the D_2O tank containing the thermo-couple guide hole.

In Fig. 3-9 the effects of ventilation on the HTO concentration in air are shown in a greater detail for the two 1-wk periods with the ventilation system working. Curves ① and ② show the changes in HTO concentration in air before and after the removal of the heavy water, respectively. A comparison of these curves clearly shows that the HTO concentration in the air after quasi-

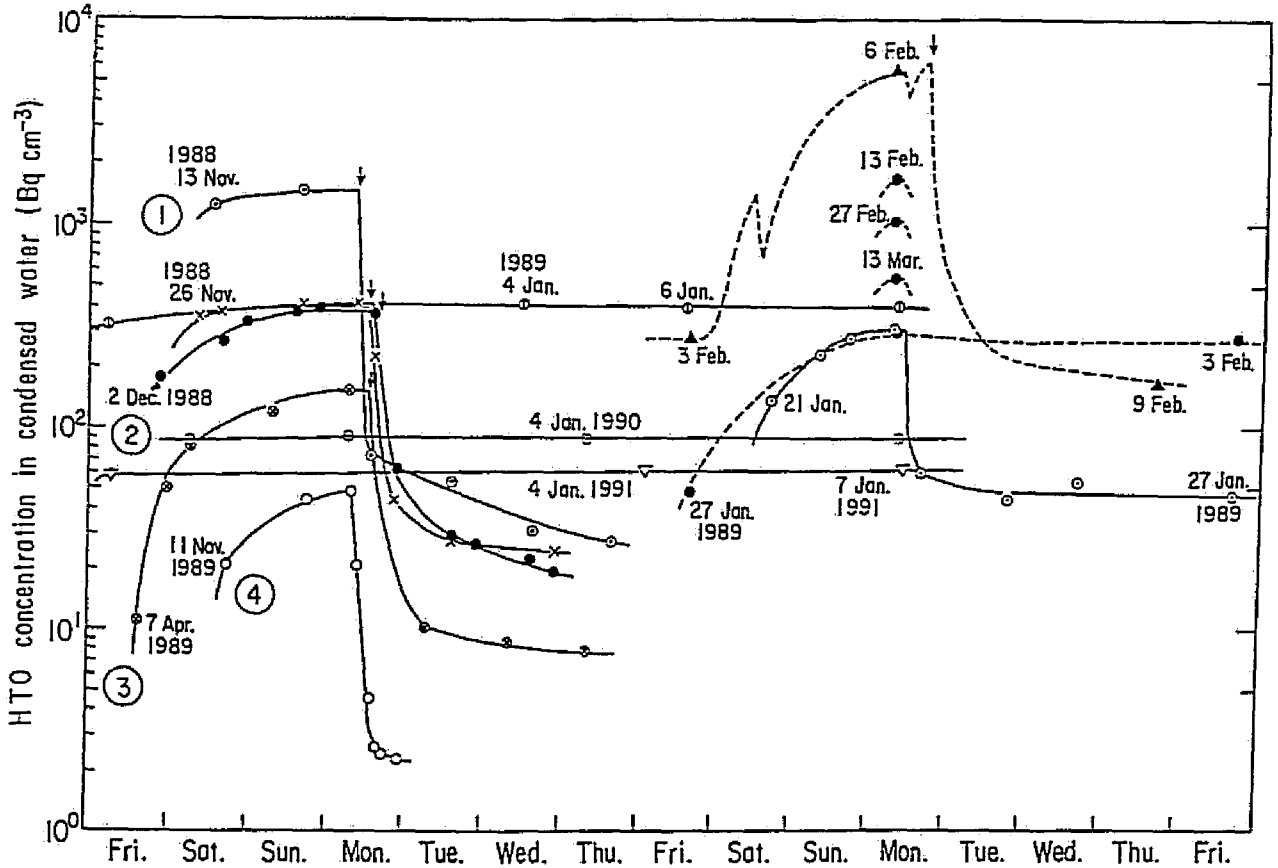

Fig. 3-9 Weekly changes in HTO concentration in condensate in containment building air as a result of the ventilation shut down and the resumption. Unexpected increases are shown on the right hand side of this figure caused by leakage during the process of dehumidifing the graphite.

equilibrium, which was attained as a result of ventilation shut down, decreased from 1.5×10^{3} Bq cm^{-3} to 4×10^{2} Bq cm^{-3}. The HTO concentration in air decreased further to 1.5×10^{2} Bq cm^{-3} in early April 1989 after the HTO in the graphite block was recovered (curve ③). Seven months after the removal of the graphite, the concentration in air was lowered by another one third (5×10^{1} Bq cm^{-3} in curve ④) resulting mainly from the reduction of the HTO inventory in the concrete. These growth curves for HTO concentrations in air during shut down of the ventilation allow for the estimation of the leak rate, μ, in the containment building, which was approximately 0.96 d^{-1} as determined by the curve fitting (Fukui 1992).

For longer periods of about 2 wk during the New Year holidays in January 1989 - 1991, the ventilation was shut down and no further increases in concentration were found in this period as shown in Fig. 3-9. Thus, it was ascertained that the steady state in concentration in the containment building air was attained within a few days after the ventilation shut down. The drastic decreases in HTO concentrations in air under steady state conditions were shown to correspond to operation of the ventilation system, followed by a moderate change in HTO concentrations in air due to decreasing of the production rate from concrete. The rate of change for this later stage, corresponds to α as expressed in Fig. 3-7 and used in eqn (3-14). The α value decreased slightly with time and was estimated to be 3.0×10^{-1} d^{-1} over a 5-mo period prior to March 1989 to 1.3×10^{-1} d^{-1} over a 7-mo period following the removal of the HTO sources in April 1989.

3.4.3.2 Estimation of amount absorbed in the building concrete

The production rate, P_{io}, could be approximated from eqn (3-18) as the product, $C_{ao}\ \mu V$, for large times ($t_k > 3$ d). Therefore, long-term monitoring of HTO concentration in air (C_{ao}) allows for the estimation of the attenuation rate, β_o of the HTO production rate, which depends on the HTO content in the concrete.

Figure 3-10 shows the change of C_{ao} over nearly a 1-y period

during which samples were collected two or more days after ventilation shut down. The data in Fig. 3-10 shows attenuation rate (β_o) in eqn (3-19) to be approximately 5.0×10^{-3} d^{-1} ($T_{1/2}$= 20 wk) until July 1989 and 3.0×10^{-3} d^{-1} ($T_{1/2}$=33 wk) since August 1989. An abrupt increase in HTO concentration is evident, resulting from the leakage of HTO during the 2-mo retrieval procedure. On the right hand side of this figure, the change in HTO concentration in the containment building, due to the leakage from the graphite, is shown after subtracting the contribution of HTO exhaled from concrete walls as background emission. This gives a half-life of 11 days which corresponds to the HTO content in the graphite in the isolation chamber. The initial production rate, P_o of 4.8×10^{1} MBq d^{-1} in eqn (3-19), was also estimated from a concentration, C_{ao} of about 4.2×10^{2} Bq cm^{-3} in late November 1988, just after the main source in the containment building had been transferred and isolated.

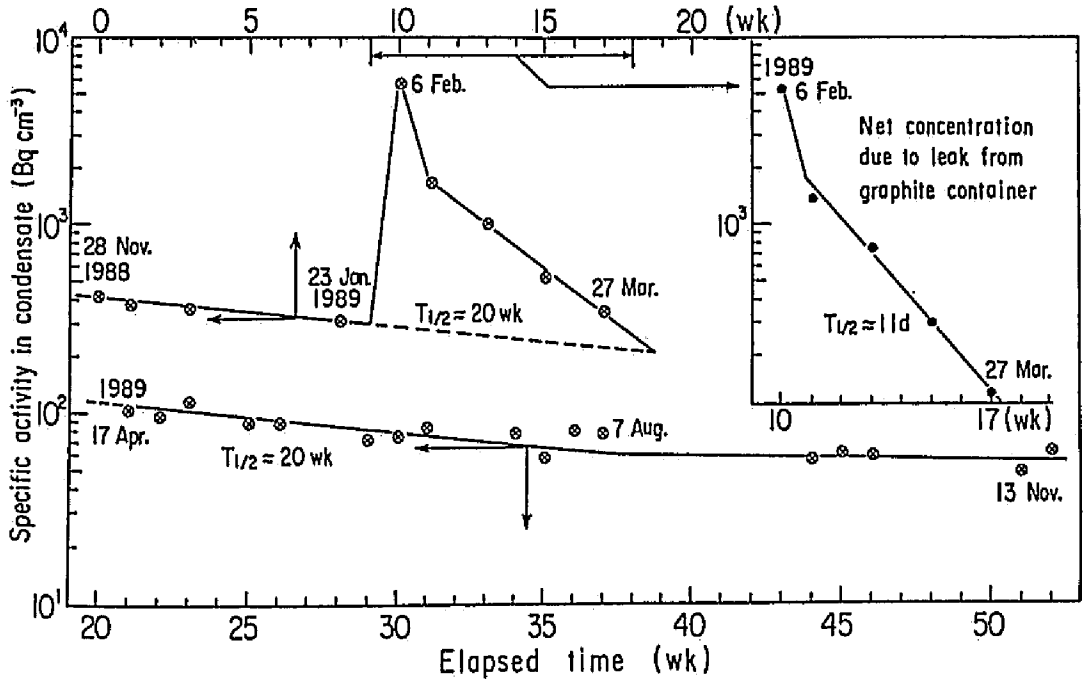

Fig. 3-10 Decrease in HTO concentrations in condensate collected in the containment building air under quasi-equilibrium conditions between air and concrete material.

Taking into consideration the history of operation of the ventilation system since late November 1988, when the heavy water as a main source of contaminant was isolated in the containment building, the amount of HTO vapor emerged and released weekly from the KUR was estimated using eqn (3-20), and is illustrated in Fig. 3-11 (closed circles), together with the amount of HTO accumulated (solid line) until March 1990. The remaining parameter values necessary for this estimation were set as follows:

$V = 1.2 \times 10^4$ m^3, $v = 4.2 \times 10^1$ d^{-1}, $Q = 4.8 \times 10^5$ m^3 d^{-1}.

The cumulative amount over a 70-wk period was calculated to be 1.6 GBq during the flushing of the stagnant air in the containment building by the initial ventilation period and 2.6 GBq (dashed line) for the subsequent stage as calculated from the second term in eqn (3-20). This total amount of 4.2 GBq was found to have been emitted almost solely from the concrete walls, because the amount lost from the sub-pool water during the same period was estimated as 5.6×10^{-1} GBq and no other sources exist in the containment building. The estimates of the HTO released resulting from an abrupt discharge from graphite are not included in the above calculation. This is so because the amount calculated in eqn (3-20) was not based on monitoring data, but on the typical evolution of HTO concentration modelled with the ventilation operating described previously.

The same approach was used to estimate the amount of HTO released by the abrupt discharge from the graphite during the 7-wk period from 6 February to 27 March 1989, as illustrated in Fig. 3-10. These discharged amounts were estimated to be 1.4 GBq for flushing the stagnant air and 2.7 GBq for continued ventilation. It was found that almost same quantity, 4.1 GBq, in comparison with the amount emerged from the concrete for a 70-wk period, was released during the short period when the amount of 4.6×10^1 GBq was retrieved from the graphite. Thus, the behavior of HTO leaked from the heavy water tank was quantitatively revealed and the models developed in this section will serve to predict the contaminant spread of volatile chemicals in air-water systems.

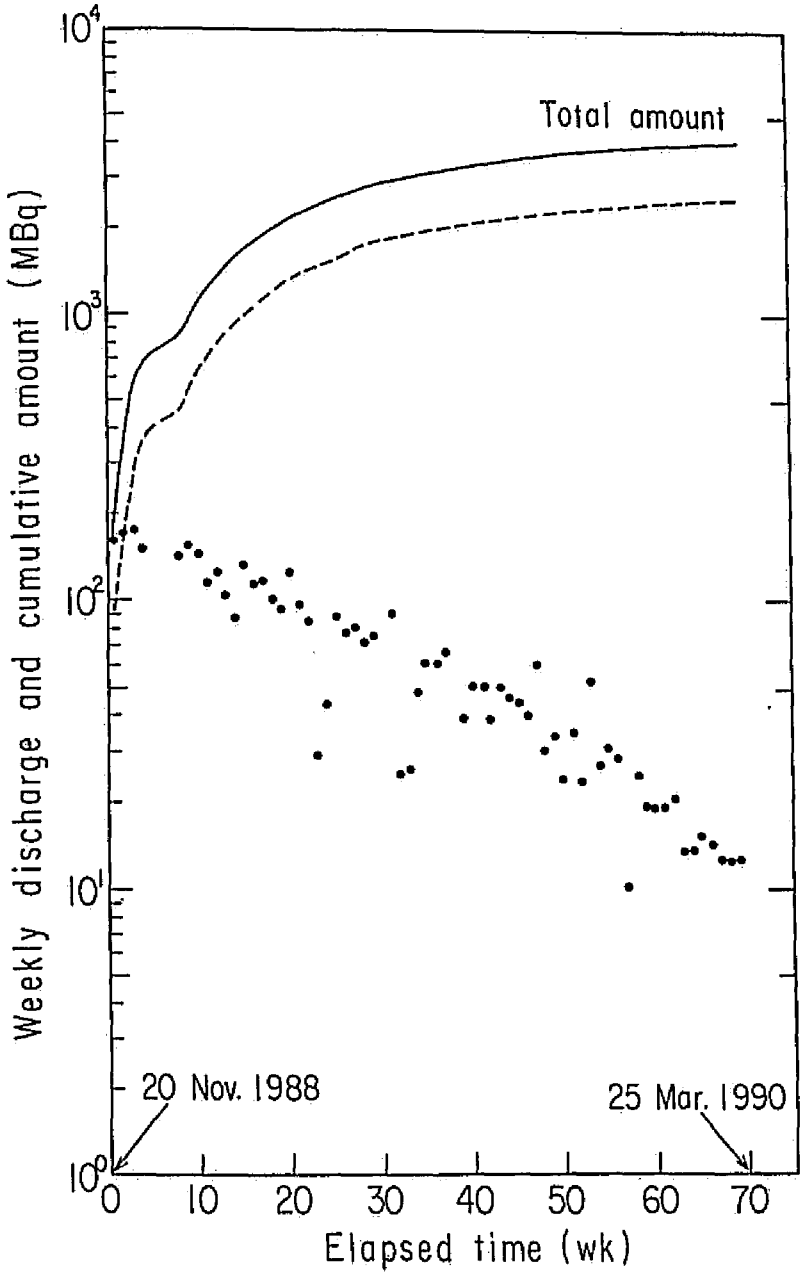

Fig. 3-11 Weekly discharges (closed circles) and cumulative amount (solid line) released by concrete material after removal of HTO sources in the containment building. The dashed line indicates the amount emitted from concrete after resumption of ventilation, which was calculated from the second term in eqn (3-20).

3．5 CONCLUSIONS

The following conclusions can be drawn from the environmental monitoring and the model development:

(1) Over a period of less than 1 y, the HTO concentrations in the water in the sub-pool (1.7 m^3) and of that in the primary coolant (30 m^3) increased by factors of ca. 60 and 5, respectively, due to the HTO leakage of 3.4×10^2 GBq (ca. 28.2 L heavy water) from the D_2O tank.

(2) The HTO increase in this water, followed by a decrease due to the removal of the sources of HTO in the reactor containment building can be explained by an exchange between water and vapor and by the dilution of the tritium-free water that had been lost by evaporation.

(3) Good agreement was obtained between the rate constants for the exchange and evaporation obtained by laboratory experiments using small glass dishes with HTO-containing water. This verified the HTO dynamics model between water and air.

(4) The model was able to predict the different levels in the increase of the HTO concentrations in the water in the sub-pool and the primary coolant, respectively, by adopting the same average concentration in the air of the containment building for these kinetic parameters. This gave a range of ambient concentrations (4×10^2- 6×10^2 Bq cm^{-3}) and can be used to determine the level of exposure to radiation by workers before the leak had been detected and before monitoring was started.

(5) With minor modification, the model showed that the decrease of HTO in the sub-pool water had a half-life of 15 wk and gave an average concentration of 3.6×10^1 Bq cm^{-3} for HTO vapor in air. This value fell well within the HTO concentration range

monitored over one year after removal of the sources of HTO.

(6) A significant amount of HTO vapor had been absorbed by the concrete construction material. This was discovered after noting increases in HTO vapor concentration in the air during the period of ventilation shut down, even after transferring and isolating all other HTO sources. The pattern of changes in HTO concentration, as influenced by the operation cycles of the ventilation system, was analogous to that of radon emanating from concrete.

(7) The amount of HTO absorbed by the concrete at a time when the HTO sources were isolated was estimated to be 4.2 GBq using calculations based on a model developed from the pattern of concentration changes according to the operation of the ventilation. This same calculational procedure revealed that the amount leaked during the retrieval of 4.6×10^{1} GBq from the graphite was 4.1 GBq.

(8) Monitoring of the air revealed that the amount of HTO absorbed in concrete over the period of ca. 20 mo decreased with a half-life of 20 wk after the main sources were removed in the containment building.

Chapter 4
RADIONUCLIDES IN COASTAL AREAS

4. 1 INTRODUCTION

More than 30% of the electricity in Japan was generated by nuclear power in 1990. Twelve nuclear power plants have been operated in the northern part of the Kinki district. As a result of a recent improvement of waste treatment techniques, liquid waste with a very low radioactivity concentration is only released as effluent into the coastal regions. Among some radionuclides detected in coastal sediments in the northern part of the Kinki district, only ^{60}Co and ^{54}Mn show quantitatively a spatial distribution (Yoshioka 1982) resulting from radioactive effluent of nuclear power plants on Urazoko Bay. Such pollution of the coastal environment will be a matter of great concern to the public from the view point of radiation protection. For this reason, and as the first stage in a continuing study, attention has been directed towards characterizing the partitioning of radionuclides in suspended particulate matter (SPM) collected at some coastal areas in the Kinki district. Some knowledge still remain to be acquired on the parameters affecting the transport of radionuclides released into a coastal area, though there are many reports on the sorption of radionuclides onto SPM and sediments (Duursma and Bosch 1970; Aston and Duurrsma 1973; Dawson and Duursma 1974; Alberts and Muller 1979; Cook et al. 1984; Higgo and Rees 1986). However, the radioactivity discharged into coastal areas from nuclear power plants, especially in Japan has decreased to approximately one-tenth GBq y^{-1} per plant. Such low releases have not led to high concentrations of radionuclides in the coastal sediments, in contrast to the released radioactivity of ^{60}Co of about one-tenth TBq y^{-1} as reported elsewhere (Ramberg 1984). Many reports exist on radionuclide adsorption on sediments

(Duursma and Eisma 1973; Means et al. 1978; Sibley and Myttenaere 1986), but there are few studies on the kinetics of radionuclide desorption from coastal sediments, which was focused on as the second stage of interest. Data from both types of studies are essential to understand the behavior of radionuclide across the sediment-water interface and to forecast long-term accumulation of these contaminants in coastal areas.

4. 2 PARTITIONING OF SOME RADIONUCLIDES ONTO SUSPENDED PARTICULATE MATTER

4.2.1 Objective and Scope

The principal objectives of this laboratory research are:

(1) To determine SPM content in water samples collected in some coastal areas, followed by the measurement of distribution coefficients for some radionuclides to compare the radionuclide affinity for an identical SPM sample; and

(2) To estimate the particulate radioactivity fraction on SPM, the size distributions of SPM and setting velocity of radionuclides, which may control the behavior of radionuclides in a coastal area.

4.2.2 Experimental

4.2.2.1 Samples and sampling locations

Water and SPM samples were taken on July 1978 at several coastal zones located in the Kinki district as shown in Fig. 4-1 (Fukui 1979). After flushing 20-L polythylene bottles with coastal water, surface seawaters were carefully sampled in these bottles so as to avoid water coming in contact with air. This enables to one minimize vigorous agitation by water-shaking during transport, which may cause decomposition of the SPM and destroy shapes of macroflocs. Sampling locations of surface seawater for determining the weight percentage of SPM by fractional filtration method are

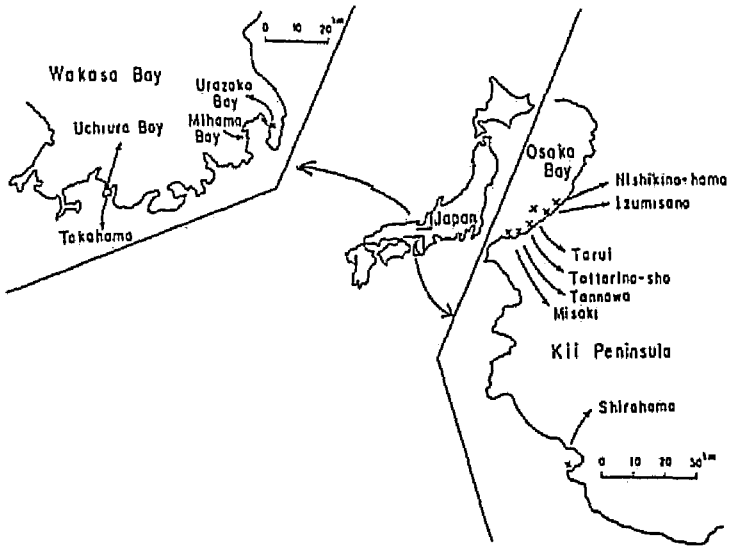

Fig. 4-1 Sampling locations of SPM in Kinki district.

as follows:

Six locations in Osaka Bay:

(1) Misaki (concrete tetra-pot),
(2) Tannowa (gravelly),
(3) Tottorino-sho (sandy),
(4) Izumisano (concrete tetra-pot),
(5) Nishikino-hama (sandy) and
(6) Tarui (5 km offshore).

Four locations at Shirahama:

(1) near Shirahama aquarism (sandy beach),
(2) near Shirahama aquarism (rocky),
(3) Shirahama Bay (1 km offshore) and
(4) Shirahama Bay (1.5 km offshore).

Two locations in Urazoko Bay:

(1) Yamatenoura (sandy) and
(2) Kamatanimoto (river mouth).

Sorption experiments of radionuclides were mainly conducted with the SPM collected from these water samples at Osaka Bay and one collected by using a plankton net of ca. 200 μm-φ at Shirahama and only stored in formalin. Plankton of about 100 mL

volume (wet) was also collected at Uchiura Bay using a plankton net. The organic matter content by combustion and the dry density were determined on this sample. The samples of coastal water and the wet SPM collected were stored in a refrigerator at ca. 5℃ to prevent excessive microbial activity in the laboratory.

4.2.2.2 Materials and methods

(1) Measurement of SPM contents and size distributions

To determine the SPM size distribution by the fractical filtration method, four kinds of filter papers (20, 5, 1 and 0.45 μm; 47 mm diameter) were set in a series. The same fractionation procedure was also used with three kinds of filter papers, excluding the 20 μm filter paper set in order of decreasing pore size, to examine the contribution of the first stage for the possibility of collecting SPM with smaller than the nominal pore size. Size distributions were determined in more detail using the Stokes diameters calculated, which were based on the relation between the settling velocity in distilled water and the differences of light transparency, in which the wet SPM collected on a filter paper was resuspended into distilled water after ultrasonic treatment (30 kHz) for defloculation for 3 min. The SPM density for the calculation of the settling velocity was determined using a pycnometer (Gay-Lussac's bottle) and the weight loss by combustion at ca, 400℃ for a few hours was used as an indicator of the organic matter content in the SPM.

(2) Radionuclides sorption by batch method

Coastal water samples filtered through the 0.45 μm membrane paper were spiked with a mixture of carrier-free or high specific activity of radionuclides (^{85}Sr, ^{137}Cs, ^{60}Co, ^{54}Mn and ^{65}Zn) and used as tracer solutions in the batch experiment. The wet SPM collected by filtering 10 L of coastal water through the 0.45 μm filter paper was carefully transferred into a 200 mL-tracer solution and stirred for a week. It is reported that the equilibrium of radionuclide sorption was attained for 7-d contact time by the sequential filtration procedure as described above (Nishiwaki et

al. 1965; Aston et al. 1973). Here, the weight of sea-salt and radioactivity on the filter papers together with the SPM were corrected by weighing the adsorbed water before and after drying the papers and the radioactivity concentrations of filtrate. Single (non-sequential) filtration was also conducted using the same SPM sample collected by filtration of 20 L of seawater, where the collected SPM was filtered separately through four kinds of filter papers with different pore sizes, as mentioned above. The distribution coefficient K_d, between radionuclide concentrations in SPM and water is conventionally defined as:

$$K_d \ (mL\ g^{-1}) = Q/C \qquad (4\text{-}1)$$

where Q: radioactivity in particulate fraction per unit mass of SPM, and

C: radioactivity in solution per unit volume of solution.

This parameter has also been referred to as the concentration factor, the partition coefficient, or the sorption factor when it does not imply equilibrium, and should be distinguished from K_s calculated by eqn (4-2), where the radioactivity in a solution is measured without filtering.

$$K_s \ (mL\ g^{-1}) = K_d \ (1 - r) \qquad (4\text{-}2)$$

where r is the removal ratio of radioactivity in solution by filtration. The final tracer concentrations for radionuclides in batch experiments were always less than 10^{-7} mol L^{-1}. The salinities of the tracer solutions were less than 30 ‰ and the pH was 8.1 ± 0.1. All experiments were performed at ambient temperature (28± 2 ℃) and in duplicate.

A Ge(Li) detector (58.5 cm^3) and Ortec 4K - γ-spectroscopy analyzer were used for radiometric assay of isotope mixure.

4.2.3 Results and Discussion

4.2.3.1 SPM concentrations and size distributions

The size distributions of SPM have not been determined in detail, especially of microflocs by filtration and/or by centrifugation. It was pointed out that macroflocs are loosely

bound and easily broken up by physical disturbances during sampling and size analysis. Sloot et al. (1981) used a continuous flow centrifuge to separate SPM into four size fractions, and reported that fractional weight percentage which contains relatively large particles (ca. 30 μm) with organic matter is more than 70%; however, the relation between particle size and that of the fraction is not clear.

Table 4-1 shows the SPM concentrations and the weight percentage of SPM in coastal water of 10 L filtered through papers with four nominal pore sizes. SPM(>20μm) at Osaka Bay contributed more than 70% and the contributions of lower size fractions (<20μm) were small. The values in parenthes is shown in this table indicate those obtained not by filtering entire water, but a 200 mL-tracer solution in which the SPM was resuspended for the partition experiment of radionuclides as mentioned earlier. Between these two filtering methods, Table 4-1 shows no significant differences in this trend, that is, the contribution of lower size fraction being small in the weight percentage of seston (SPM). Moreover, for the SPM collected at Tarui, the percentage of first fraction (> 5 μm) was nearly 90%, and the same as those percentages obtained for the first stage (20 μm) of four sequential filterings when three kinds of filter papers, excluding the 20-μm filter paper, were used in series.

Each size fraction for SPM collected at Urazoko Bay and Shirahama shows a smaller decrease in the weight percentage in the order of decreasing pore size than those samples from Osaka Bay (see Table 4-1). This may stem from the decomposition of SPM by microbial activity, as the water samples were not stored cool during transport to a laboratory. Terashima (1969) showed that the percentage of first fraction of coastal water sampled at Mihama Bay (see Fig. 4-1) with a 10μm milipore filter paper was ca. 50%, which is the same extent in those of the fractions (20 μm) for SPM at Shirahama.

It is interesting that SPM concentrations are higher in heavily populated areas; the maximum concentration is 6.27 mg L^{-1}

at Osaka Bay and the lowest is 0.89 mg L^{-1} at Shirahama (Table 4-1). Among samples taken at the seashore of Osaka Bay, the lowest concentration, 3.07 mg L^{-1} was observed at Misaki, a southern part which has a lower population density. A slightly lower concentration 2.93 mg L^{-1} was found at Tarui offshore, 5 km in Osaka Bay, the average concentration of the SPM is reported as 3.19 mg L^{-1} in Osaka Bay (CORC 1985). At Kamatanimoto, where the sampling site was the mouth of a small river, a rather high SPM concentration of 4.01 mg L^{-1} was found. High values in this low population area are likely because of the drainage from housing areas located upstream. This suggests that sampling locations should be carefully selected so that they are located beyond the sources of artificial pollution. After all, the SPM content in the coastal water near nuclear power plants can be estimated less than 2 mg L^{-1} of which value will be used as a parameter for scavenging in latter section.

Table 4-1 Concentrations of SPM in water and weight percentage by fractional filtration.

Sampling location	Total suspended matter (mg/l)	Weight percentage			
		Fraction			
		I (20 μm)	II (5 μm)	III (1 μm)	IV (0.45 μm)
Misaki	3.07(4.40)†	84.4(86.4)	6.4(3.2)	4.8(6.6)	4.4(3.9)
Tannowa	3.95(5.64)	90.4(85.1)	2.2(5.5)	2.8(6.4)	4.6(3.0)
Tottorino-sho	4.73(4.55)	83.1(86.6)	4.0(2.9)	3.6(7.5)	9.3(3.1)
Izumisano	6.27(5.37)	71.7(91.2)	15.1(2.4)	6.6(3.9)	6.6(2.2)
Nishikino-hama	4.08(5.32)	75.4(90.2)	6.6(1.3)	9.0(4.5)	9.0(4.1)
Tarui, offshore 5 km	(2.92)	—	(89.4)	(5.5)	(5.1)
Shirahama (sandy)	2.38	51.5	27.3	10.6	10.6
Shirahama (rocky)	0.89	51.9	14.5	18.9	14.5
Shirahama, offshore 1 km	0.92	60.1	17.9	8.9	13.1
Shirahama, offshore 1.5 km	1.55	59.7	25.5	8.3	6.5
Urazoko Bay (Yamatenoura)	1.71	36.7	20.4	25.4	17.5
Urazoko Bay (Kamatanimoto)	4.01	58.9	26.1	8.3	6.7

† Values in parenthesis indicate those obtained not by filtering entire water, but a 200 ml-tracer solution for sorption experiment.

For the measurement of the Stokes diameter, a significant difference in extinction is necessary in photo cell. Therefore, SPM collected in Osaka Bay through a 0.45 μm filter paper was resuspended. It is reported that homogenizing the sample by shaking produced similar distributions of microflocs which is reproducible and can not easily be reduced further in size (Eisma 1986).

The cumulative frequency curves vs. Stokes diameter are shown in Fig. 4-2 for five samples. It was found that the mean size of particles in suspension of surface water at the Ems river in Netherlands is less 10 μm (Duinker et al. 1985). Data in Fig. 4-2, however, reveals that more than 90% (Wt) of the seston is greater than 10 μm, and more than 80% (Wt) is less than 50 μm in size. The mass median diameter of SPM seems to be ca. 30 μm. This is roughly in agreement with the results obtained for the sequential fractionation method by filter papers.

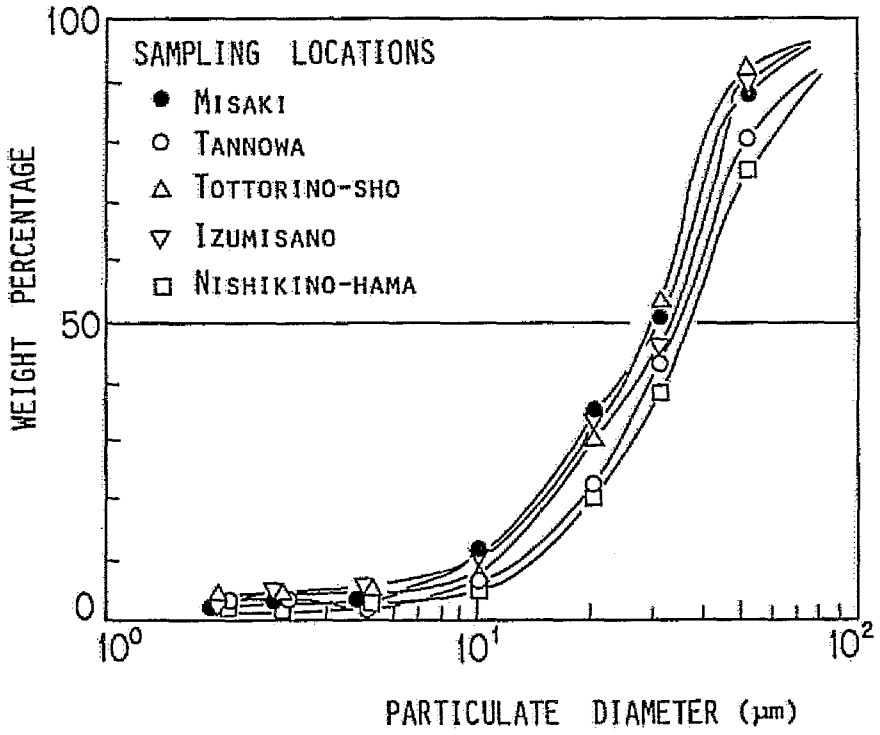

Fig. 4-2 Cumulative frequency curves of particulate diameter of SPM measured by the light extinction method.

Assuming the mass median diameter to be 30 μm and using the particle density of 1.1 - 1.6 g cm^{-3} obtained by drying, the settling velocity by the Stokes law can be roughly estimated to be 4.2 - 25 cm d^{-1}. Note that for a 10-fold increase in the size of particles, the settling velocity increases by an order of 10^2.

4.2.3.2 Distribution coefficients of radionuclides for SPM

Distribution coefficients, K_ds of five radionuclides on SPM obtained by fractional separation method are shown in Table 4-2. For the > 20 μm fraction, K_ds for ^{54}Mn, ^{65}Zn and ^{60}Co are the largest in comparison with smaller fractions, whereas no tendency on the magnitude of K_d could be seen for ^{85}Sr and ^{137}Cs. This fact suggests that radionuclides in particulate with a high K_d value are more retained onto a filter paper of first fraction because the smaller particle than the nominal pore size of filter paper set for the first stage may be trapped due to a decrease in effctive pore size during filtrtation. For the first size fraction in Table 4-2, the ratios K_s/K_d, ranged from 0.13 to 0.42 for ^{54}Mn, 0.66 - 0.92 for ^{65}Zn, 0.10 - 0.45 for ^{60}Co, and 0.88 - 1.0 for ^{85}Sr and ^{137}Cs.

In Table 4-2, K_ds for SPM, which was taken by a plankton net at Shirahama and stored in formalin for one week, is shown. The reason that K_ds is lowered by ca. two orders of magnitude for highly associated elements (^{65}Zn, ^{54}Mn and ^{60}Co) may stem from the inhibition of formalin on adsorption of transition metals as organic chelates and/or the lack of absorption by living organics. Low K_d values for ^{137}Cs with seston are certainly attributed to the high concentration of Na ion dissolved in coastal water.

The weight loss on combustion (at 400 ℃ for 3 h) of SPM sampled at Uchiura Bay was ca. 34%, and the ratio of clay to non-clay minerals in the dried SPM was estimated ca. 2. This suggests that the SPM contains much clay in comparison with that reported elsewhere (Duinker et al. 1985), which was obtained for the low concentrations of SPM. This may be attributed to the locations of sample collection performed in the bay.

Table 4-2 Distribution coefficients of radionuclides onto suspended particulate matter by fractional filtration.

Sampling location	Nominal pore size (μm)		^{85}Sr	^{137}Cs	^{54}Mn	^{65}Zn	^{60}Co
Misaki	20	K_d	3.4×10^{1}	1.4×10^{2}	1.7×10^{4}	2.4×10^{3}	2.1×10^{4}
		K_s/K_d	0.96	1.0	0.31	0.72	0.26
	5	K_d	6.9×10^{1}	1.3×10^{2}	1.5×10^{3}	1.5×10^{2}	1.9×10^{3}
	1	K_d	5.3×10^{1}	3.1×10^{1}	6.4×10^{2}	2.9×10^{2}	8.3×10^{2}
	0.45	K_d	7.6×10^{1}	4.2×10^{1}	4.2×10^{2}	1.4×10^{2}	2.7×10^{2}
Tannowa	20	K_d	2.1×10^{1}	7.3×10^{1}	6.4×10^{3}	1.4×10^{2}	6.0×10^{3}
		K_s/K_d	1.0	1.0	0.42	0.92	0.45
	5	K_d	2.0×10^{1}	5.9×10^{1}	1.0×10^{2}	5.4×10^{1}	5.9×10^{1}
	1	K_d	4.2×10^{1}	4.7×10^{1}	9.3×10^{1}	8.8×10^{1}	7.2×10^{1}
	0.45	K_d	1.0×10^{2}	5.2×10^{1}	1.4×10^{2}	1.8×10^{2}	1.8×10^{2}
Tottorino-sho	20	K_d	4.3×10^{1}	2.7×10^{1}	3.5×10^{4}	1.7×10^{3}	5.1×10^{4}
		K_s/K_d	1.0	1.0	0.13	0.73	0.10
	5	K_d	3.2×10^{1}	1.5×10^{1}	7.8×10^{2}	2.5×10^{2}	9.0×10^{2}
	1	K_d	2.8×10^{1}	1.9×10^{1}	4.4×10^{2}	2.4×10^{2}	9.7×10^{2}
	0.45	K_d	5.0×10^{1}	5.8×10^{1}	6.3×10^{2}	2.3×10^{2}	1.8×10^{3}
Izumisano	20	K_d	3.5×10^{1}	2.4×10^{1}	1.8×10^{4}	2.0×10^{3}	1.5×10^{4}
		K_s/K_d	1.0	1.0	0.19	0.66	0.24
	5	K_d	3.2×10^{1}	4.5×10^{1}	3.7×10^{2}	3.5×10^{2}	6.1×10^{2}
	1	K_d	3.2×10^{1}	5.5×10^{1}	3.2×10^{2}	3.9×10^{2}	5.2×10^{2}
	0.45	K_d	6.1×10^{1}	6.0×10^{1}	3.2×10^{2}	8.5×10^{2}	3.4×10^{2}
Nishikino-hama	20	K_d	2.8×10^{1}	2.1×10^{1}	1.1×10^{4}	2.0×10^{3}	2.1×10^{4}
		K_s/K_d	1.0	1.0	0.29	0.76	0.18
	5	K_d	2.6×10^{1}	1.7×10^{2}	5.2×10^{2}	4.2×10^{2}	1.0×10^{3}
	1	K_d	2.8×10^{1}	4.9×10^{1}	2.3×10^{2}	1.4×10^{2}	4.6×10^{2}
	0.45	K_d	2.5×10^{1}	5.5×10^{1}	1.5×10^{2}	2.0×10^{2}	2.2×10^{2}
Tarui	5	K_d	1.2×10^{1}	3.2×10^{1}	7.0×10^{3}	7.7×10^{2}	2.6×10^{4}
		K_s/K_d	1.0	0.94	0.25	8.81	0.09
	1	K_d	1.3×10^{1}	2.9×10^{0}	9.2×10^{1}	3.3×10^{1}	1.4×10^{3}
	0.45	K_d	7.7×10^{0}	2.2×10^{1}	1.2×10^{2}	4.1×10^{1}	4.7×10^{2}
Shirahama	20	K_d	8.4×10^{0}	1.6×10^{1}	1.8×10^{2}	5.5×10^{2}	6.9×10^{2}
		K_s/K_d	0.88	0.95	0.93	0.76	0.93
	5	K_d	1.4×10^{1}	1.8×10^{1}	8.4×10^{1}	3.1×10^{2}	5.2×10^{2}
	1	K_d	9.2×10^{0}	4.0×10^{1}	4.4×10^{1}	1.4×10^{2}	1.7×10^{2}
	0.45	K_d	2.1×10^{1}	3.2×10^{1}	2.9×10^{1}	2.3×10^{2}	2.0×10^{2}

It is necessary to recognize the difference in K_d values obtained by sequential fractionation with those from a single filtration using a specific filter paper.

Figure 4-3 shows that K_ds for resuspended seston from a single filtration with the 20 μm filter paper are much smaller than those for seston from smaller size fractions (5, 1 and 0.45 μm) which gave almost identical values for same radionuclides. The ratios of K_d for the 20 μm filter paper to the average for the other three were 0.56 for ^{85}Sr, 0.55 for ^{137}Cs, 0.64 for ^{54}Mn, 0.43 for ^{65}Zn and 0.65 for ^{60}Co, respectively (see Table 4-3).

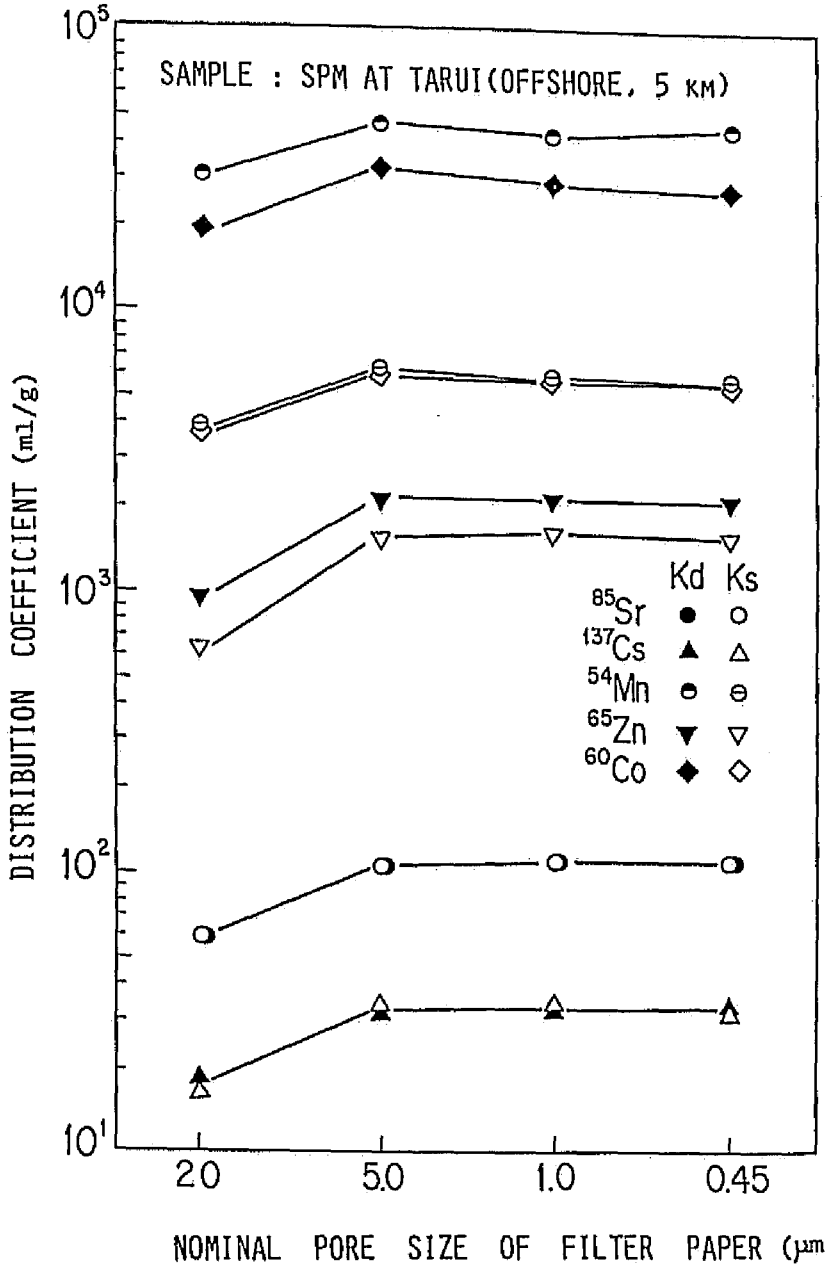

Fig. 4-3 Distribution coefficients of radionuclides for SPM in water of 20 L sampled at Tarui offshore (5 km), where the SPM collected was resuspended into a 800 mL tracer solution and each 200 mL of suspension was filtered by a single filtration method through four filter papers with different pore sizes.

So, it was revealed that the sequential fractionation method does not give the acculate K_d values when a 20 μm filter paper was used as a first stage in stead of a filter paper with a pore size less than 5 μm due to the less collection efficiency. This also indicates that the single separation by a 5 μm in stead of a 0.45 μm filter paper is recommended from a view point of expediting filtration.

Table 4-3 Distribution coefficients of radionuclides by single filtration using four kinds of filter paper.

Nominal pore size (μm)		^{85}Sr	^{137}CS	^{54}Mn	^{65}Zn'	^{60}Co
20	K_d	6.0×10^{1}	1.8×10^{1}	3.0×10^{4}	9.2×10^{2}	1.9×10^{4}
	K_s/K_d	1.0	1.0	0.13	0.67	0.18
5	K_d	1.1×10^{2}	3.3×10^{1}	4.8×10^{4}	2.1×10^{3}	3.2×10^{4}
	K_s/K_d	0.98	1.0	0.13	0.75	0.18
1	K_d	1.1×10^{2}	3.3×10^{1}	4.4×10^{4}	2.2×10^{3}	2.9×10^{4}
	K_s/K_d	1.0	1.0	0.13	0.76	0.19
0.45	K_d	1.1×10^{2}	3.4×10^{1}	4.6×10^{4}	2.2×10^{3}	2.8×10^{4}
	K_s/K_d	0.97	0.96	0.12	0.73	0.20
$\frac{K_d \text{ for } 20\ \mu m}{\text{Average } K_d \text{ for others}}$		0.56	0.55	0.64	0.43	0.65

SPM sample: Tarui offshore 5 km.

For samples at Osaka Bay, average K_d values (mL g^{-1}) for radionuclides, which were corrected for those in Table 4-2 with the collection efficiency of the filter paper mentioned above, are as follows:

^{85}Sr: $(5.8\pm1.5)\times10^{1}$, ^{137}Cs: $(1.0\pm0.9)\times10^{2}$,
^{65}Zn: $(3.8\pm2.0)\times10^{3}$, ^{54}Mn: $(2.8\pm1.6)\times10^{4}$,
^{60}Co: $(3.5\pm2.6)\times10^{4}$.

These average values are not so different from those for plankton reported elsewhere (IAEA 1985), except that the K_d values for ^{65}Zn in this study is an order in magnitude larger.

All distribution coefficients discussed above were corrected for the weight of sea-salt and radioactivity attached on a filter paper. Generally, a large volume of water samples and a filtration were required for monitoring of radioactivity in natural environment. Thus, it may be worthwhile to get another correction factor for an apparent distribution coefficient which may include errors arising from the filtration procedure. These correction factors determined for the single separation were also found to be different from those for a 20-μm filter and for the other three kinds of membrane filters (see Table 4-4). Small fluctuations of the correction factors among the three kinds of filters indicate that the actual K_d can be determined by multiplying the apparent K_ds with these averaged factors, that is, 0.39 for ^{85}Sr, 0.50 for ^{137}Cs, 0.35 for ^{54}Mn, ^{65}Zn and ^{60}Co, respectively.

Table 4-4 Ratios of actual K_d to apparent K_d which is not corrected for sea-salt and radioactivity attached on filter papers.

Nominal pore size (μm)	^{85}Sr	^{137}Cs	^{54}Mn	^{65}Zn	^{60}Co
20	0.33	0.65	0.22	0.46	0.22
5	0.41	0.51	0.36	0.37	0.37
1	0.37	0.48	0.34	0.34	0.37
0.45	0.38	0.51	0.35	0.34	0.35

SPM sample: Tarui offshore 5 km.

4.2.3.3 Particulate radioactivity fraction

It is important to distinguish between the 'particulate' and 'dissolved' radioactivities in the solution to recognize the difference of behavior between them. This has been pointed out by recent studies using K_d and the concentration of SPM (Fukui 1979; Assinder et al. 1985; Gschwend and Wu 1985). For a low concentration of SPM, the fraction of radioactivity as a suspension in the solution is given by the following equation (Fukui 1979):

$$\beta = (1 + 1 \times 10^{6} K_d^{-1} C_p^{-1})^{-1} \quad (4\text{-}3)$$

where K_d is defined in eqn (4-1) with units of mL g^{-1} and C_p is the mass of SPM per unit volume of solution (mg L^{-1}). The other version of this equation, involving terms with different units, have been given by a few researchers (Beasley et al. 1982; Shokovitz 1983; Assinder et al. 1985). Consider total radioactivity T both in solid and liquid phases,

$$T = Q\, w + (V_{sn} - v)\, C \quad (4\text{-}4)$$

where

w : mass of SPM,

V_{sn}: volume of suspension, and

v : volume of SPM in suspension.

Hence, the fraction of particulate radioactivity in coastal water is expressed as:

$$\beta = w\, Q/T. \quad (4\text{-}5)$$

Equation (4-5) can be used, when the volume of particulates, v, can not be ignored for higher SPM concentration, and finally expressed as:

$$\beta = (1 + 1 \times 10^{6} K_d^{-1} C_p^{-1} - K_d^{-1} \rho_p^{-1})^{-1} \quad (4\text{-}6)$$

where

ρ_p : particle density (g mL^{-1}).

As the term, $K_d^{-1} \rho_p^{-1}$, is usually much smaller than unity, eqn (4-6) reduces to eqn (4-3). In Table 4-5, particulate radioactivity fractions are given for rather high distribution coefficients obtained earlier; C_p value was assumed to be 2.0 mg L^{-1}, which seems to be the average SPM concentration in the non-polluted coastal water of the Kinki district.

Table 4-5 Particulate radioactivity fraction, β of radionuclides for SPM concentration, 2 mg L^{-1}.

	$^{85}Sr \fallingdotseq {}^{137}Cs$	^{65}Zn	$^{54}Mn \fallingdotseq {}^{60}Co$
K_d (mL g^{-1})	1×10^{2}	2.5×10^{3}	5×10^{4}
β	2×10^{-4}	5×10^{-3}	9×10^{-2}

Considering the settling velocity of 4.2 - 25 cm d^{-1} for 30 μm particles and the particulate radioactivity fractions, the role of SPM as a scavenger cannot be ignored because the scavenging phenomenon is persistent. This is especially true for radionuclides with large distribution coefficients, though the fraction, β, was at most 0.1 for ^{54}Mn and ^{60}Co. These parameters will be necessary for predicting the behavior, not only of radionuclides released from nuclear power plants, but also of other toxic metals originating from industrial wastes.

4.2.4 Conclusions

Following conclusions were drawn in this study:

(1) The SPM content obtained for coastal water were less than 2 mg L^{-1} for the samples collected from lower population density near nuclear power plants, and 3 - 6 mg L^{-1} from locations near in highly populated areas of the southern Kinki district.

(2) The mass median diameter of SPM was ca. 30 μm, and the estimated settling velocity was ca. 4.2 - 25 cm d^{-1}.

(3) Most SPM (70 - 90% Wt) in coastal water was retained on the initial filter of sequential fractionation using three or four stages and no significant differences in weight percentage of SPM collected could be seen between 20 and 5 -μm nominal pore size of the initial filter.

(4) Highest values of K_d were found in the first fraction of nominal pore size, 20 μm filter paper when filtering was performed sequentially with 20, 5, 1 and 0.45-μm filter paper. When the filtrations were not performed in series, however, but were conducted from the same tracer solution in parallel, the K_d values were identical for the smaller filter sizes (5, 1 and 0.45 μm) and were greater, by ca. 150% than those derived from the 20 μm filter paper.

(5) The degree of association of the radionuclides with SPM was $^{85}Sr < ^{137}Cs < ^{65}Zn < ^{54}Mn < ^{60}Co$ and the mean values of K_d for the SPM in Osaka Bay were $(5.8 \pm 1.5) \times 10^1$ for ^{85}Sr, $(1.0 \pm 0.9) \times 10^2$ for ^{137}Cs, $(3.8 \pm 2.0) \times 10^3$ for ^{65}Zn, $(2.8 \pm 1.6) \times 10^4$ for ^{54}Mn, and $(3.5 \pm 2.6) \times 10^4$ (mg L^{-1}) for ^{60}Co, respectively.

(6) The particulate radioactivity fraction of the SPM in coastal water was estimated at less than 0.1 for elements with the highest K_d value of ca. 5×10^4 (mg L^{-1}), which are highly associated with the SPM (2 mg L^{-1}). This scavenging effect by SPM might be, however, considerable, because it is persistent with the settling velocity.

4. 3 ASSOCIATION OF SOME RADIONUCLIDES WITH COASTAL SEDIMENTS

4.3.1 Objective and Scope

The objectives of this section are to:

(1) evaluate the impact of aqueous-phase composition on desorption of radionuclides from sediments;

(2) determine variations in distribution coefficients for radionuclides in the adsorption/desorption processes; and

(3) examine the decrease in radionuclide adsorption under suboxic condition.

4.3.2 Materials and Methods

4.3.2.1 Sorptive materials

Several samples of sea sediments, limnetic sediments, and a subsoil were collected for use in this study in summer 1980. Sampling locations are shown in Fig. 4-4. Sea sediments were sampled at Mihama and Takahama, located in Wakasa Bay of the Kinki district. These surface sediments (0-20 cm), designated as M and T, respectively, were taken from a water depth 2 - 30 m using an "Ekman Dredge" grab sampler. Sediment samples (designated as O_s) were taken at the site for the New Kansai International Airport at Osaka Bay. Sediments and seawater samples were stored at 2 - 5 ℃ to prevent the growth of microorganisms. Within a few days after sampling in summer 1980 (Fukui 1981a), these wet sediment samples were sieved in seawater to remove particles >2 mm in diameter (gravel, pebbles, and shells). The seawater used in the batch experiments was filtered through a 0.45 μm membrane. Sediments used in all batch experiments were not treated except for wet sieving.

Some limnetic sediments and a subsoil, which were designated as I and L, respectively, were sampled at the site of the KUR. The sample I-1 was taken from the bottom of the Ima-ike pond

outlet in the KUR site. Aquatic plants grow in this pond during the summer months, and as a result the sediment organic matter content is high (12% loss of weight on ignition). The sediment, I-2, was sampled from the waste water reservoir located upstream of the Ima-ike pond inlet.

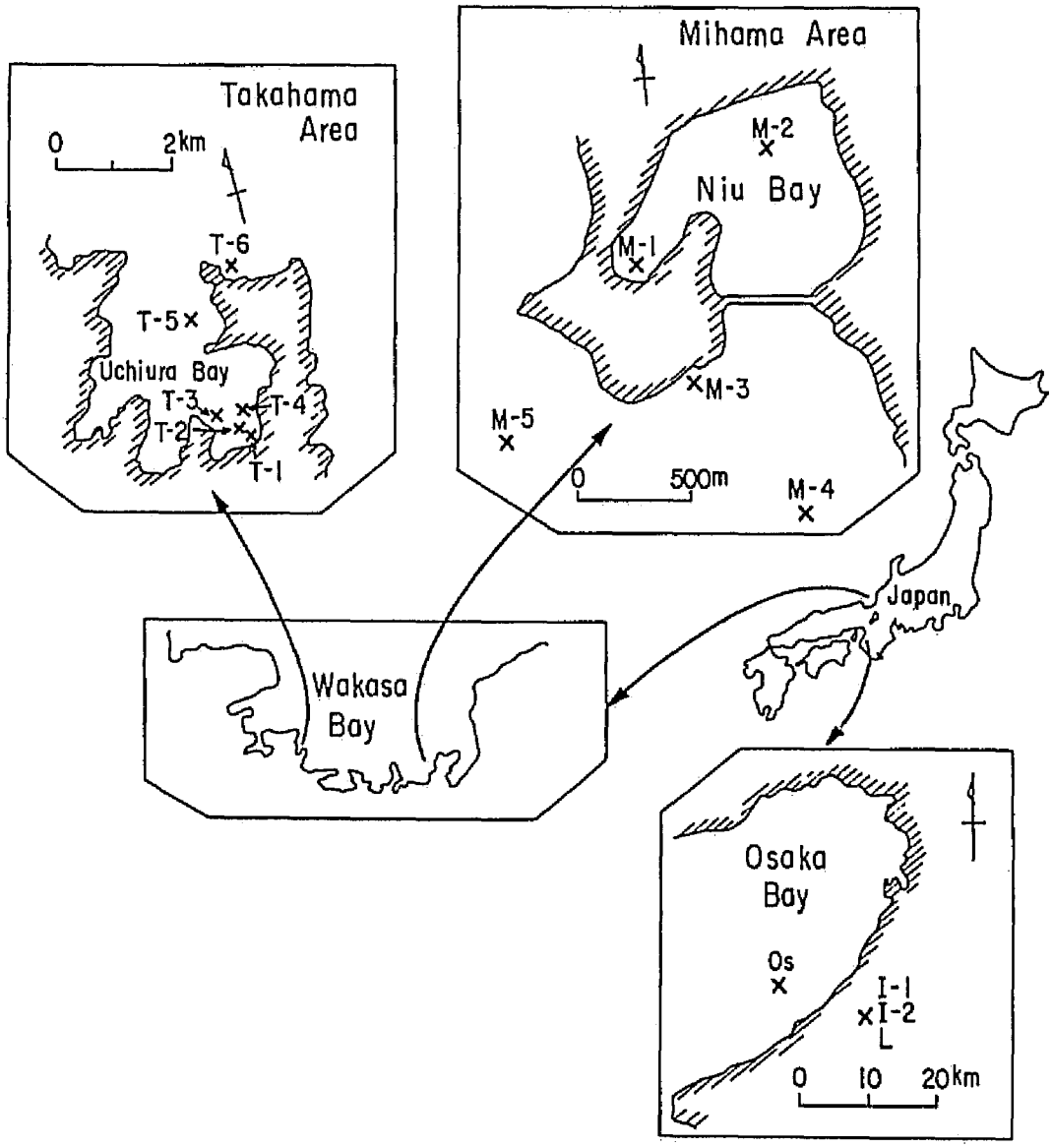

Fig. 4-4 Locations of sampling sites for coastal sediments (T-1 ~6, M-1~5, O_s), limnetic sediments (I-1, I-2), and a subsurface soil (L).

These limnetic samples, I-1 and I-2, were sieved wet using fresh water. The soil sample, L, taken 30-cm below surface was dried at 60℃ and treated using a 2-mm sieve. Unconfined groundwater at the soil sampling site is located about 1-2 m below the ground surface. These sediments and soil samples are classified by their texture as follows:

Coarse sand (2000 -250 μm): M-1, M-3, M-5, T-6, I-2
Fine sand (250 - 50 μm): T-1, T-2, T-3, T-4, T-5, M-4, L
Silt (<50 μm): M-2, O_s, I-1

Note that the numbers associated with each sample code name designate the location of the same sampling site as shown in Fig. 4-4. Color of wet samples was generally light brown for coarse sand, dark blue for fine sand and black for silt.

4.3.2.2 Trace metals and radiometric assay

Same radionuclides (^{85}Sr, ^{137}Cs, ^{65}Zn, ^{54}Mn and ^{60}Co) as used in section 4.2 were selected for use in this study because these trace metals are the major contaminants in effluents discharged from nuclear power plants located on the coastal areas of Japan. The final tracer concentrations of stock solution used for the experiments were carrier-free for ^{137}Cs and ^{54}Mn, and generally <0.01 mg L^{-1} ($<10^{-7}$ mol L^{-1}) for ^{85}Sr, ^{60}Co, and ^{65}Zn in the Cl^- soluble form. The radioactive concentrations of the solutions were usually adjusted to the order of a few tens of Bq mL^{-1} for each, and the five radionuclides were used as mixture in the solution.

A 5-mL solution was sampled into a polyethylene tube (5 cm in length, 1 cm in diameter), and radioactivity was measured using a Ge(Li) detector for 300 to 4000 sec to get sufficient total counts for a reliable calculation of the distribution coefficients.

Approximately 0.1-2 g of sediment or soil samples were placed in polyethylene tubes for radiometric assay, and 5 mL of 1N-HCl was added so that the volume and geometric conditions for solid samples in the counting tubes were similar to those of liquid

samples. Differences among K_{ds} values obtained from the solid:liquid ratio and those (K_{dl}) from the calculation using only the concentration change in the solution in the adsorption process were found to be insignificant, as shown in Fig. 4-5.

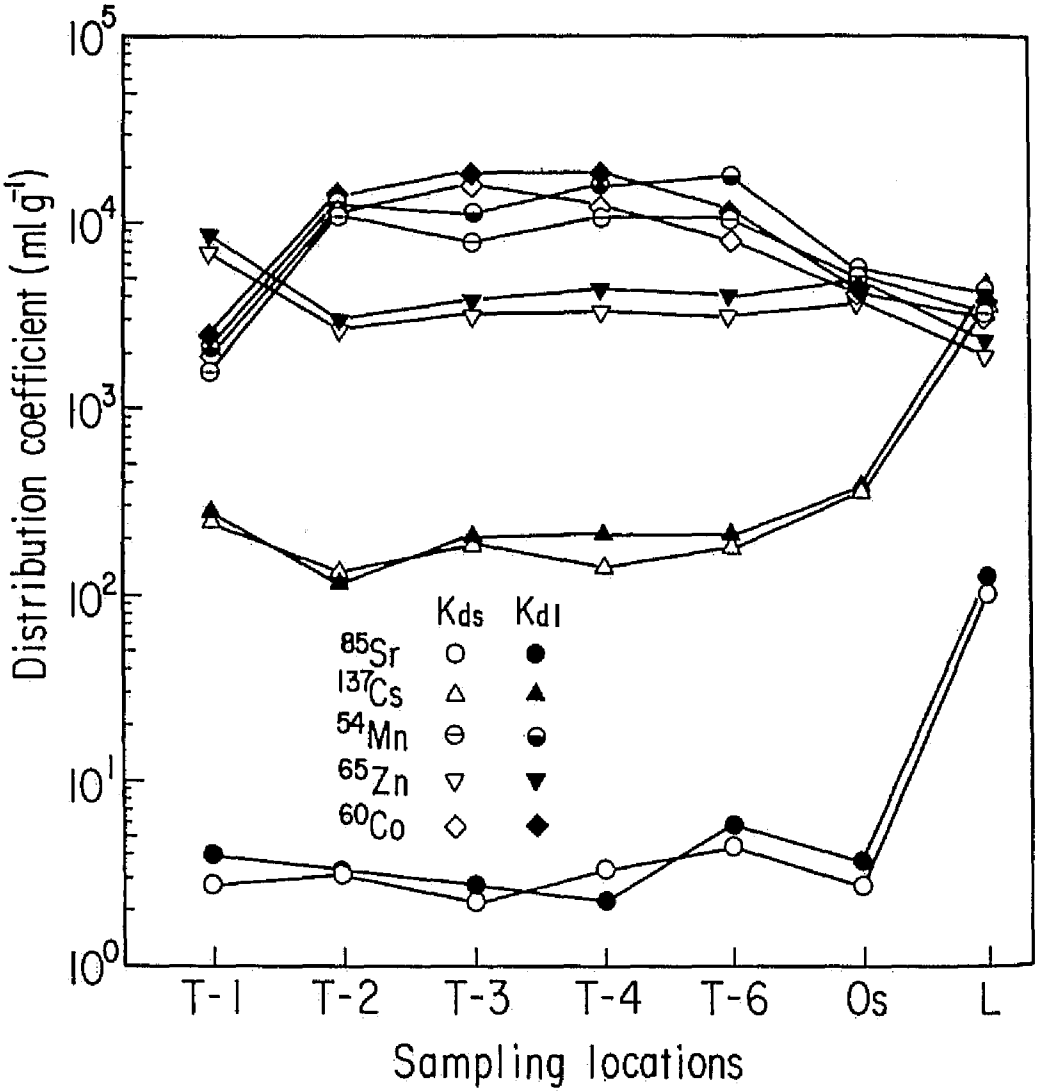

Fig. 4-5 Distribution coefficients obtained in the adsorption process both for the concentration ratio of soild:liquid (K_{ds}) and the concentration changes only in solution (K_{dl}) for various samples. Contact time : 2 wk.

4.3.2.3 Extracting solutions for desorption

Six types of aqueous solutions were used for studing desorption kinetics, as follows:

(1) seawater, fresh water, and groundwater were used for studying metal desorption under aqueous-phase composition found at the sampling locations;
(2) distilled water was used for examining the dissolution previously sorbed on solid phase;
(3) HCl (1 N and 6 N) was used for ascertaining metal desorption, destroying a part of the mineral lattices;
(4) ammonium acetate (1 M) was used for assessing the extent of readily exchangeable fractions;
(5) ammonium oxalate (0.2 M) was employed for studying desorption under suboxic conditions (Aoyama and Urakami 1982); and
(6) EDTA-2Na (0.01 M) was used for examing the possible formation of chelate compounds with the heavy metals in the solution.

4.3.2.4 Distribution coefficients and adsorption/desorption procedure in batch experiments

Desorption kinetics were examined using the two experimental procedure (A and B) described below:

A) About 50 g of sediment and soil samples were equilibrated in a 200-mL beaker, with stock solutions tagged with the five radionuclides mentioned above. Coastal sediments were equilibrated in seawater, pond sediments in fresh water, and a subsoil in groundwater. Intermittent shaking for a few minutes twice a day over a 2-wk contact period was allowed for equilibration. The sediments and soil samples were then washed quickly with distilled water to remove the excess tagged water attached to the samples, and ca. 2 mL of wet-tagged samples were transferred into 50 mL of the extracting solutions mentioned above.

These solid-liquid batch systems were allowed to equilibrate for more than 2 wk. For two days, these samples were allowed to settle without shaking to promote the removal of suspended

particles and to facilitate the filtration of supernatants. The extent of desorption was determined directly by measuring the ratio, ε (Q_e/Q_i), where Q_i and Q_e are the initial and final concentrations of radioactivity in the solid samples. The initial concentrations were determined for samples taken from the adsorption experiment. Samples T-1, T-4, T-6, O_s, I-1, I-2, and L, were used for this experiment.

B) The change in distribution coefficients was investigated by replacing a large volume of solution for extraction. For the first 2 wk, a sample of ca. 2 mL of untagged coastal sediments was initially transferred, using a syringe, into 50 mL of seawater tagged with five radionuclides for adsorption; 40 mL of solution was replaced by untagged seawater and allowed to settle for another 2 wk for desorption. The same dilution procedure was repeated two more times. This resulted in a 2-wk adsorption, followed by six weeks for desorption. The mixing procedure for batch systems for each two weeks is the same as that described in experiment, A.

The coastal sediments used in these experiments were: M-1~ M-5, T-2, T-3, and T-6. Only seawater was used as extracting solution (pH 8.1).

The values of distribution coefficients for both adsorption and desorption were calculated as follows:

$$K_{ad} = \{C_0/C - (V_0 + v_a)/V_0\}V_0/w \qquad (4\text{-}7)$$

$$K_{de} = \{C_0/C_i - (V_0 + v_a)/V_0\}V_0/w - V_dC_{i-1}/wC_i \qquad (4\text{-}8)$$

where

K_{ad}: distribution coefficient for adsorption calculated from the concentration change in the solution phase (mL g^{-1}),

C_0: initial concentration in the solution phase,

C : concentration in solution phase after a 2-wk period of adsorption,

V_0: volume of solution in batch: 50 (mL),

v_a: solution volume attached with the wet sediment sample (mL),

w : sediment weight in dry (g),

K_{de}: distribution coefficient for desorption (mL g^{-1}),
C_i: concentration in solution in batch just before the i-th time renewal of solution ($i > 2$), and
V_d: volume of solution renewed at a time: 40 (mL).

Desorption experiment B, was also performed with the minor revisions of bubbling N_2 gas after every new adsorption-desorption step into batch solutions for a few hours in order to evaluate the effect on radionuclide association under suboxic conditions. This procedure lowered the redox potential in solution by a few tens of mV.

Sediment pretreatment such as washing with fresh water or drying by heating was avoided in order not to change the physical-chemical-biological properties of the sediment:soil. The dry weights of the solid materials were obtained from the weight differences by heating a batch container after removing the solutions at the end of the runs. The solute concentrations in batch experiment, B, were measured without filtration to avoid contamination by radionuclides for the solution from the porous filter support, as at each desorption step, the solute concentrations were diluted by a factor of 0.2 (10 mL : 50 mL).

A two-day settlement of the batch system was enough to promote removal of suspended particles in a small volume of solution. An error in the measurement of solution concentration by the presence of suspended particulate matter (SPM) could be inferred from the fraction of particulate radioactivity, β, as expressed in eqn (4-6) in section 4.2. Figure 4-6 shows the β value to the variable K_dC_p, which is calculated by neglecting the third term, $K_d^{-1}\rho_p^{-1}$, which is usually much smaller than unity. As is clear in this figure, the β value is less than 0.1, provided that the K_dC_p value is smaller than 10^5. This indicates that the presence of SPM concentration of less than a few mg L^{-1} does not significantly affect the solution concentration, i.e., the K_{ad} and/or K_{de} for sediments obtained in a laboratory batch experiment, and no filtration procedure would be required for determining the K_d values.

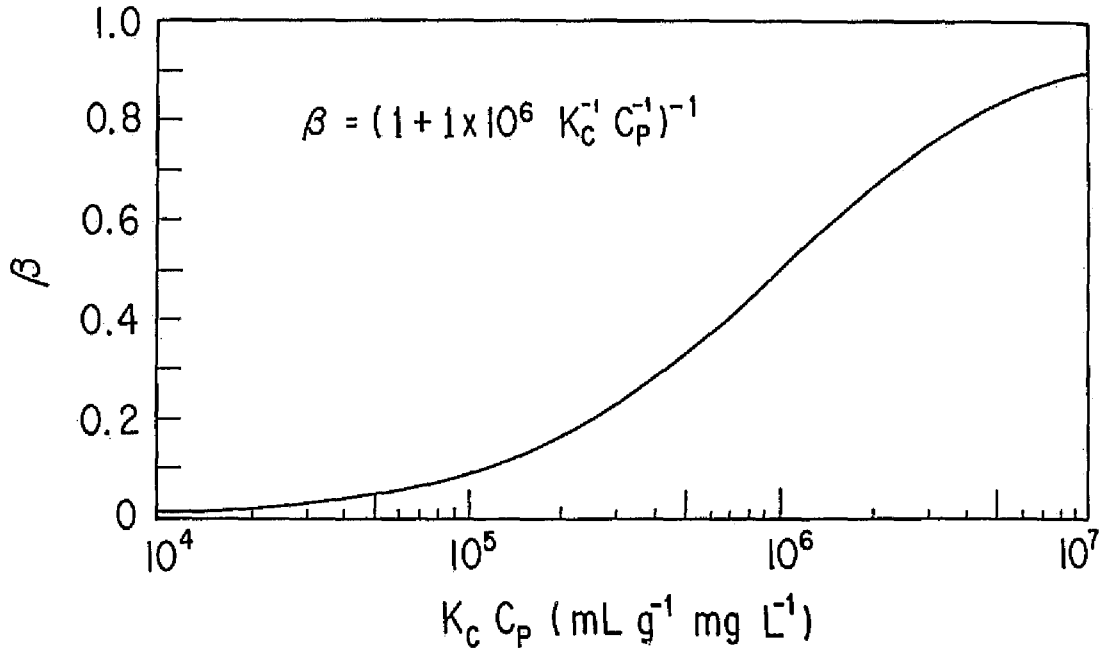

Fig. 4-6 Fraction of particulate radioactivity, β, in the solution vs. K_dC_p, where K_d (mL g^{-1}) is the distribution coefficient on SPM and C_p (mg L^{-1}) is the SPM concentration in the solution.

4.3.3 Results and Discussion

4.3.3.1 Radionuclide desorption into various extractant (Experiment A)

In Figs. 4-7, 4-8 and 4-9, data characterizing radionuclide desorption are shown as the ratio, ε (Q_e/Q_i). Figure 4-7 shows that for the limnetic samples (I-1, I-2, and L), it is difficult to desorb most of the tracer elements not only into distilled water but also into the limnetic water taken from the site. For coastal sediments, the ratio, ε obtained in distilled water are generally greater than those in seawater, especially for ^{85}Sr, which indicates that ion exchange as the sorption mechanism is important only for this element (Förtner and Schoer 1984).

Figure 4-7, however, suggests that for the other four radionuclides the ion-exchange mechanism cannot be dismissed as being similar to the chemical dissolution and physical sorption, because the ratio, ε, in seawater are somewhat lower than that in distilled water; that is, a slight effect of seawater containing sodium, potasium, and other divalent cations on the desorption can be seen. For sediment sample, T-4, the ratios, ε for all radionuclides, fall between 0.5 and 0.7 in distilled water. These values suggest that all radionuclides may loosely bind onto sediment coatings, because the same trend can be seen in other extractants such as HCl (Fig. 4-8) and EDTA-2Na (Fig. 4-9).

Figure 4-8 shows that more than 80 - 90% of the trace elements, except for ^{137}Cs, adsorbed on all samples were desorbed by HCl. The differences in the ratios obtained for ^{137}Cs by 1 N and 6 N HCl, indicate diffusion into the solid particles (Fukui 1978)

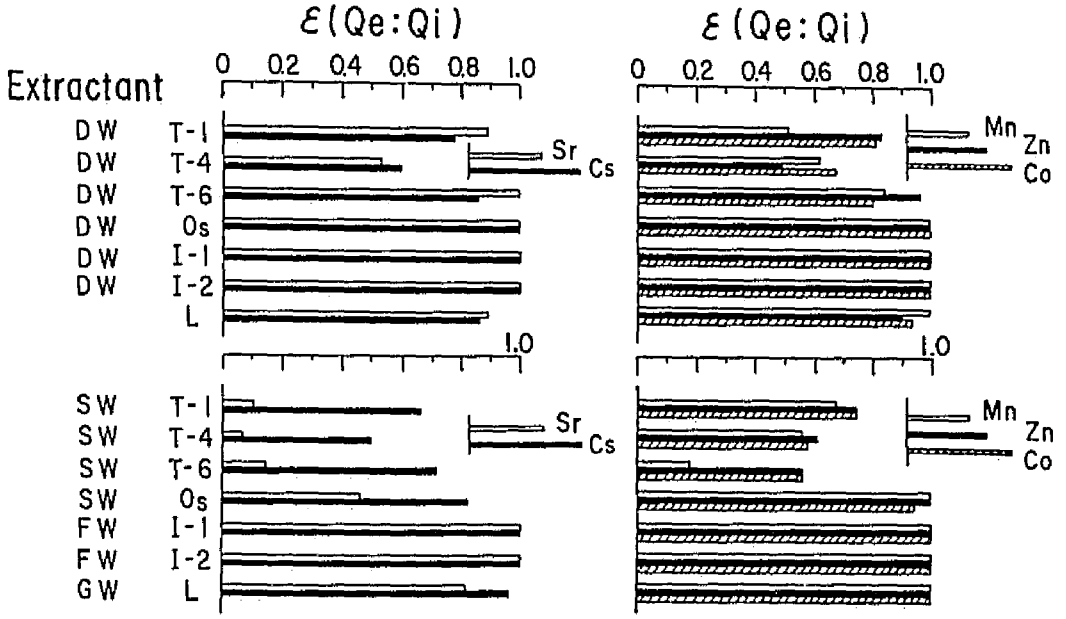

Fig. 4-7 The ratios, ε (Q_e:Q_i) of residual radioactivitiy after extraction to the amount sorbed initially.
Extractants: SW, seawater; FW, fresh water; GW, groundwater; DW, distilled water.

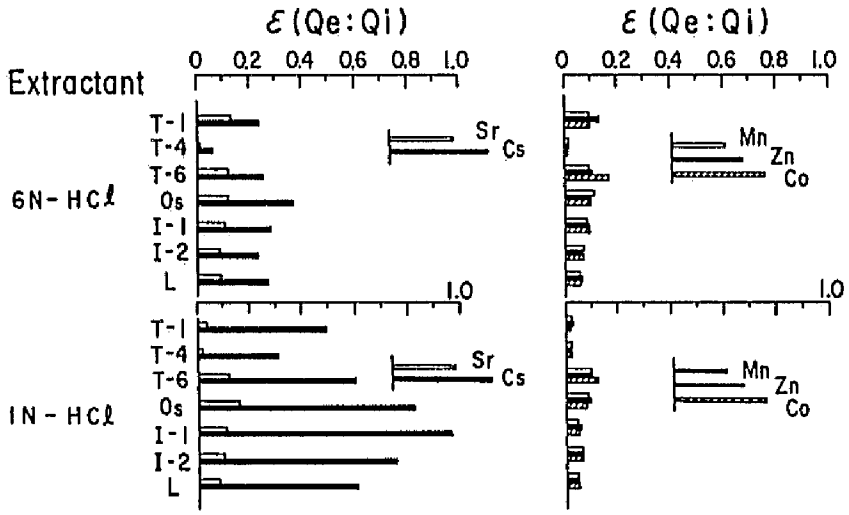

Fig. 4-8 The ratios, ε (Q_e:Q_i) are shown as defined in Fig. 4-7, where both 1 N and 6 N HCl solutions are used as the extractant in the desorption experiments.

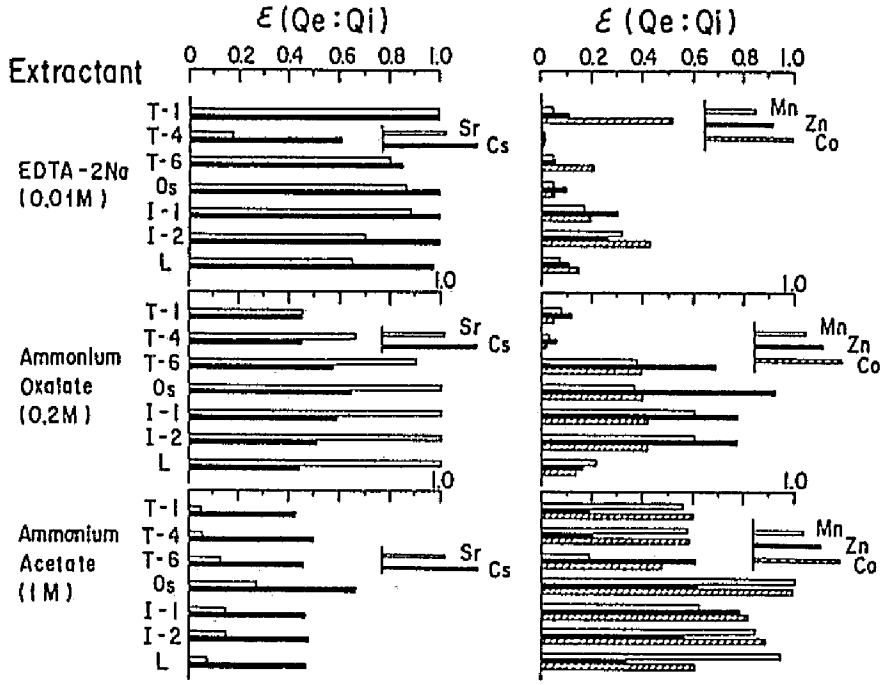

Fig. 4-9 The ratios, ε (Q_e:Q_i) are shown, where EDTA-2Na, ammonium oxalate, and ammonium acetate are used as the extractant in the desorption experiments.

because higher concentrations of HCl would destroy more of the lattice of solid particles, thus allowing ^{137}Cs to diffuse more readily out of the inter-granule regions into the solution. It was also reported that HCl could extract most of the transition metals absorbed on these samples by decomposing organometals and/or Fe- and Mn- oxyhydroxides (Koons et al. 1980). For heavy metals, the model of surface complexation is widely accepted in the field of aquatic chemistry, though in Fig. 4-8, $<10\%$ of adsorbed transition metals remain as a component of irreversible residues by HCl extraction.

Figure 4-9 shows the ratios, ε for five radionuclides desorbed with ammonium acetate, ammonium oxalate, and EDTA- 2Na. The ratios for ammonium acetate are smaller, especially for ^{85}Sr and ^{137}Cs, compared with those for the aqua-ecosystem water(seawaters, limnetic waters), as shown in Fig. 4-7. This data indicates that ammonium ion in this solution can more readily desorb trace metals adsorbed by the ion-exchange mechanism than by the sodium ion abundant in seawater.

The EDTA-2Na data in Fig. 4-9 show an opposite trend compared with that mentioned above; i.e., the ratios for ^{65}Zn, ^{54}Mn and ^{60}Co are much smaller than those for ^{85}Sr and ^{137}Cs. This indicates the complex formation of these three radionuclides with EDTA-2Na, which results in increased solubility. Manganese-54 and ^{60}Co are also easily desorbed by ammonium oxalate solution (pH 6.2, Eh 60 mV) due mainly to the suboxic condition that may decompose oxides and the co-precipitates on the sediment surface, followed by increasing the ionic strength in solution. Zinc was less desorptive in ammonium oxalate than ^{54}Mn and ^{60}Co. As a results, the degree of association of radionuclides in the following extractants with coastal sediments are:

ammonium acetate: $^{54}Mn > ^{60}Co > ^{65}Zn > ^{137}Cs > ^{85}Sr$
ammonium oxalate: $^{85}Sr > ^{65}Zn > ^{137}Cs > ^{54}Mn > ^{60}Co$
EDTA-2Na: $^{137}Cs > ^{85}Sr > ^{54}Mn > ^{65}Zn > ^{60}Co$

4.3.3.2 Change in distribution coefficients for sediments by successive dilution with seawater (Experiment, B)

In Fig. 4-10, the relative concentrations ($C_i:C_o$) of ^{85}Sr and ^{137}Cs in seawater are shown for desorption from eight sediments taken from different locations. Recall that in this series of experiments, sediments in seawater with initial concentration, C_o, were subjected to the adsorption step for the first 2 wk, followed by three successive dilutions, i.e., desorption steps, each also 2-wk long. Note that for each sediments, the time scale is shifted to the right hand side by 2 wk to avoid overlapping of curves presented in Fig. 4-10.

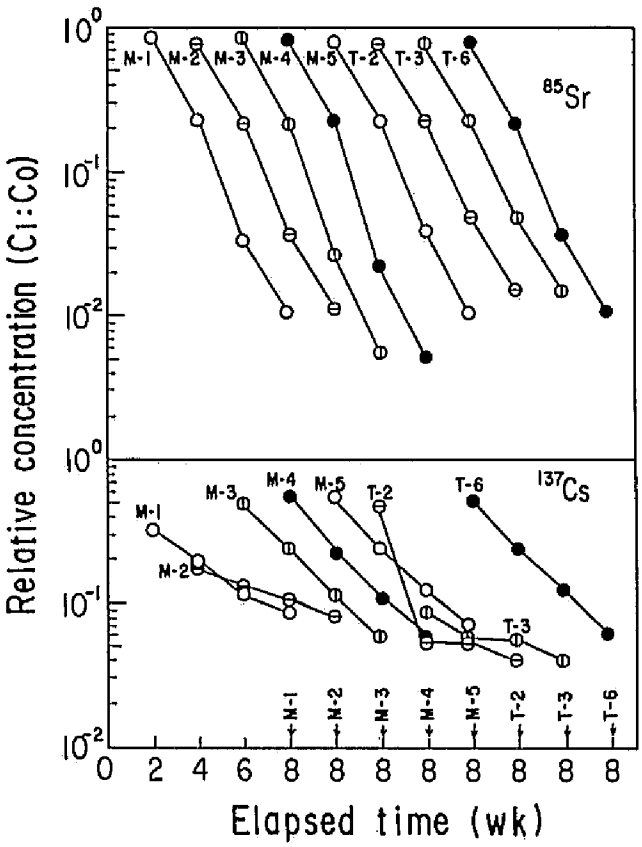

Fig. 4-10 Change in relative concentrations ($C_i:C_o$), where C_i is the concentration just before 40 mL of seawater in the batch was replaced every 2 wk, after ca. 2 mL untagged sediments were put into the tagged 50-mL seawater.

Strontium, which has a weak affinity for the sediments, shows the greatest decrease: the slope has a value of ca. 0.2, close to the dilution factor. The slopes for ^{137}Cs are less than those for ^{85}Sr because of slow desorption, controlled by intraparticle diffusion with slow reaction, which is verified by column experiments using distilled water and $CaCl_2$ aq. as leachants (Fukui and Katsurayama 1976a). This trend is more apparent for the sediments M-2, T-2, and T-3, which are abundant in silt.

Figure 4-11 shows the changes in the distribution coefficients for the adsorption step (K_{ad}; closed circle) and the desorption step (K_{de}; open circle), which were calculated only from the change of concentrations in the liquid phase, based on eqns (4-7) and (4-8). Most of the distribution coefficients become larger with each successive renewal of seawater, and the differences between K_{ad} and K_{de} values are usually one order of magnitude or so larger. This trend indicates somewhat irreversible desorption and/or disequilibrium except for ^{137}Cs, for which ratio, $K_{de}:K_{ad}$ was smallest. The ratios, $K_{de}:K_{ad}$ for ^{85}Sr were greater than 10 after successive dilution, though K_{ad} itself was smaller than 10 (mL g^{-1}) except for silty sediment, M-2. This may suggest the slow reaction of ^{85}Sr with metal-oxyhydroxide (Jackson and Inch 1980). The affinity of the radionuclides for the coastal sediments was as follows:

$$^{54}Mn \geqq {}^{60}Co > {}^{65}Zn > {}^{137}Cs > {}^{85}Sr$$

Most distribution coefficients, K_{ad}s, calculated from eqn (4-7) using only the concentration changes by the dilution in the aqueous phase, were at most two-fold higher than those obtained by direct measurements of the concentration ratio in the liquid-solid phases for these radionuclides (Fukui et al. 1989). This result is considered to be a rather good agreement between these methods for obtaining K_ds, and no serious effect of adsorption loss for these radionuclides onto the batch wall is shown.

Generally, the recovery ratio of radioactivity, ξ, by liquid and solid phases to that initially loaded in a batch can be derived by eqn (4-9):

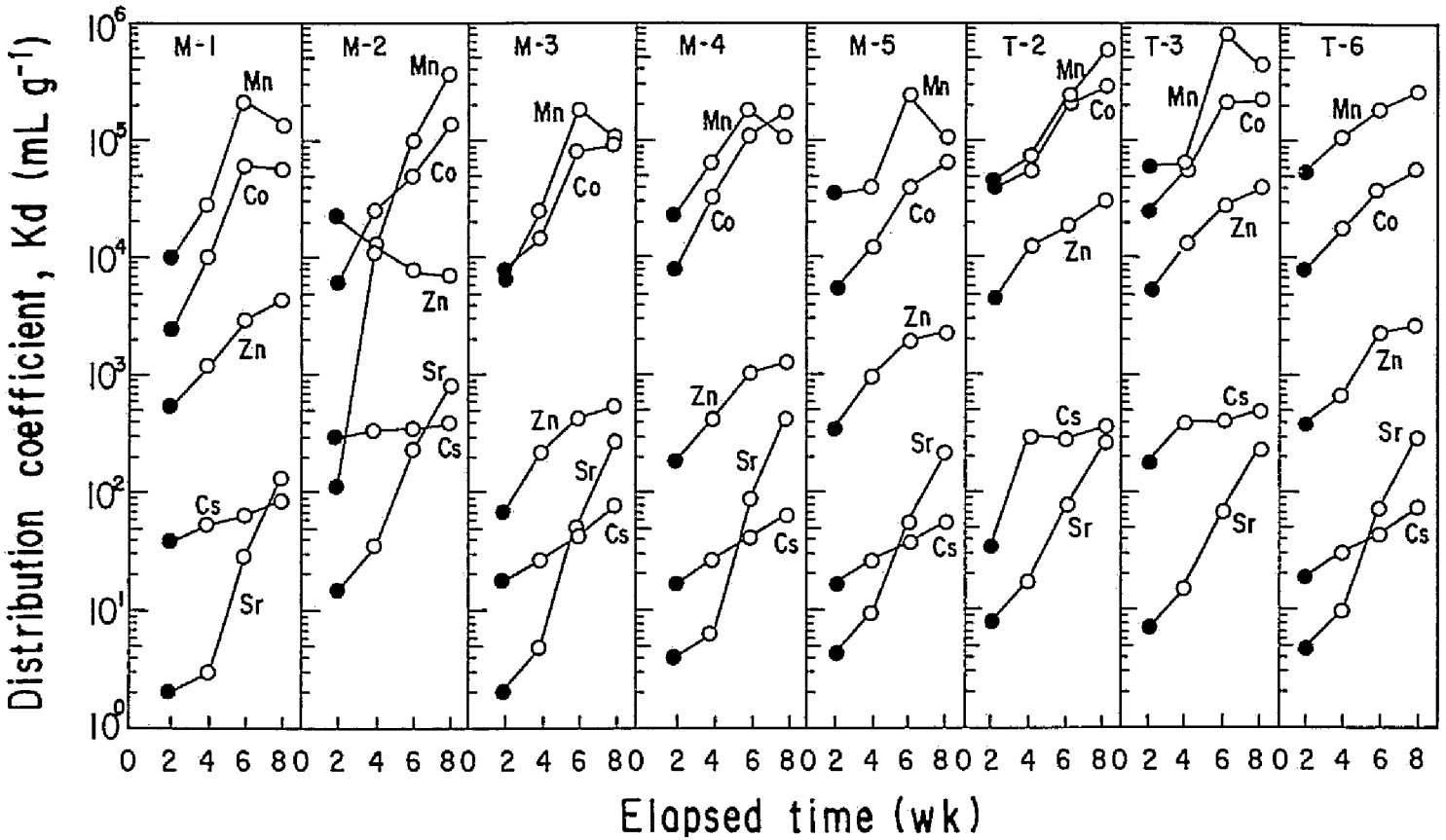

Fig. 4-11 Distribution coefficients obtained both for adsorption (K_{ad}: closed circle) and desorption processes (K_{de}: open circle), where 40 mL of seawater in batch were renewed every 2 wk.

$$\xi = (wQ + V_o C) V_o^{-1} C_o^{-1} \quad (4\text{-}9)$$

where

Q : radioactive concentration in solid phase (unit g^{-1});

C_o and C : inlet and outlet concentration (unit mL^{-1}); and

V_o and w : volume of solution (mL) and mass of sorbent (g).

Then, the activity loss to a batch wall a, could be expressed as:

$$a = (1 - \xi) C_o V_o \quad (4\text{-}10)$$

The ratio of the distribution coefficient, K_d'/K_d, can be derived as eqn (4-11) setting $v = 0$ in eqns (4-7) briefly, where K_d' is the apparent distribution coefficient calculated by ignoring adsorption loss to a wall, i.e., $a = 0$, and K_d is obtained after correction for the loss and/or by measurement of concentrations directly in liquid-solid phases.

$$K_d'/K_d = (1 - C/C_o)/(\xi - C/C_o) \quad (4\text{-}11)$$

Figure 4-12 indicates that the K_d' values estimated without correction for adsorption loss differ appreciably from K_d values when the relative concentration, C/C_o, after equilibrium is close

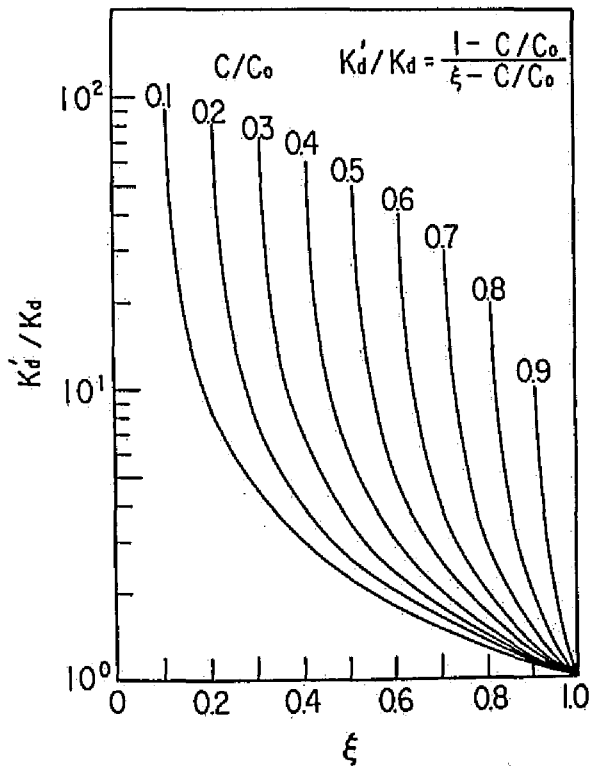

Fig. 4-12 Ratio of distribution coefficients, K_d'/K_d vs. recovery ratio, ξ, for batches. The value K_d' was estimated without correction for adsorption losses on walls and the correction was made for the K_d value.

to the recovery ratio, ξ. This means that the decrease of concentration C_o to C was caused by the adsorption loss on a wall and no adsorption took place on the geologic materials in a batch. It can also be seen that the larger the concentration change $(1-C/C_o)$, after the equilibrium is attained in the liquid phase, the greater the ratio (K_d'/K_d) for inherently small ξ values.

Suboxic conditions were achieved by bubbling N_2 gas for a few hours after adsorption and each subsequent desorption step (Fukui 1981a). Figure 4-13 shows the decreases in relative concentration of ^{60}Co measured under oxic (solid lines) and suboxic (dashed lines) conditions, where for each sediment the time scale is shifted again by 2 wk to the right, for the same purpose as in Fig. 4-10. The slopes of the ^{60}Co data are close to those of ^{85}Sr rather than ^{137}Cs, indicating the irreversibility of ^{60}Co in seawater once uptake has occurred because the changes of concentration for ^{60}Co in liquid phases approximately follow the dilution factor mentioned above. The same trend as shown in Fig. 4-10 for ^{85}Sr was due to a lesser amount of radiactivity adsorbed. The relative concentration for ^{60}Co for all sediments range between 1×10^{-3} and 1×10^{-1} under suboxic conditions, and between 2×10^{-4} and 1×10^{-2} under oxic conditions, which indicates that the distribution coefficients of ^{60}Co are smaller under suboxic condition.

In Table 4-6, the ratios K_d^o/K_d^s, that were obtained from both concentrations in liquid and solid phases under oxic conditions (K_d^o) and suboxic conditions (K_d^s), are shown for eight sediments. These ratios are usually smaller than unity for ^{85}Sr and ^{137}Cs and range between 2 and 10 for the other three radionuclides in the order $^{65}Zn<^{60}Co<{}^{54}Mn$. This indicates that the K_d^o values obtained for ^{85}Sr and ^{137}Cs become smaller under oxic conditions, due to the decrease in adsorption sites by ion-exchange mechanisms because of the existence of oxide coatings, whereas Fe-oxides, oxyhydroxides, and other coatings on sediment surfaces would decompose gradually, followed by a decrease of association for transition metals under suboxic conditions.

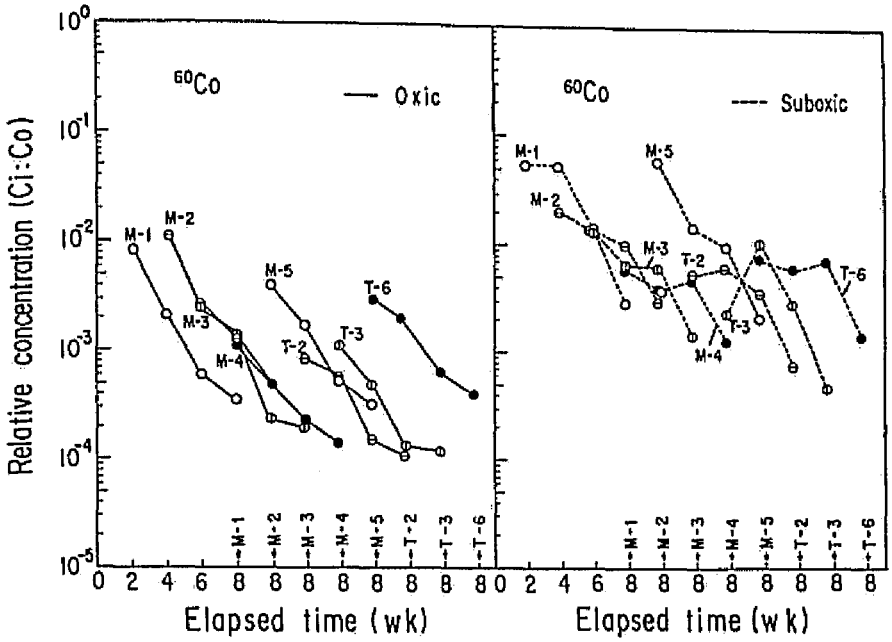

Fig. 4-13 Change of relative concentrations (C_i/C_o) for ^{60}Co both in oxic and suboxic conditions, where the experimental procedure is the same as that in Fig. 4-10.

Table 4-6 Ratios of distribution coefficients obtained for oxic conditions (K_d^o) to those for suboxic conditions (K_d^s).

Sample	^{85}Sr	^{137}Cs	^{54}Mn	^{65}Zn	^{60}Co
M-1	0.93	0.54	8.7	4.4	7.4
M-2	0.30	0.26	2.3	0.57	3.5
M-3	2.66	0.35	6.3	2.3	8.1
M-4	1.77	0.33	9.0	3.5	8.0
M-5	0.59	0.30	7.6	1.9	5.2
T-2	0.77	0.39	13.3	2.3	7.1
T-3	0.35	0.41	7.5	1.7	2.4
T-6	0.74	0.33	12.8	2.9	4.6
Average (K_d^o/K_d^s)	1.01 ±0.81	0.36 ±0.09	8.5 ±3.5	2.4 ±1.2	5.8 ± 2.2

4.3.4 Conclusions

The kinetics of radionuclides adsorption/desorption from artificially spiked environmental solid samples were examined by batch experiments using six types of aqueous solutions for extraction. The essential sorption mechanisms for retension were shown to be mainly ion exchange for ^{85}Sr in the early stage of sorption, though the small amount on sediments showed some irreversible sorption, and both ion exchange and intraparticle diffusion for ^{137}Cs.

For ^{54}Mn, ^{60}Co, and ^{65}Zn, the combination of ion exchange and complexes with organic ligands appeared to have some effect on the sorption and/or metal-oxyhydroxides. These sorption mechanisms were also inferred from similar patterns in desorption of trace metals for successive dilution with aqua-ecosystem water, ammonium acetate and EDTA-2Na solutions.

The affinity of trace elements for coastal sediments was in the order of $^{54}Mn \geqq ^{60}Co > ^{65}Zn > ^{137}Cs > ^{85}Sr$ in seawater.

Hysteresis in sorption was observed for these elements, as indicated by larger distribution coefficients measured for desorption than for adsorption. Most ^{85}Sr is easily desorbed by seawater; however, the ratio of distribution coefficient (K_{de}/K_{ad}) observed with a successive dilution method was greatest for ^{85}Sr (which may be adsorbed by irreversible and non-exchangeable mechanisms) and smaller for ^{137}Cs (likely due to slow reaction controlled by intraparticle diffusion).

For ^{54}Mn and ^{60}Co especially, the trend of decreasing distribution coefficients was observed in suboxic conditions both in adsorption and desorption processes. These results, especially the fact of hysteresis suggest that for the radionuclide migration in sediments an irreversible reaction should be considered in the model expression, which will be dealt with in the following section.

4. 4 PREDICTING THE FATE OF COBALT-60 IN A COASTAL AREA

4.4.1 Objective and Scope

An assessment of spatial distribution of sediment pollution resulting from radionuclides released from nuclear energy facilities into coastal areas only from the results of environmental monitoring is difficult in Japan due to the low discharges. Therefore, an assessment for regional pollution in Uchiura Bay, located in northern part of the Kinki district, was performed by using a mathematical model with available parameters to predict the accumulation trends of radionuclides, especially in sediments. Calculation also addressed estimating the ratio of the amount present in the bay sediment to that lost from the bay, and making sure the attainment of equilibrium of radioactivity between coastal water and sediments as well as in Urazoko Bay (Fukui et al. 1989c).

4.4.2 Site and Currents

4.4.2.1 Site

Since 1974 liquid wastes with extremely low concentrations have been discharged from the Takahama Power Station, unit No. 1 (PWR Type, 826 MW, designated as TPS-1) into Uchiura Bay (1.2 km width, 4 km length, and 7.6 km^2). Since 1975 another nuclear reactor of the same type (TPS-2) has been operated at the same site. These plants are located to the south-east of Uchiura bay, i.e., the south-west of the Otomi peninsula as shown in Fig. 4-14. Secondary coolant, ca. 77 $m^3\ s^{-1}$, taken from the east side of the Otomi peninsula has been released into Uchiura Bay via these plants and no other comparable flows exist in the bay. The additional Power Plants, unit No. 3 and No. 4 were constructed in 1982. Secondary coolant from these plants has been discharged in different manner from unit No. 1 and No. 2. This resulted in altering the steady-state flow pattern in the bay, hence the calculation for the

assessment in this project was carried out for the duration of a 8-y period of FY 1974-1981.

4.4.2.2 Steady-state current vectors

For the long-term estimation of pollutants in coastal areas, the steady-state current vectors are more important than the short-term non-steady currents caused by the tidal wave and/or the wind-forced wave. In the surveyed area, the Fishery Laboratory, Fukui prefecture and the Agency of Fishery have investigated the current flows by conducting the buoy trace tests which showed that the elevation of surface water temperature near the discharge point was ca. 5-7 ℃; flows first towards the north-west, and then towards the mouth. As a result, stratified counter currents exist in the lower layer. The boundary of the interface between these two layers was observed ca. 10 m deep in the summer season. For shallow reaches where no stratification is expected, and in this study sixteen compartments, as shown in Fig. 4-14, were adopted together with the convective-diffusive equation.

Prior to predicting the contaminant spread in the bay, the continuity equation was used to reproduce the convective flows on the basis of water mass conservation for the two stratified water layers by taking into consideration the topography of the sea bed. The obtained current vectors showed an average flow of ca. 5 cm s^{-1} towards the north near the center of the upper layer as shown in Fig. 4-14. Figure 4-15 shows the flow vectors obtained for the lower layer. On the whole, the calculated flow vectors agreed well with the observations based on the buoy trace tests and reproduced the two-layer flow model; the maximum velocity observed near the surface of upper layer were, however, ca. three-fold faster than the calculated velocity due to the averaging through the depth of the layer.

The origin of the Cartesian coordinate system for the investigated area is set at 35° 31′ north latitude, and 135 ° 28′ east longitude, and the x, y axes are directed clockwise by 24° .

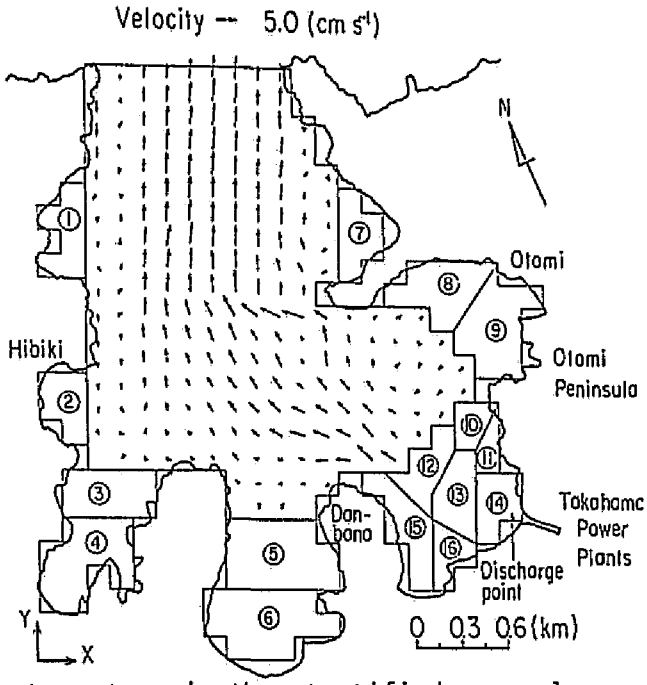

Fig. 4-14 Current vectors in the stratified upper layer, which were represented by solving the continuity equation. Numbers 1-16, show compartments considered in the box model.

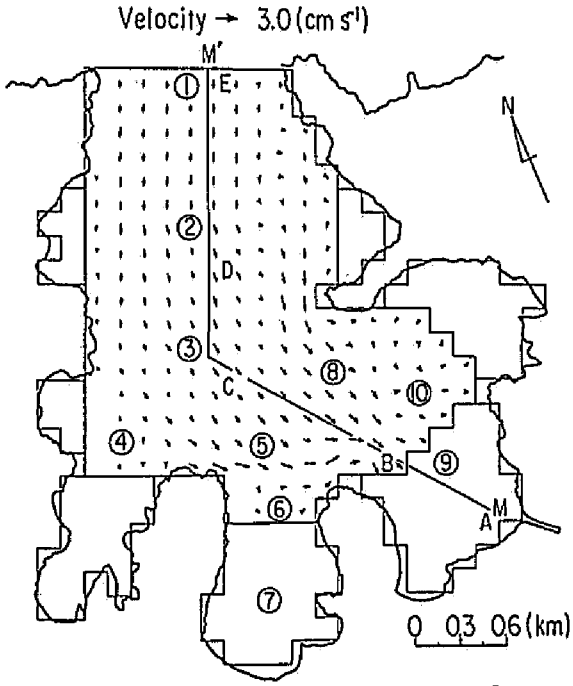

Fig. 4-15 Current vectors obtained for the lower layer. Numbers 1-10, show sampling locations of sediments.

4.4.3 Assessment Model

4.4.3.1 Dispersion equation

The advective-dispersion equation for turblent, incompressible flow of a conservative solute is generally expressed as:

$$\partial (h\,C)/\partial t = -\partial (M_x C)/\partial x - \partial (M_y C)/\partial y - h\,\partial (w\,C)/\partial z + \partial h/\partial x\,(K_x\,\partial c/\partial x) + \partial h/\partial y\,(K_y\,\partial c/\partial y) + \partial h/\partial z\,(K_z\,\partial c/\partial z) - R_v - R_d - R_a \qquad (4\text{-}12)$$

where

- C : concentration in water (unit cm^{-3}),
- h : water depth of the upper/lower layer (cm),
- M_i : i component of the integrated flow velocity, i.e., $\int u\,dx$ or $\int v\,dy$ ($cm^2\ s^{-1}$),
- u, v, w : x-y-z-component of flow vector ($cm\ s^{-1}$),
- K_i : i component of the eddy diffusivity ($cm^2\ s^{-1}$),
- R_v : scavenging rate (unit $cm^{-2}\ s^{-1}$),
- R_d : radioactive decay rate in water (hC), i.e., λhC (unit $cm^2\ s^{-1}$), and
- R_a : sink rate of radioactivities for the lower layer by the sorption of sediments (unit $cm^{-2}\ s^{-1}$).

4.4.3.2 The equation for sorption by sediments

As shown in Fig. 4-16, the sediment layer is modeled by dividing it into three zones based on observations of radionuclide profiles. The uppermost part of the sediment is assumed to be well mixed and the concentrations in the interstitial water were set equal to those in the overlying water in the lower layer. Below this mixing zone, the diffusivity in the middle part of sediment, including the impacts of the agitation effect by inner wave and/or bioturbation, was accomodated by assigning a value two orders of magnitude larger than molecular diffusion coefficient. The molecular diffusion coefficient, $4\times10^{-6}\ cm^2\ s^{-1}$, was adopted in the lowest zone of the interstitial water. Instantaneous equilibrium for cobalt was assumed between water and sediments in the uppermost zone, and an analytical solution (Fukui et al. 1981b) for

diffusive substances in reactive porous media was adopted to estimate the amount sorbed in the two stagnant zones.

In this study the two-site sorption model was adopted, i.e., expressing the association of radionuclides with sediments by the equation of the so-called linear isotherm for the fast adsorption superimposed with the irreversible first-order kinetics for the slow reaction such as precipitation, reactions with oxides and mineralization. This coupled equation is expressed as:

$$\partial Q / \partial t = \partial Q_h / \partial t + \partial Q_f / \partial t \qquad (4\text{-}13)$$

where

Q : total amount sorbed to sediments (unit g^{-1}),

Q_h : amount sorbed by linear isotherm relation, (unit g^{-1}), that is, $Q_h = K_d C$, and

Q_f : amount sorbed irreversibly by the first-order kinetics, (unit g^{-1}), i.e.,

$$\partial Q_f / \partial t = k C \qquad (4\text{-}14)$$

where

k : rate constant for the first-order reaction, ($cm^3\ g^{-1}\ s^{-1}$).

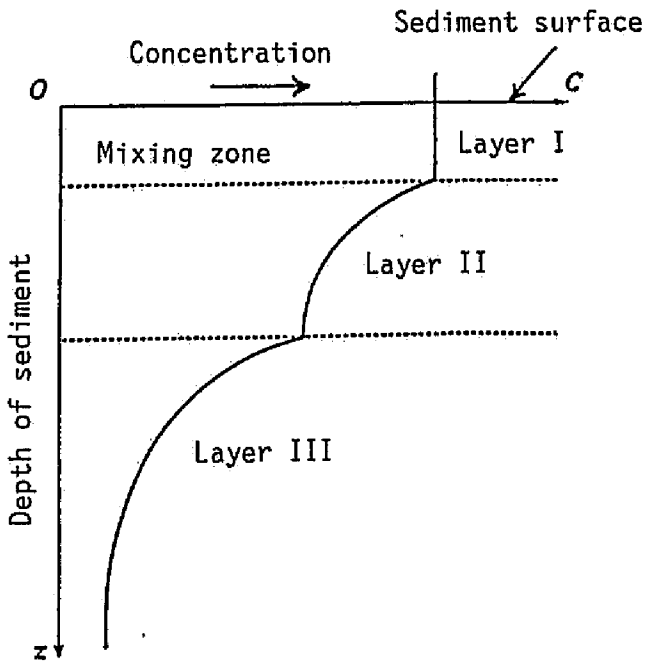

Fig. 4-16 Modeling the sediment region for assessment.

4.4.3.3 Modeling the compartments

Mass balance equation between compartments in the shallow reaches, as shown in Figs. 4-14 and 4-15, are expessed as:

$$\partial S_i / \partial t = -\delta S_i - \lambda S_i - \Sigma \mu_i S_i + \Sigma \mu_j S_j + q \qquad (4\text{-}15)$$

where

S_i : radioactivity at time t in the i^{th} compartment (unit),
S_j : radioactivity at time t in the j^{th} compartment (unit) adjacent to the i^{th} compartment,
δ : rate of dilution in the i^{th} compartment (s^{-1}),
λ : rate of loss due to decay (s^{-1}),
μ_i : rate of transfer from the i^{th} compartment (s^{-1}), ($i \neq j$)
μ_j : rate of transfer from the j^{th} compartment (s^{-1}), and
q : rate of new input to or loss from compartment i.

The estimated amount of radioactivities obtained from eqn (4-15) at each time step is converted to the concentration in each compartment considering the topography of the sea bed, i.e., the volume of the boxes, and used as the boundary concentrations for solving eqn (4-12).

4.4.4 Parameters for Assessment

4.4.4.1 Diffusion/Dispersion

The dispersion will be a function of many factors such as geomorphology, wind forced waves, tides and salinity, which may vary within and between seasons. The values of the order of 10^5 - 10^6 cm^2 s^{-1} were estimated and used for the dispersion coefficient in the Irish Sea and in the North Sea (Plandle 1984). The values 10^3 - 10^6 $cm^2 s^{-1}$ depending on the time elapsed after observations are obtained for the open coastal area of Tokai, Japan (Fukuda 1980). The dispersive effect may be small in the semi-closed bay such as Uchiura Bay as shown in Fig. 4-14. Horizontal dispersion coefficients, K_x and K_y of 10^4 cm^2 s^{-1} were adopted in this area.

The dispersion experiment in vertical direction is difficult because the oceanic structure is more complex. In this study, the

coefficient of vertical dispersion was assumed to be 3×10^{1} cm^2 s^{-1}, based on the following values: 7 cm^2 s^{-1} at 10 m depth of Tokai offshore (Fukuda 1975) and 1 to 200 cm^2 s^{-1} in the South Pacific Ocean (South Pacific Commission 1983).

4.4.4.2 Scavenging of radionuclides

The rate of loss of radioactivity due to the settling of particulate matter suspended in water, which appeared in eqn (4-12), is generally expressed as:

$$R_v = \beta v_s C \qquad (4\text{-}16)$$

where

β : particulate radioactivity fraction approximated by eqn (4-3),

v_s : settling velocity (cm s^{-1}), and

C : concentration of radioactivity in water.

The values used to estimate β in eqn (4-3) were : 1×10^{4} mL g^{-1} for the partitioning coefficient, K_d, for ^{60}Co; and 2 mg L^{-1} of depth-averaged particulate concentration, C_p. Stokes velocity of 4.2 cm d^{-1} obtained in section 4.2.3 was adopted for the settling velocity. This value seems rather small compared with 4×10^{-3} cm s^{-1} reported by McCave (1970). However, recent experimental evidence has shown that biological activity and infrequent storm events disturb the sediment record and induce resuspension (Edgington and Robbins 1976), resulting in a smaller value for the apparent settling velocity. This will also play a large role in the transport of particulate matter in water and further research is needed on this topic.

4.4.4.3 Distribution coefficients

It has been recognized that the K_d values obtained for desorption process are larger than those for adsorption process, as discussed in section 4.3. This adsorption-desorption hysteresis was dealt with in the estimation as follows: the distribution coefficients for adsorption (K_d) were adopted for the calculation when $\partial C/\partial t > 0$, and values for desorption (K_d') were used when $\partial C/\partial t < 0$ in the interstitial water. Furthermore, the desorption

processes were not considered to be taking place when the sorbed amount, $K_d'C$, is greater than K_dC obtained for the concentration in aqueous phase at different time steps before and after the desorption event.

These chemical parameters are essential for assessment and seem to be readily obtained by the in situ method in stead of the in vitro batch experiment. However, it is generally difficult to measure the radioactivity in coastal water, even near the discharge point. In this study, therefore, the intrinsic data for sediment samples taken from the locations (water depth : 14 - 45 m) shown in Fig. 4-15 (designated as 1- 10) were obtained by the batch experiments as follows:

(1) about 2.5 mL of wet sediment, which was sieved only by sea water, was transferred using a syringe into 50 mL of sea water tagged with ^{60}Co and ^{137}Cs, and

(2) after 2 wk, 40 mL of solution was replaced by untagged sea water and allowed to settle for another 2 wk for desorption.

Table 4-7 shows distribution coefficients for ^{137}Cs and ^{60}Co obtained both during adsorption and desorption. Temperature effect is evident for both radionuclides, though K_d values for ^{137}Cs decreased when ambient temperature increased from 5 ℃ to 28℃, whereas those for ^{60}Co showed a normal correlation. This suggests that adsorption reaction of ^{60}Co with coastal sediments may not be governed by the ion-exchange mechanism, but enhanced by chemical reaction and/or bio-sorption due to increasing the temperature. Small variations in K_d value for ^{137}Cs indicate the high precision in the procedure for the measuring procedure. Some of desorption coefficients (K_{dh}) for ^{60}Co were one order of magnitude or more larger than adsorption coefficients (K_{ah}), especially for silt rather than sand. This results suggests strong sorption of ^{60}Co to organic coatings and/or Fe, Mn-oxides formed on the particle surface of sediments (Hamilton 1986). In this simulation, the same K_d values were used for the area with similar texture of sediments and the K_d values interpolated depending on the water temperature were adopted during different seasons.

Table 4-7 Distribution coefficients for ^{137}Cs and ^{60}Co obtained in adsorption and desorption processes.

	Adsorption			Desorption			
Sampling location	^{137}Cs K_{an}	^{137}Cs K_{al}	K_{al}/K_{an}	^{137}Cs K_{dn}	^{137}Cs K_{dl}	K_{dl}/K_{dn}	K_{dn}/K_{an}
1	$9.5\cdot10^{1}$	$2.3\cdot10^{2}$	2.4	$1.3\cdot10^{2}$	$3.0\cdot10^{2}$	2.3	1.4
2	$6.6\cdot10^{1}$	$2.7\cdot10^{2}$	4.0	$1.3\cdot10^{2}$	$3.2\cdot10^{2}$	2.4	2.0
3	$9.8\cdot10^{1}$	$2.7\cdot10^{2}$	2.8	$1.5\cdot10^{2}$	$3.2\cdot10^{2}$	2.1	1.5
4	$8.9\cdot10^{1}$	$2.6\cdot10^{2}$	2.9	$1.3\cdot10^{2}$	$3.1\cdot10^{2}$	2.3	1.5
5	$7.5\cdot10^{1}$	$1.9\cdot10^{2}$	2.5	$1.1\cdot10^{2}$	$2.6\cdot10^{2}$	2.4	1.4
6	$7.0\cdot10^{1}$	$1.9\cdot10^{2}$	2.7	$9.5\cdot10^{1}$	$2.1\cdot10^{2}$	2.2	1.4
7	$6.4\cdot10^{1}$	$1.7\cdot10^{2}$	2.7	$9.3\cdot10^{1}$	$2.3\cdot10^{2}$	2.4	1.5
8	$8.2\cdot10^{1}$	$2.4\cdot10^{2}$	2.9	$1.2\cdot10^{2}$	$2.6\cdot10^{2}$	2.2	1.4
9	$1.1\cdot10^{2}$	$3.3\cdot10^{2}$	3.0	$1.6\cdot10^{2}$	$4.2\cdot10^{2}$	2.6	1.5
10	$1.4\cdot10^{2}$	$3.2\cdot10^{2}$	2.3	$1.7\cdot10^{2}$	$4.2\cdot10^{2}$	2.5	1.2
	^{60}Co K_{an}	^{60}Co K_{al}	K_{al}/K_{an}	^{60}Co K_{dn}	^{60}Co K_{dl}	K_{dl}/K_{dn}	K_{dn}/K_{an}
1	$5.5\cdot10^{3}$	$1.2\cdot10^{3}$	0.22	$3.2\cdot10^{4}$	$3.4\cdot10^{3}$	0.11	5.8
2	$1.7\cdot10^{3}$	$7.9\cdot10^{2}$	0.46	$3.3\cdot10^{4}$	$7.7\cdot10^{3}$	0.24	19.0
3	$4.3\cdot10^{3}$	$1.3\cdot10^{3}$	0.30	$1.2\cdot10^{4}$	$6.7\cdot10^{3}$	0.58	2.7
4	$8.2\cdot10^{3}$	$2.9\cdot10^{3}$	0.35	$7.5\cdot10^{4}$	$3.1\cdot10^{3}$	0.41	9.1
5	$4.4\cdot10^{3}$	$1.6\cdot10^{3}$	0.37	$3.0\cdot10^{4}$	$3.0\cdot10^{3}$	0.10	6.8
6	$6.0\cdot10^{3}$	$2.3\cdot10^{3}$	0.38	$4.5\cdot10^{4}$	$9.2\cdot10^{3}$	0.20	7.5
7	$5.0\cdot10^{3}$	$2.3\cdot10^{3}$	0.47	$8.7\cdot10^{4}$	$4.9\cdot10^{3}$	0.06	17.4
8	$7.6\cdot10^{3}$	$1.8\cdot10^{3}$	0.24	$4.3\cdot10^{4}$	$1.0\cdot10^{4}$	0.24	5.7
9	$6.3\cdot10^{3}$	$2.6\cdot10^{3}$	0.42	$4.7\cdot10^{4}$	$2.3\cdot10^{4}$	0.50	7.5
10	$1.8\cdot10^{4}$	$2.1\cdot10^{3}$	0.12	$6.2\cdot10^{4}$	$2.2\cdot10^{4}$	0.36	3.5

Suffixes, a, d, h, and l in the K value indicate adsorption process, desorption one, high(28 ±5°C) and low(5±2°C) temperature respectively.

4.4.4.4 Rate constant

Prior to solving eqn (4-12) coupled to eqn (4-13), it is necessary to estimate the rate constant, k, in eqn (4-14). In the following estimation of this parameter value using batch techniques will be discussed.

A mass balance equation can be expressed for the two-site sorption model as:

$$CV + (Q_h + Q_f)w = C_0V \qquad (4\text{-}17)$$

where

V, w : volume of solution (cm^3) and mass of solid phase (g),

C, C_0 : concentrations of outlet and inlet in liquid phase (unit cm^{-3}), and

Q_h, Q_f: concentrations sorbed by the linear isotherm and the first-order kinetics (unit g^{-1}).

Setting $Q_h = K_dC$ in eqn (4-17), it can be rewritten as follows:

$$Q_f = C_0V/w - (V/w + K_d)C \qquad (4\text{-}18)$$

Differentiating eqn (4-18) with time, t and substituting into eqn (4-14), an analytical solution expressing the change in concentration in the batch solution can be easily derived as:

$$\ln(C/C_0) = -k't \qquad (4\text{-}19)$$

where

$$k' = k/(V/w + K_d) \qquad (4\text{-}20)$$

Equation (4-18) is valid for $Q_f > 0$, subject to the following condition:

$$C/C_0 < 1/(1+K_dV^{-1}w^{-1}) \qquad (4\text{-}21)$$

This indicates that the eqn (4-19) is valid in the range of the concentration change expressed in eqn (4-21) in the batch solution (Fukui et al. 1989b).

The k' value, is obtained graphically from the slope of semi-logarithmic plots of C/C_0 against time, hence the k value is derived from eqn (4-20). Table 4-8 shows the rate constants and distribution coefficients obtained for ^{60}Co by the procedure mentioned above, for four different conditions of temperature set in a dark place. As indicated in Table 4-8, temperature effects on the K_d values were confirmed showing a peak value around 35℃,

which may suggest the high activity of microrganisms in sediments. For an appreciable change in temperature, 5 - 35 ℃, the k values show only a small change ranging from 1.3×10^{-3} to 2.7×10^{-3} cm^3 g^{-1} s^{-1}. In the assessment, the value, 2.5×10^{-3} cm^3 g^{-1} s^{-1} was adopted in the compartment adjacent to the discharge point of the secondary coolant because of thorough mixing by hydrodynamic agitation. For the other areas, the smaller rate constant, 1×10^{-4} cm^3 g^{-1} s^{-1} was assumed, due to rather calm hydraulic condition and insufficient mixing of the coastal water in the lower layer overlying the sediment.

Table 4-8 Rate constants and K_ds for ^{60}Co determined by coupled adsorption model in batch experimrnts.

Constant	5 ℃	15 ℃	35 ℃	55 ℃
k' (s^{-1})	1.2×10^{-6}	3.3×10^{-7}	1.2×10^{-7}	1.8×10^{-7}
k($cm^3g^{-1}s^{-1}$)	1.3×10^{-3}	2.7×10^{-3}	1.6×10^{-3}	1.8×10^{-4}
K_d (28 days)	8.6×10^{3}	1.5×10^{4}	1.6×10^{4}	1.1×10^{3}

4.4.4.5 Parameters in the compartment model

The rates of the volume exchange between the adjacent compartments were estimated to be 10^{-5} - 10^{-4} s^{-1} for the adjacent boxes including discharge point and 10^{-8} - 10^{-6} s^{-1} for the other stagnant reaches considering the data base of current observations and flow vectors reproduced after sevral times of the trial and error procedure. The box volumes range from 10^5 to 10^6 m^3 estimated on the basis of the sea bed topography and the surface areas. The decay constant for ^{60}Co is 4.17×10^{-9} s^{-1}.

Figure 4-17 shows the monthly amount of ^{60}Co discharged as the secondary coolant over the period, FY 1974-1981, which relate the term q in the eqn (4-15). The yearly discharge ranged from 5 to 25 MBq and the total amount was 124 MBq for the eight years without correction for decay. The concentrations at t = 0 in water

and the concentration gradient at the mouth of the bay were set at zero as intial and boundary conditions for the calculation. The area of interest is represented by the rectangular grid network (150 m) and an explicit finite-difference scheme was used to solve the equation mentioned above with a value for the time step, 300 s. In a simple one-dimensional case, stability requires $\Delta x/\Delta t > u$, hence $\Delta t < \Delta x/u_{max}$ where u_{max} is the maximum velocity that may occur (Plandle 1984). For the present case, the $u_{max} \leqq 10$ cm s^{-1} (see Figs. 4-14 and 4-15), and $\Delta x/u_{max}$ is estimated as 1500 s. Therefore, a time step of 300 s adopted in this project is small enough to satisfy the stability requirement mentioned above.

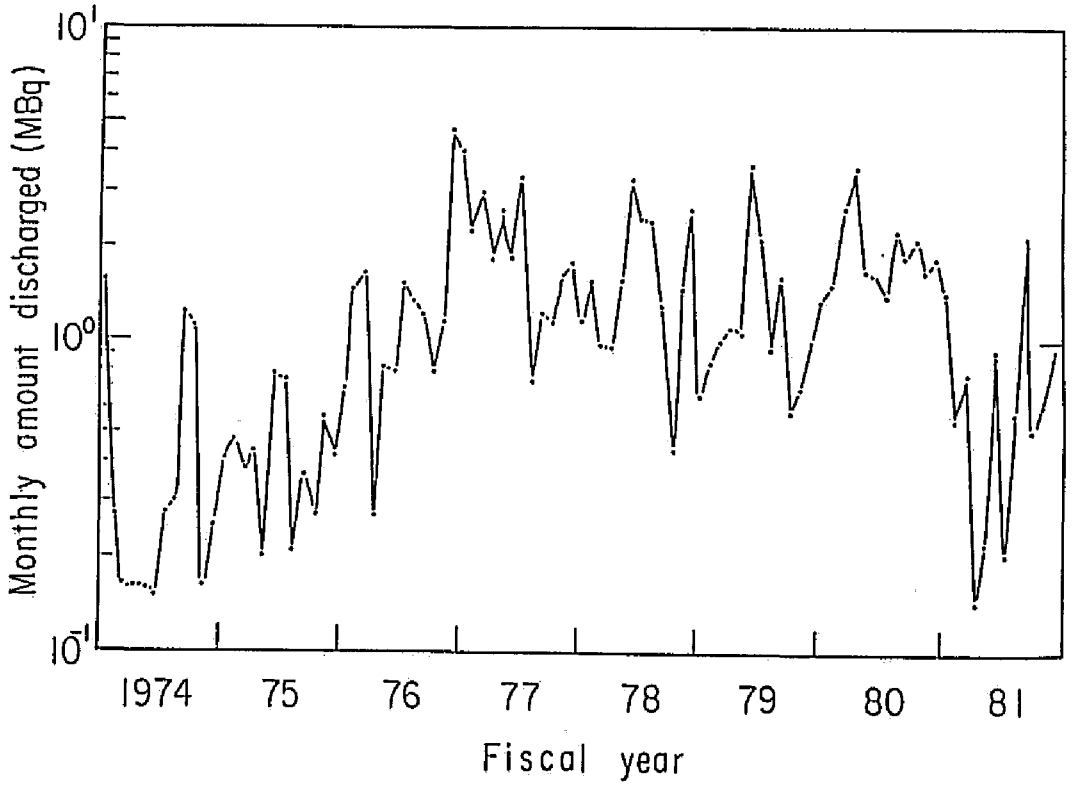

Fig. 4-17 Monthly amount of ^{60}Co discharged into Uchiura bay.

4.4.5 Results and Discussion

Figure 4-18 shows the contour of concentrations on 31 March 1982 in both the upper (solid lines) and the lower (dashed lines) layers. On the whole, the concentrations in water in the upper layer are larger than those in the lower layer due to the stratification caused by the discharge of effluent, which elevated the temperature by ca. 5 - 7 ℃, and also greater flow vectors in the upper layer than in the lower layer (Figs. 4-14 and 4-15). However, direct validation for the distributions by radiometric assay is difficult as the concentrations in water are much less than the detection limit.

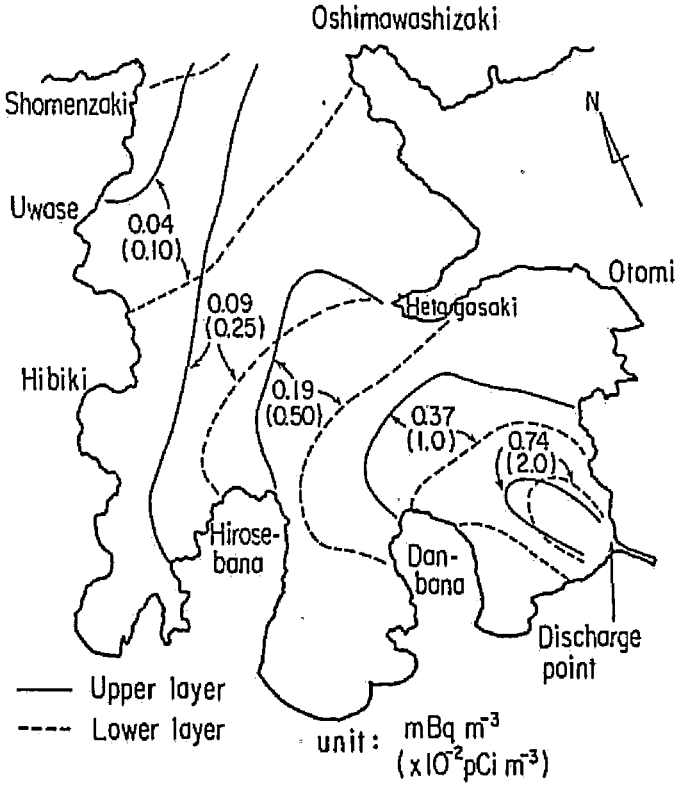

Fig. 4-18 Contaminant spread in coastal water simulated over eight years starting from April 1974. Contours of solid and dashed lines denote concentrations in water both in upper and lower layers, respectively.

In Uchiura Bay, monitoring data has shown that ^{60}Co in sediment, ranging in concentration from 0.4 to 1.5 mBq g^{-1}, has been detected only near the discharge point of the effluent (designated as A in Fig. 4-15), however, no temporal trends could be recognized in the concentrations. Spatial distributions of concentrations for ^{60}Co in the sediments, computed over eight years, at the end of March 1982 are shown in Fig. 4-19. It seems quite reasonable that the spatial distribution of concentrations in sediments is more consistent with that of the water in the lower layer than in the upper layer. As is evident from this figure, the concentrations at the mouth of the bay are almost three orders of magnitude less than those at the discharge point. The trend of decrease is more apparent from Fig. 4-20, which gives a view of concentrations both in waters and sediments along the cross section M-M' (A ~ E) as given in Fig. 4-16.

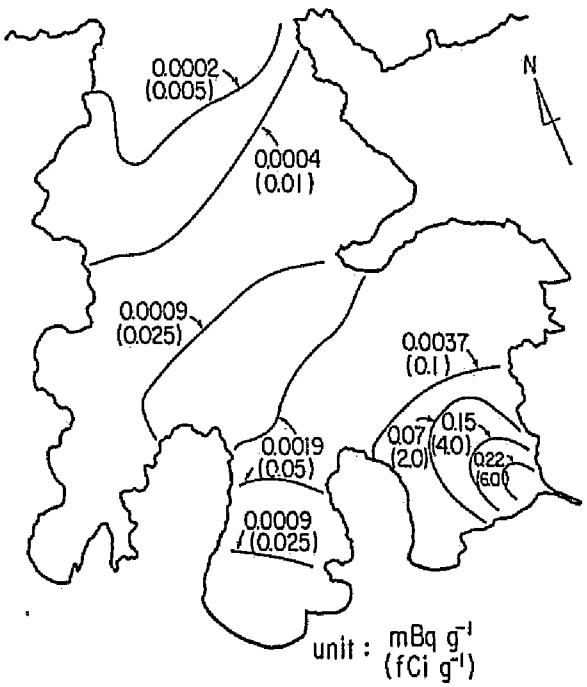

Fig. 4-19 Distributions of ^{60}Co adsorbed in the mixing zone of sediments in Uchiura Bay, which were simulated over eight years starting from April 1974.

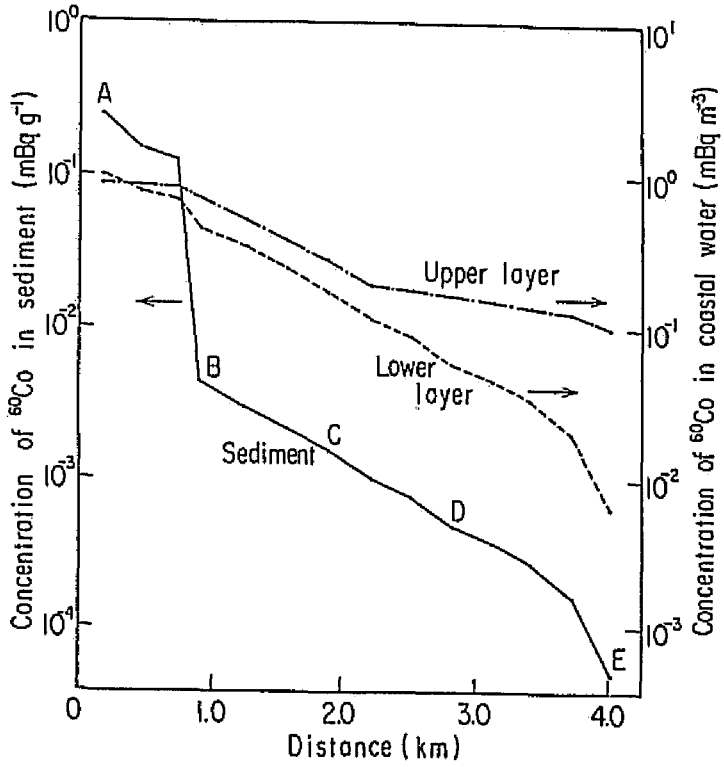

Fig. 4-20 Attenuation of ^{60}Co concentrations calculated for both sediments and waters in two stratified layers at the end of March 1982. Locations A~E on the cross section, M-M' are indicated in Fig. 4-15.

Serious decrease in the concentration in sediments can be seen between the location of A and B, whereas both concentrations in water show mild decreases along the distance. The discontinuity of the concentration in sediments may be due to the difference in the values of rate constant k, used for the calculation as described previously. This also cannot be validated directly by radiometric assay as the spatial distribution of radionuclide in sediments had not been provided by the environmental monitoring in the bay. None the less, the concentration ca. 0.2 mBq g^{-1}, produced by the calculation for the location near the discharge point was found not to be so different, compared with the observed values 0.4 - 1.5 mBq g^{-1}, and the rate of decrease in the concentration in sedimentsis about one order/2km as shown for the location between

B and D. This indicates that the mathematical simulation seems provide reasonable estimates of the contaminant spread in space and time below the extremely low level of detection in the bay of interest. This is the primary objective of present study, and no physical models with sorption kinetics different from a single-valued K_d concept as presented in this chapter have been reported, though the ambiguity of the so-called K_d values in assessment was pointed out (NCRP No.76 1984).

Fig. 4-21 shows the concentration histories simulated in sediments at the locations A~E, and the amount of ^{60}Co sorbed by sediments in the whole bay over eight years.

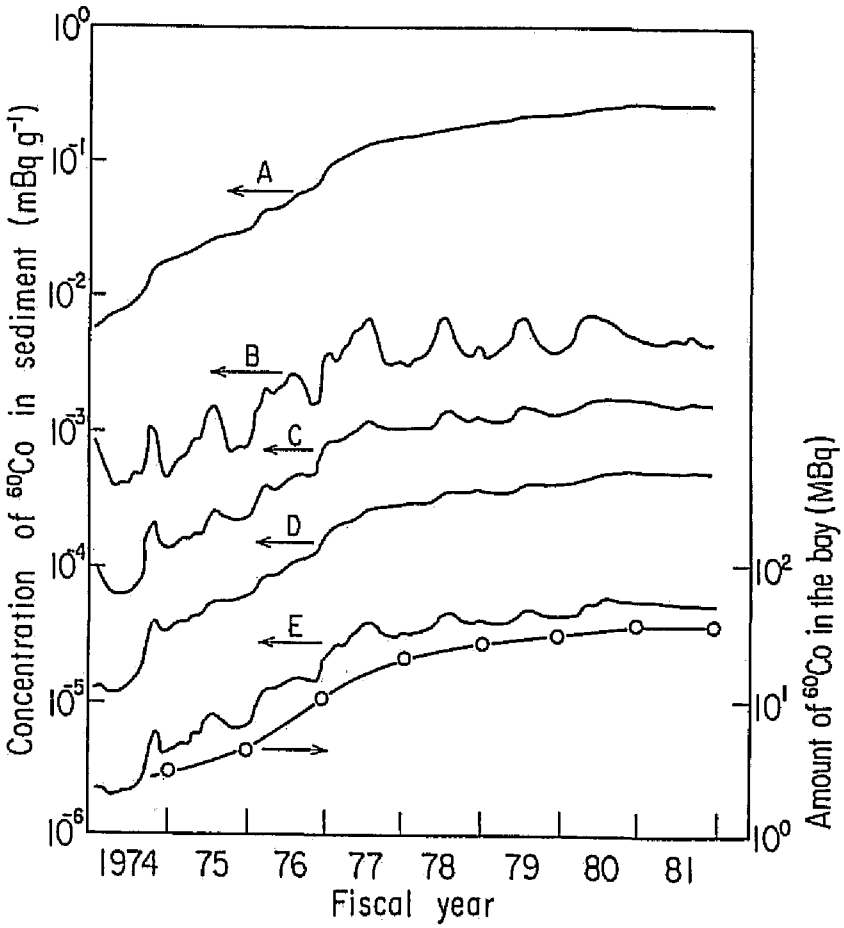

Fig. 4-21 Concentration histories of ^{60}Co at five locations A~E, calculated over eight years and the amount accumulated by sediments in Uchiura bay.

It is evident from Fig. 4-21 that the concentrations in sediments approach steady state about five years after the commencement of discharge. No more than ca. 35 MBq had accumulated in the sediments in the bay. After allowing the radioactive decay, about 44 MBq had been discharched from Uchiura Bay into Wakasa Bay, indicating that about 44 % of the radioactivity discharged during eight years were accumulated in Uchiura Bay.

4.4.6 Conclusions

This work estimated the impact on the coastal environment by the discharge of extreamly low level liquid rad-wastes from Takahama Power Plants, unit No. 1 and No. 2 into Uchiura Bay. Current vectors reproduced by using the continuity equation well described flow patterns of counter currents in two stratified layers. After eight years of simulation, the concentration of ^{60}Co in the sediment near discharge point was estimated to be 0.2 mBq g^{-1}, which was the same as the order of the observed by monitoring. The decrease in concentration in sediments at the mouth of the bay was ca. three to four orders of magnitude less than at the discharge point, 4 km away. During the eight year period, about 35 MBq was stored in the sediment in the bay, which was ca. 44% of the total discharged amount and the remainder was released into Wakasa Bay. The model simulations suggest that no further contamination is likely to occur in Uchiura Bay, provided the discharge rate of radioactivity would not increase in this coastal area.

Chapter 5
SUMMARY

The primary objective of this work was to obtain a better understanding of how radionuclides are distributed and behave in the environment, such that exposure to workers and general public can be assessed. Ideally, environmental fate prediction requires the acquisition of data on the physical and chemical properties of the substance under consideration and the routes of transfer to and through the environment as well as the resulting distribution. However, this requires an investigation of a wide range of topics, even limiting the substances related to radiation hazards.

In this thesis, particular interest was addressed on describing: (1) the distributions and variations of ^{222}Rn content in groundwater and soil air arising from Earth's crust, (2) the distributions of volatile substance, i.e., tritiated water vapor released incidentally in a building and the generalization by modeling the behavior, and (3) the prediction of radionuclides, especially ^{60}Co, discharged routinely from nuclear power plants into a coastal area.

The main findings are summarized as follows:

Chapter 2;

The variation and distribution of ^{222}Rn concentrations were investigated in unconfined groundwater to obtain information as to establishment of how to measure the representative concentration in shallow groundwater and the effects of meteorological parameters on the concentration.

Vertical distributions in concentrations which decrease near groundwater table were clearly obtained in summer rather than in winter owing to the stability, caused by the density difference of water along the depth.

The continuous extraction of shallow groundwater more than 1 m^3 caused pronounced increase of the concentration, and led to the determination of the representative concentration, which

coincides with that of deep groundwater of the same geology.

A method was developed for continuous monitoring of unconfined groundwater in order to examine the effects of meteorological parameters on the groundwater. In this system, part of the groundwater was circulated and sprayed from a nozzle in the same casing and the radon gas released was measured; the remaining water was reinjected into another casing. The main effect observed was a decrease in radon concentration due to dilution by infiltrating water following precipitation, and an increase due to return to the equilibrium between ^{222}Rn and ^{226}Ra. The concentrations diluted by the precipitaion, usually returned to the former levels within a week.

Concentration profiles of radon in soil air were also studied to understand the variation in vertical transport in the ground caused by fluctuations of meteorological parameters. A method of trapping ^{222}Rn was developed to measure the concentration profiles by circulating and bubbling soil air in a porous cup into toluene.

For locations where the water table is close to the ground surface, observations showed a peak concentration in the vertical profile of ^{222}Rn at about 40-cm depth and revealed that the concentration in soil air decreases as soil moisture increases near the water table.

Flux density of ^{222}Rn at the ground surface was estimated to be in the range of 6.9 to 2.6×10^{1} mBq m^{-2} s^{-1} during calm conditions at this site. Soil air in a buried vessel was also circlated continuously to monitor ^{222}Rn gas in the ground near the surface using an ionization chamber. The circulation system was again found to be suited for monitoring of ^{222}Rn in soil air because less opportunity for this type of air exchange to occur in underground air space.

A rise of the water table following precipitation caused a burst of ^{222}Rn concentration resulting from upflow in the ground. However, the concentration in the soil air soon decreased with the intake of air above the surface due to

increasing atmospheric pressure following precipitation. The concentration in soil air again increased via the phenomenon accompaning the recovery of equilibrium between ^{222}Rn and ^{226}Ra in soil moisture.

Chapter 3;

The distributions and behavior of a volatile substance were investigated by monitoring and modeling the changes in concentration of tritiated water (HTO) vapor after an accidental release in a containment building.

Mathematical models have been developed to predict the transfer of HTO in water pools in the building in which approximately 3.4×10^{2} GBq of HTO vapor had leaked over a period of more than one year from a heavy water facility. The model simulations suggest that the mechanism of HTO vapor transfer between air and water is controlled by two key parameters: the kinetic constant for HTO exchange and the evaporation rate constant from water to air. A model was constructed based on data from laboratory experiments involving small glass dishes containing various volume of HTO. The model was validated by estimating the increasein HTO concentration in water pools of various depths in the containment building. After the leakage from the D_2O facility had been stopped, the decrease in HTO concentration in the sub-pool water could be described by this model with a half-life of 15 weeks.

A mathematical model was also developed to estimate the average HTO vapor concentration in air, which is strongly dependent on the operation of the ventilation system even after the removal of the sources of the HTO. This is due to the continued release of HTO from the construction material and is anologous to the dynamics of radon exhalation. The amount which emerged from the concrete was estimated by the model developed on the basis of the monitoring data of the HTO concentration in air, which decreased with a half-lifeof 20 wk.

Of the amount of HTO spilled from the D_2O facility, ca.13.6% (4.6×10^{1} GBq) was retrieved from graphite blocks and 1.3% was

estimated to have been absorbed in the concrete material.

Chapter 4;

Efforts were specifically focused on the prediction of a contaminant spread in a coastal area. The research addressed not only the acquisition of data necessary for the assessment but also for a better understanding of the kinetics of trace elements in saline water.

Distribution coefficients, K_ds, for uptake of several radionuclides by suspended particular matter (SPM) were determined in laboratory batch experiments using samples collected in the coastal areas of the Kinki district. Most SPM in coastal water was retained on the initial filter of four sequential filtering stages (20, 5, 1 and 0.45 μm pore size). Maximum K_d values were measured for the SPM retained on this first stage. When filtration was performed not in series, but in parallel, using the same tracer solution, the K_d values were identical for smaller pore sizes (5, 1 and 0.45 μm) and were greater by 150 % than those measured for the 20 μm size.

The degree of association of the radionuclides with the SPM, as measured by K_d, was $^{85}Sr < {}^{137}Cs < {}^{65}Zn < {}^{54}Mn < {}^{60}Co$.

The fraction of particulate radioactivity associated with the SPM in coastal water was estimated to be $\leqq 0.1$ for radionuclides with K_d of ca. 5×10^4 mL g^{-1}, i.e., which are highly associated with the SPM (2 mg L^{-1}). However, the scavenging effect of SPM seemed to be considerable because scavenging effect based on the settling velocity which was estimated to be 4 - 25 cm d^{-1}, is persistent.

The adsorption/desorption kinetics of the five radionuclides mentioned above were studied for several coastal sediments using various aqueous solutions as extractants in batch systems. In a 2-wk desorption experiment, >90% of most radionuclides sorbed were extracted by 6N-HCl, whereas in 1N-HCl, ca. 30% of the ^{137}Cs was retained by the sediments due to its fixation following intraparticle diffusion.

For longer desorption periods (6 wk), reversible sorption

with sediments could be seen only for ^{137}Cs compared with other four radionuclides in sea water. The EDTA-2Na solution extracted >70% of ^{65}Zn, ^{54}Mn and ^{60}Co, and the ammonium oxalate extracted >60% of ^{54}Mn and ^{60}Co. Readily exchangeable cations extracted by ammonium acetate were >80% for ^{85}Sr, ca. 50% for ^{137}Cs, and 40% for ^{60}Co and ^{54}Mn.

Distribution coefficients for these radionuclides in coastal sediments, obtained in desorption experiments, were one order of magnitude or larger than those obtained in the adsorption experiments. Especially for ^{85}Sr, larger-than- expected distribution coefficients were obtained in the desorption experiment, most likely as a result of the irreversible formation of metal-oxyhydroxides during a slow reaction. These data indicate that the use of a single K_d is inappropriate to forecast the behavior of radionuclides associated with sediments.

The environmental impact of ^{60}Co released from nuclear power plants into Uchiura Bay was estimated by a quasi-three dimensional transport model which is applicable to coastal areas where water bodies are stratified by the thermocline. The processes included in the model were: advection, dispersion, interactions with sediments, radionuclide decay and scavenging by the SPM. Sorption of ^{60}Co by the sediments was described using a model with hysteresis process. Model calculations showed that the decrease rate of concentration in the sediment was ca. one order/2 km along the center line of the bay and equilibration had been attained between water and sediments. During the period of assessment about 44% of ^{60}Co dicharged from the nuclear power plants was stored in the sediments and the remainder flowed into Wakasa Bay via Uchiura Bay. Extremely low-level of ^{60}Co in both sediments and water were judged not likely to pose significant public health hazard near the site.

All processes and models of the radionuclide behavior as dealt with in this thesis will serve to have better understanding of how pesticides and/or herbicides behave in the agro-environment because of their analogue in environmental processes.

REFERENCES

Alberts, J.J.; Muller, R.N. The distribution of $^{239,240}Pu$, ^{238}Pu and ^{137}Cs in various particle size classes of Lake Michigan sediments. J. Envirn. Qual. 8: 20-22; 1979.

Amano, H.; Kasai, A. The transfer of atmospheric HTO released from nuclear facilities during normal operation. J. Environ. Radioactivity 8: 239-253; 1988.

Anazawa, Y.; Kokubu, M.; Fujita, K. Monitoring of tritium in the working environment. Hoken Butsuri (Jpn J. Health Phys.) 7: 27-35; 1972. (in Japanese)

Assinder, D.J.; Kelley, K.; Aston, S.R. Tidal variations in dissolved and particulate phase radionuclide activities in the Esk Estury ,England, and their distribution coefficients and particulate activity fractions. J. Environ. Radioactivity 2: 1-22; 1985.

Aston, S.R.; Duursma, E.K. Concentration effects on ^{137}Cs, ^{65}Zn, ^{60}Co and ^{106}Ru sorption by marine sediments, with geochemical implications. Neth. J. Sea Res. 6: 225-240; 1973.

Aoyama, I.; Urakami, Y. Local redistribution and partial extraction of heavy metals in bottom sediments of an estuary. Environ. Pollut. Ser.B 4: 27-43; 1982.

Beasley, T.M.; Carpenter, R.; Jennings, C.O. Plutonium, ^{241}Am and ^{137}Cs ratios, inventries and vertical profiles in Washington and Oregon continental shelf sediments. Geochim. Cosmochim. Acta 46: 1931-1946; 1982.

Belot, Y.; Gauthier, D.; Camus, H.; Caput, C. Prediction of the flux of tritiated water from air to plant leaves. Health Phys. 37: 575-583; 1979.

Bichard, G.F.; Libby, W.F. An inexpensive radon earthquake prediction concept. EOS (Trans. Am. Geophys. Union), 57: 957; 1976. (Abst.)

Bissell, V.C.,; Peck, E.L. Monitoring snow water equivalent by using natural soil radioactivity. Water Resour. Res. 9: 885-890; 1973.

Blue, T.E.; Holcomb, D.E.; Jarzemba,M.S. Steady-state adsorption

of radon on charcoal canister in cavities in the soil. Radiation Protection Dosimetry 29: 199-202; 1989.

Champ, D.R.; Brown, R.M.; Cooper, E.L.; Cornett, R.J. Emergency response to a spill of tritiated heavy water— The interface between emergency responce, routine monitoring and research. in: Recovery operations in the event of a nuclear accident or radiological emergency, IAEA-SM-316/9, 23-38, Vienna, 1990.

Clement, W.E.; Wilkening, M. Atmospheric pressure effects on ^{222}Rn transport across the earth-air interface. J. Geophys. Res. 79: 5025-5029; 1974.

Cook, G.T.; Baxter, M.S.; Duncan, H.D.; Malcolmson, R. Geochemical associations of Plutonium and γ—emitting radionuclides in Caithness soils and marine particulates. J. Environ. Radioactivity 1: 119-131; 1984.

CORC; Coastal Oceanography Research Committee, Coastal Oceanography of Japan Islands: p.652, Oceangr. Soc. Japan, 1985. (in Japanese)

Dawson, R.; Duursma, E.K. Distribution of radioisotopes between phytoplankton, sediment and seawater in a dyalysis compartment system. Neth. J. Sea Res. 8: 339-353; 1974.

Duinker, J.C.; Hillebrand, M.T.J.; Nolting, R.F.; Wellershaus, S. The river Ems: processes affecting the behaviour of metals and organochlorines during esturing mixing. Neth. J. Sea Res. 19: 19-29; 1985.

Duursma, E.K.; Bosch, C.J. Theoretical, experimental and field studies concerning diffusion of radioisotopes in sediments and suspended particles of the sea. Part B: Methods and experiments. Neth. J. Sea Res. 4: 395-469; 1970.

Duursma, E.K.; Eisma, D. Theoretical, experimental and field studies concerning reactions of radioisotopes with sediment sand suspended particles of the sea. Part C: Applications to field studies. Neth. J. Sea Res. 6: 265-324; 1973.

Edgington, D.N.; Robbins, J.A. Pattern of deposition of natural fallout of radionuclides in the sediments of lake Michigan and their relation to limnological processes. p.705 in :Environmental Biochemistry, Vol.2, Ann Arbor Science Publisher, Michigan, 1976.

Eisma, D. Flocculation and de-flocculation of suspended matter in estuaries. Neth. J. Sea Res. 20: 183-199; 1986.

Fleischer, R. L.; Mogro-Campero, A. Radon enhancements in the earth: Evidence for intermittent upflow? Geophy. Res. Lett. 6: 361-364; 1979.

Fleischer, R. L. Theory of alpha recoil effects on radon release and isotopic disequilibrium. Geochim. Cosmochim. Acta 47: 779-784; 1983.

Förstel, H. Uptake of elementary tritium by the soil. Radiation Protection Dosimetry 16:75-81; 1986.

Förstner, U.; Schoer, J. Diagenisis of chemical associations of ^{137}Cs and other artificial radionuclides in river sediments. Environ. Technol. Lett. 7: 295-306; 1984.

Fukuda, M. Sea conditions off Tokai-mura. NIRS-M-10: 13-21; 1975.

Fukuda, M. Oceanic diffusion in the coastal area. JAERI-M 8730: 1980.

Fukui, M.; Katsurayama, K. Studies on the sorption model of Cs and Sr ion through a saturated sandy layer. Doboku Gakkai Ronbun Hokoku-shu 254: 37-48; 1976a. (in Japanese)

Fukui, M.; Katsurayama, K. Surveying studies on the groundwater around the construction site of the high flux reactor at the Research Reactor Inst., Kyoto Univ. KURRI-TR-162; 1976b. (in Japanese)

Fukui, M. Evaluation of a combined sorption models for describing Cs tansport in a soil. Health Phys. 35: 555-562; 1978.

Fukui, M. Investigation on the processes of disperision and settling of radionuclides in seawater. in : Studies on the distribution and behavior of radionuclides in environment, 11-16; Nucl. Safety Res. Assoc.; Oct. 1979. (in Japanese)

Fukui, M. Studies on the processes of diffusion and deposition of radionuclides in sea, ibid., 10-38; Sept. 1981a. (in Japanese)

Fukui, M.; Uchida, S.; Katsurayama, K. A convenient method for estimating the contaminated zone of a subsurface aquifer resulting from radioactive waste disposal into ground. Hoken Butsuri 16: 11-21; 1981b. (in Japanese)

Fukui, M.; Katsurayama, K. The ^{222}Rn content of groundwater in strata of the Plio-Pleistocene Osaka Group in the Sennan area, Japan. J. Hydrol. 60: 197-207; 1983a.

Fukui, M. Studies on the distribution of ^{222}Rn both in the surrounding water and in the ground. in : Studies on the distribution and behavior of radionuclides in environment, 22-41; Nucl. Safety Res. Assoc.; Oct. 1983b. (in Japanese)

Fukui, M. ^{222}Rn concentrations and variations in unconfined groundwater. J. Hydrol. 79: 83-94; 1985a.

Fukui, M. Continuous monitoring of ^{222}Rn concentration in unconfined groundwater. J. Hydrol. 79: 371-380; 1985b.

Fukui, M. Soil water effects on concentration profiles and variations of ^{222}Rn in a vadose zone. Health Phys. 53: 181-186; 1987.

Fukui, M. Uptake of radionuclides onto suspended particulate matter in coastal water. J. Nucl. Sci. Technol. 25: 934-942; 1988.

Fukui, M.; Yoshimoto, T.; Yamasaki, K.; Saito, M.; Okamoto, K. Kinetics of radioactivities in air in Kyoto University Reactor (KUR) installations and impact assessment. J. At. Energy Soc. Jpn. 31: 1393-1401; 1989a. (in Japanese)

Fukui, M.; Fujikawa, Y. et al. Partitioning of radionuclides for coastal sediments and adsorptive behavior. ibid. 31: 1165-1175; 1989b. (in Japanese)

Fukui, M.; Shirai, H.; Kuruba, K.; Maekawa, M.; Katsurayama, K. Fate of radionuclides released from a nuclear power facility into a coastal area. The 1989 International Chemical Congress of Pacific Basin Societies, held in Honolulu, Abs, INOR-348, Dec., 1989c.

Fukui, M. Recent concerns over the management of radioactivities released from reseach reactor installations. Proc. of 24th scientific meeting of the Research Reactor Institute, Kyoto University: 103-108; 1990. (in Japanese)

Fukui, M. Contamination by tritium of waters and concrete in a research reactor containment due to leakage of heavy water. Proc. 8th Congress of the International Radiation Protection Association, held in Montreal, 1992. (to be published)

Garland, J.A. Absorption and evaporation of tritiated water vapor by soil and grassland. Water, Air, and Soil Pollut. 13: 317-333; 1980.

Goldsmith, W.A.; Haywood, F.F.; Leggett, R.W. Transport of radon which diffuses from uranium mill tailings. Natural radiation environment, U.S.DOE, 1585-1601; 1980.

Graves, B.(ed.) Radon in ground water. Proc. of the NWWA Conference, April 7-9, 1987, New Jersey, Lewis Publishers, 1987.

Gschwend, P.M.; Wu, Shlan-chee. On the constancy of sediment-water partition coefficients of hydrophobic organic pollutants. Environ. Sci. Technol. 19: 90-96; 1985.

Hamilton, E.I. K_d values: an assessment of field v laboratory measurements. in : Application of distribution coefficients to radiological assessment models. 35-63; Elsevier Applied Sci. Publishers, 1986.

Hatsuda, Z. Radon content and its change in soil air near the ground surface. Mem. Coll. Sci., Kyoto Univ. Ser. B, 20: 285-306; 1953.

Hems, G. Acceptable concentration of radon in drinking water. Air Water Pollut. 10: 769-774; 1966.

Hess, C.T.; Stephen, A.N.; Willem, F.B.; Robert, E.C.; Edward, G.C.; Hess A.L. Radon-222 in portable water supplies in Maine. The geology, hydrology, physics and health effects. Land and Water Resources Center, University of Maine, Orono, Me. 1979.

Higgo, J.J.W.; Rees, L.V.C. Adsorption of actinides by marine sediments: Effect of the sediment/seawater ratio on the measured distribution ratio. Environ. Sci. Technol. 20: 483- 490; 1988.

IAEA Exploration for uranium ore deposits, IAEA, Vienna, 1976.

IAEA Sediments K_ds and concentration factors for radionuclides in the marine environment, Tech. Rept. Ser. 247, Vienna, 1985.

IAEA Nuclear techniques in the exploration and expliotation of energy and mineral resources, IAEA, Vienna, 1991.

Ikeda, K.; Murashita, T.; Taguchi, Y.; Ino, M. Studies on earthquake prediction in the eastern part of Tokai District— On automatic observations of radon concentration in groundwater. Bull. Geol. Surv. Japan 32: 151-166; 1981.(in Japanese)

Itihara, M.; Yoshikawa, S.; Inoue, K. Stratigraphy of the Plio-Pleisticene Osaka Group in Sennan-Senhoku area, south of Osaka Japan. J. Geosci. Osaka City Univ. 19: 1-29; 1975.

Jackson, R.E.; Inch, K.J. Hydrogeochemical processes affecting the migration of radionuclides in a fluvial sand aquifer at the Chalk River Nuclear Laboratories. Ottawa: National Hydrology Research Institute; NHRI Paper no.7, Scientific series No.104; 1980.

Kataoka, T.; Ikebe, Y. Influence of ^{222}Rn concentration under the ground on natural gamma-ray flux density exposure rate. Health Phys. 37: 669-675; 1979.

Kiefer, J.; Wicke, A.; Glaum, F.; Porstendorfer, n.n. ^{226}Ra and ^{222}Rn content of drinking water. Proc. 5th Congress of the International Radiation Protection Soc.: 1107-1110; 1980.

Kimura, S.; Asakura, H.; Ochiai, T. Study of groundwater flow measurement by artificial radioactive nuclide tracer. Nogyo Doboku Shikenjo Hokoku 7: 91-118; 1969. (in Japanese)

Kimura, S.; Ohhira, N.; Komae, T. Study of water circulation by taking advantage of radon existing in natural environment. Nogyo Doboku Shikengyo Hokoku, 13: 1-34; 1975. (in Japanese)

King, Chi-Yu. Radon emanation on San Adreas Fault. Nature 271: 516-519; 1978.

Kline, J. R.; Stewart, M. L. Tritium uptake and loss in grass vegetation which has been exposed to an atmospheric source of tritiated water. Health Phys. 26: 567-573; 1974.

Koons, R.D.; Helmke, P.A.; Jackson, M.L. Association of trace elements with iron oxides during rock weathering. Soil Sci. Soc. Am. J. 44: 155-159; 1980.

Kraner, H.W.; Schroeder, G.L.; Evance, R.D. Measurements of the effects of atmospheric variables on radon-222 flux and soil gas concentrations. in : The Natural Radiation Environment (Chicago, IL: Univ. of Chicago Press); 1964.

Kurzeja, R.J., Murphy Jr, C.E., Taylor, R.W. Dispersion of HT and HTO following an unplanned release of tritium to the atmosphere. Fusion Technol. Part B, 14: 1111-1114; 1988.

Langhorst, S.M.; Morris, J.S.; Bull, S.R. Tritium monitoring methodology and application at a research reactor. Health Phys. 40: 823-827; 1981

Liss, P.S., Slater, P.G. Flux of gases across the air-sea interface. Nature 247: 181-184; 1974.

McCave, I.N. Deposition of fine-grained suspended sediment from tidal currents. J. Geophy. Res. 21: 4151-4159; 1970.

Means, J.L.; Crerar, D.A.; Borscik, M.P.; Duguid, J.O. Adsorption of Co and selected actinides by Mn and Fe oxides in soils and sediments. Geochim. Cosmochim. Acta. 42: 1763-1773; 1978.

Megumi, K.; Mamuro, T. Radon and thoron exhalation from the ground. J. Geophys. Res. 78: 1804-1808; 1973.

Mochizuki, S.; Sekikawa,. T. Radon-222-exhalation and its variation in soil air. in : Natural Radiation Environment III, U.S.DOE, 105-116; 1980.

Murphy Jr, C. E. The relationship between tritiated water activities in air, vegetation and soil under steady-state conditions. Health Phys. 47: 635-639; 1984.

NCRP No.76. National Council on Radiation Protection and Measurements, Radiological assessment: Predicting the transport, bioaccumulation and uptake by man of radionuclides released to the environment. NCRP Reports, No.76, Betheda, MD.; 1984.

NCRP No.97. ibid: Measurement of radon and radon daughters in air. NCRP Report, No.97, Betheda, MD.; 1988.

Neretnicks, I. Diffusion in rock matrix: An important factor in radionuclide retardation? J. Geophys. Res. 85: 4379-4397; 1980.

Nielson, K.K.; Rogers, V.C.; Gee, G.W. Diffusion of radon through soils: A pore distribution model. Soil Sci. Soc. Am. J. 48: 482-487; 1984.

Nishimura, S. Automatic measurement of radon in soil gas for earthquake prediction. Radioisotopes 28: 29-32; 1979. (in Japanese)

Nishiwaki, Y.; Kawai, H.; Honda, Y.; Kimura, Y.; Morishima, H.; Koga, T.; Ono, R. On the accumulation and distribution of some radionuclides in the suspended matter in seawater. Radioisotopes 14: 368-373; 1965. (in Japanese)

Noguchi, M. Radioactivity measurement of Radon by means of liquid scintillaton fluid. Radioisotopes 13: 362-366; 1964. (in Japanese)

Noguchi, M.; Wakita, H. A method for continuous measurement of radon in groundwater for earthquake prediction. J. Geophys. Res. 82: 1353-1357; 1977.

Nuclear Regulatory Commission. Characterization of uranium tailings cover materials for radon flux reduction. Washington D.C., NUREG/CR-1081, FBDU-218-2, 1980.

Nuclear Regulatory Commission. Calculation of radon flux attenuation by earthern uranium mill taillings covers. Washington D.C.: NRC; Regulatory Guide 3.64; 1989.

Numata, S.; Minami, K.; Fujii, Y.; Okamoto, M. Containment of tritiated water vapor by concrete walls of fusion reactor building J. Nuclear Sci. and Technol. 28: 84-90; 1991.

Okabe, S. Time variation of the atmospheric radon content near the ground surface with relation to some geophysical phenomena. Mem. Coll. Kyoto Univ., Ser. A, 28: 99-115; 1956.

Okada, S. (Ed.) Tritium data book. Special research program on the nuclear fusion supported by the Ministry of Education, Japan. p.651; 1988. (in Japanese)

Plandle, D. A modelling study of the mixing of ^{137}Cs in the seas of the European continental shelf. Phil. Trans. R. Soc. Lond. A 310: 407-436; 1984.

Pohl, E.; Pohl-Ruling, J. Determination of environmental or occupational ^{222}Rn in air and water and ^{226}Ra in water with feasible and rapid methods of sampling and measurement. Health Phys. 31: 343-348; 1976.

Ramberg, L. Sedimentation of cobalt-60 and cesium-137 release in Tvaren Baltic Bay. J. Environ. Radioactivity 1: 151-164; 1984.

Rogers, V.C.; Nielson K.K. Correlations for predicting air permeabilities and ^{222}Rn diffusion coefficients of soils. Health Phys. 61; 225-230; 1991.

Sasser, M.K.; Watson, J.E. An evaluation of the radon concentration in North Carolina groundwater supplies. Health Phys. 34: 667-671; 1978.

Schery, S.D.; Gaerddert, D.H.; Willkening, M.H. Factors affecting exhalation of radon from a gravelly sandy loam. J. Geophys. Res. 89: 7299-7309; 1984.

Sepall, O.; Mason, S. G. Vapor/liquid partition of tritium in tritiated water. Can. J. Chem. 38: 2024-2025; 1960.

Shibata, T.; Okamoto, S.; Kimura, I. et al. Initial calibration of the Kyoto University Reactor. Ann. Repts. of the Research Reactor Institute, Kyoto University 1: 5-94; 1968.

Sholkovitz, E.R. The geochemistry of plutonium in fresh and marine water environment. Earth-Sci. Rev. 19: 95-161; 1983.

Sibley, T.H.; Myttenaere, C. (eds). Application of distribution coefficients to radiological assessment methods. Essex: Elsevier Applied Science Publishers; 1986.

Sloot, H.A. van der; Duinker, J.C. Isolation of different suspended matter fractions and their trace metal contents. Environ. Technol. Letters 2: 511-520; 1981.

South Pacific Commission. Radioactivity in the south pacific. South Pacific Resional Environmental Programme (SPREP/Topic Review 14). Noumea, New Caledonia; 1983.

Tarnner, A.B. Radon migration in the ground: A Review. in: The Natural Radiation Environment, University of Chicago Press; 1964.

Terashima, Y. Ph. D. Dissertation, Kyoto Unv. 1969.

UNSCEAR: United Nation Scientific Committee on the Effects of Atomic Radiation, Ionizing Radiation, Sources and Biological Effects; 1982.

Vaadia, Y.; Vaisel, Y. Water absorption by the aerial organs of plants. Physiol. Plantarum 16: 44-51; 1963.

Wakita, H.; Notsu, K.; Nakamura, Y. Ground upheaval observed in the lower Tamagawa area and variation of radon concentration in groundwater. Jishin 26: 71-81; 1976. (in Japanese)

Wilkening, M. Radon in the environment. Studies in Environmental Science 40, Elsevier, Amsterdam, 1990

Yoshioka, M.; Co-60 contents in marine environment. KURRI-TR-235: 21-33; 1982. (in Japanese)

List of Publications

For this dissertation;

(1) Fukui, M. ^{222}Rn concentrations and variations in unconfined groundwater. J. Hydrol. 79: 83-94; 1985.

(2) Fukui, M. Continuous monitoring of ^{222}Rn concentration in unconfined groundwater. J. Hydrol. 82: 371-380; 1985.

(3) Fukui, M.; Katsurayama, K.; Nishimura, S. Dynamics of Radon-222 near below ground surface. J. At. Energy Soc. Jpn. 28: 972-979; 1986. (in Japanese)

(4) Fukui, M. Soil water effects on concentration profiles and variations of ^{222}Rn in a vadose zone. Health Phys. 53: 181-186; 1987.

(5) Fukui, M. Modeling the behavior of tritiated water vapor in a research reactor containment building. Health Phys. (in press)

(6) Fukui, M.; Hayashi, M. Retreival of tritium leaked from a heavy water facility and the indoor monitoring. J. At. Energy Soc. Jpn. (in press in Japanese)

(7) Fukui, M. Uptake of radionuclides onto suspended particulate matter in coastal water. J. Nuclear Sci. and Technol. 25: 934-942; 1988.

(8) Fukui, M.; Fujikawa, Y.; Ioka, T.; Kimura, Y., Honda, Y.; Katsurayama, K. Partitioning of radionuclides for coastal sediments and adsorptive behavior. J. At Energy Soc. Jpn. 31: 1165-1175; 1989. (in Japanese)

(9) Fukui, M. Desorption kinetics and mobility of some radionuclides in sediments. Health Phys. 59: 879-889; 1990.

(10) Fukui, M.; Shirai, H.; Kuruma, K.; Maekawa, M.; Iigima, T.; Katsurayama, K. Estimation of behavior of radioactivity discharged into Uchiura Bay. J. At. Energy Soc. Jpn. 33: 594-602; 1991. (in Japanese)

Other publications for scientific journals since 1981;

(1) Fukui, M. Study on the nonlinear sorption models of radionuclides through saturated soils by water. Hoken Butsuri (Jpn J. Health Phys.) 16: 111-121 (1981). (in Japanese)

(2) Fukui, M.; Uchida, S.; Katsurayama, M. A convenient method for estimating the contaminated zone of a subsurface aquifer resulting from radioactive waste disposal into ground. Hoken Butsuri 16: 11-21 (1981). (in Japanese)

(3) Fukui, M.; Katsurayama, K. The ^{222}Rn content of groundwater in strata of the Plio-Pleistocene Osaka Group in the Sennan area, Japan. J. Hydrol. 60: 197-207; 1983.

(4) Fukui, M. Atomic Enegy of Canada Limited, Whiteshell Nuclear Research Establishment. Hoken Butsuri 18: 425-430; 1983. (in Japanese)

(5) Fukui, M. Research program of nuclear fuel waste management in Canada. J. At. Energy Soc. Jpn. 26: 8-15; 1984. (in Japanese).

(6) Fukui, M.; Okamoto, K.; Maki, H.; Yoshimoto, T.; Katsurayama, K. The evaluation of gaseous radioactive materials in the reactor room and in the exhaust from the Research Reactor. Hoken Butsuri 20: 3-12; 1985. (in Japanese)

(7) Woodburn, K.B.; Rao, P.S.C.; Fukui, M.; Kizza, P.N. Solvophobic approach for predicting sorption of hydrophobic organic chemicals on synthetic sorbents and soils. J. Contam. Hydrol. 1: 227-241; 1986.

(8) Kimura, Y.; Ogawa, Y.; Fukui, M.; Tsujimoto, T.; Honda, Y.; Katsurayama, K, Studies on the interaction of radiocobalt with dissolved organic matter in seawater. Hoken Butsuri 22: 429-438; 1987. (in Japanese)

(9) Fukui, M. Models of sorption and migration of radionuclides in geologic media. J. At Energ Soc. Jpn. 29: 498-507; 1987. (in Japanese)

(10) Kimura, Y.; Ogawa, Y.; Fukui, M.; Tsujimoto, T.; Honda, Y.; Katsurayama, K. Studies on the physico-chemical behavior of ^{60}Co, ^{106}Ru and ^{144}Ce in seawater. Hoken Butsuri 23: 105-119; 1988. (in Japanese)

(11) Fukui, M.; Yoshimoto, T.; Yamasaki, K.; Saito, M.; Okamoto, K. Kinetics of radioactivities in air in Kyoto University Reactor (KUR) installations and impact assessment. J. At. Energy Soc. Jpn. 31: 1393-1401; 1989. (in Japanese)

(12) Kimura, Y.; Ogawa, Y.; Fukui, M.; Tsujimoto, T.; Honda, Y.; Katsurayama, K. Studies on the physico-chemical behavior of ^{60}Co, ^{106}Ru and ^{144} Ce in fresh water. Hoken Butsuri 24: 237-247; 1989.

(13) Fukui, M. Management and disposal of low-level radioactive waste in the US. Hoken Butsuri 24: 259-270; 1989. (in Japanese)

(14) Fujikawa, Y.; Fukui, M. Adsorptive solute transport in fractured rock: Analytical solutions for delta-type source condition. J. Contam. Hydrol. 6: 85-102; 1990.

(15) Fukui, M. Factors affecting distribution coefficients used in environmental impact assessment on disposal of radioactive wastes. J. At. Energy Soc. Jpn. 32: 142-148; 1990. (in Japanese)

(16) Fujikawa, Y.; Fukui, M. Analysis of radioactive cesium and cobalt adsorption to rocks using the two-site kinetic model equations. J. Contam. Hydrol. 8: 43-69; 1991.

(17) Fujikawa, Y.; Fukui, M. Variations in adsorption mechanisms of radioactive cobalt and cesium in rocks. J. Contam. Hydrol. (in press)

In Appreciation

The author extends his thanks and heartfelt gratitude to Professor Takashi Matsumura (Research Reactor Institute, Kyoto University), Professor Toshisuke Maruyama and Dean Kazutake Kyuma (Faculty of Agriculture, Kyoto University) for their valuable discussions and warm encouragements for accomplishment of this dissertation.

The author was certainly indebted to Emeritus Professor Kousuke Katsurayama, Kyoto University through the years for his interest and appreciation.

The author is greatful to Dr. Masayasu Noguchi (Japan Atomic Energy Research Institute) for his advice in radon measurement by the liquid scintillation counting and Professor Susumu Nishimura (Faculty of Science, Kyoto University) for his suggestions and providing an instrument for radon gas measurement.

Financial support has partially come from the Nuclear Safety Research Association for the study in the chapters 2 and 4, and from the special research aid of the Research Reactor Institute, Kyoto University. Organization by the Nuclear Safety Policy Section, Fukui Prefecture for the assessment in the coastal area and the technical help in its programs by the Century Research Center are greatfully acknowledged.

Sincere appreciation is extended to Professor P.S.C. Rao, Soil Science Department, University of Florida, U.S.A. and Dr. T.T. Vandergraaf, Head, Geochemistry Section, Whiteshell Laboratories, AECL Research, Canada for their constructive comments and helpful suggestions on improving the task.

The author would like to express his thanks to all the members including students in the Research Reactor Institute, Kyoto University for their support and cooperation.

In a very special way his warmest thanks and heartfelt gratitude go to technical secretary, Mrs. Sayoko Fukui, for her skills and professional attitude.